ADAPTIVE MODEL-FOLLOWING CONTROL FOR HYPERTHERMIA TREATMENT SYSTEMS

by

Reid Leonard Kress

A Dissertation Submitted to the Faculty of the

DEPARTMENT OF AEROSPACE AND MECHANICAL ENGINEERING

In Partial Fulfillment of the Requirements
For the Degree of

DOCTOR OF PHILOSOPHY
WITH A MAJOR IN MECHANICAL ENGINEERING

In the Graduate College

THE UNIVERSITY OF ARIZONA

1 9 8 8

Order Number 8816315

Adaptive model-following control for hyperthermia treatment systems

Kress, Reid Leonard, Ph.D.

The University of Arizona, 1988

U·M·I
300 N. Zeeb Rd.
Ann Arbor, MI 48106

PLEASE NOTE:

In all cases this material has been filmed in the best possible way from the available copy. Problems encountered with this document have been identified here with a check mark __✓__.

1. Glossy photographs or pages _____
2. Colored illustrations, paper or print _____
3. Photographs with dark background _____
4. Illustrations are poor copy _____
5. Pages with black marks, not original copy __✓__
6. Print shows through as there is text on both sides of page _____
7. Indistinct, broken or small print on several pages __✓__
8. Print exceeds margin requirements _____
9. Tightly bound copy with print lost in spine _____
10. Computer printout pages with indistinct print _____
11. Page(s) 20, 139 lacking when material received, and not available from school or author.
12. Page(s) _____ seem to be missing in numbering only as text follows.
13. Two pages numbered _____. Text follows.
14. Curling and wrinkled pages _____
15. Dissertation contains pages with print at a slant, filmed as received _____
16. Other _____

_____

_____

ADAPTIVE MODEL-FOLLOWING CONTROL FOR HYPERTHERMIA TREATMENT SYSTEMS

by

Reid Leonard Kress

A Dissertation Submitted to the Faculty of the

DEPARTMENT OF AEROSPACE AND MECHANICAL ENGINEERING

In Partial Fulfillment of the Requirements
For the Degree of

DOCTOR OF PHILOSOPHY
WITH A MAJOR IN MECHANICAL ENGINEERING

In the Graduate College

THE UNIVERSITY OF ARIZONA

1 9 8 8

THE UNIVERSITY OF ARIZONA
GRADUATE COLLEGE

As members of the Final Examination Committee, we certify that we have read the dissertation prepared by Reid Leonard Kress

entitled Adaptive Model-Following Control For Hyperthermia Treatment Systems

and recommend that it be accepted as fulfilling the dissertation requirement for the Degree of Doctor of Philosophy.

Robert B. Roemer	4/17/88
Robert B. Roemer	Date
Thomas C. Cetas	4/27/88
Thomas C. Cetas	Date
Arne J. Pearlstein	4/29/88
Arne J. Pearlstein	Date
Kullervo Hynynen	4/20/88
Kullervo Hynynen	Date
	Date

Final approval and acceptance of this dissertation is contingent upon the candidate's submission of the final copy of the dissertation to the Graduate College.

I hereby certify that I have read this dissertation prepared under my direction and recommend that it be accepted as fulfilling the dissertation requirement.

Robert B Roemer	4/17/88
Dissertation Director Robert B. Roemer	Date

STATEMENT BY AUTHOR

This dissertation has been submitted in partial fulfillment of requirements for an advanced degree at The University of Arizona and is deposited in the University Library to be made available to borrowers under rules of the Library.

Brief quotations from this dissertation are allowable without special permission, provided that accurate acknowledgement of source is made. Requests for permission for extended quotation from or reproduction of this manuscript in whole or in part may be granted by the head of the major department or the Dean of the Graduate College when in his or her judgment the proposed use of the material is in the interests of scholarship. In all other instances, however, permission must be obtained from the author.

SIGNED: Reid Leonard Kress

ACKNOWLEDGEMENTS

The author would like to express his sincere thanks to Dr. R. Roemer, Dr. T. Cetas, Dr. K. Hynynen and Dr. A. Pearlstein for their constant advice, guidance and encouragement during the course of the research. Special thanks also go to Scott Clegg for his numerous suggestions and stimulating discussions. The author would also like to thank Dennis Anhalt, Chris Diederich, Charles Johnson, Peggy Kundrat, Win-Li Lin, Eduardo Moros, Debbi Newkirk and Marc Olsen for their technical support and advice.

The author would like to give greatest thanks to his family especially to his wife Ann and his daughter Jessica, for their love, patience and support.

This research was supported in part by a University Fellowship and by NCI Grant CA 29653.

TABLE OF CONTENTS

TABLE OF CONTENTS--Continued

TABLE OF CONTENTS--Continued

Page

LIST OF FIGURES

LIST OF FIGURES--Continued

LIST OF FIGURES--Continued

LIST OF TABLES

ABSTRACT

The purpose of this research was to develop three real-time adaptive temperature controllers for hyperthermia heating systems. Each scheme is made adaptive by using a transient Gaussian estimation routine to estimate the tissue blood perfusion and by then using these estimated values either in an optimizing routine, in an observer, or in both. The optimizing routine uses a steady-state Gaussian estimation technique to optimize the power distribution until the best possible match is obtained between the steady-state temperatures predicted by a treatment model and a prespecified ideal temperature distribution. The observer uses a treatment model to control unmeasured locations. The first adaptive control scheme uses the optimizing routine alone, the second uses the observer alone and the third uses both the optimizing routine and the observer. The performance of each of the adaptive control schemes is compared to a standard proportional-integral-derivative (PID) control scheme for one-dimensional simulations of typical treatments. Results comparing the deviation of the controlled temperature distribution to the ideal desired temperature distribution for all locations and all times indicate that the adaptive schemes perform better than the PID scheme. It can be concluded that adaptive control yields improved performance if good a priori knowledge of the treated region tissue and perfusion region

boundaries is available. While these control schemes were designed for eventual implementation on a scanned focused ultrasound hyperthermia treatment system, the techniques are applicable to any system with the capability to vary specific power with respect to location and with an unknown distributed energy sink proportional to the temperature elevation.

CHAPTER 1

INTRODUCTION

Hyperthermia is defined in Hand and James (1986) as therapy (generally used in the treatment of tumors) in which tissue temperature is elevated to 41 °C or higher by external means in opposition to the thermoregulatory processes which control body temperature around the normal set-point. Past researchers such as Dewhirst et al. (1984), Van Der Zee et al. (1986) and Oleson, Sim and Manning (1984) have demonstrated a strong correlation between the minimum sampled intratumoral temperature and the complete response rate of a tumor to hyperthermia therapy. The detrimental effects of elevated temperatures on normal healthy tissues have also been demonstrated by Barlogie et al. (1979), Larkin et al. (1977), and Pettigrew et al. (1974).

A hyperthermia system with no automatic control system is typically controlled by a human operator. With a single applicator heating system, the operator would turn the power up or down. With a multiple applicator heating system, the operator would adjust the power in each applicator. Compared to an uncontrolled system or a system controlled by a human operator, a hyperthermia treatment employing a sophisticated control system should be much more

effective in elevating the temperature of the tumor tissues to desired toxic levels while attempting to maintain the temperature in the surrounding healthy tissues below the toxic level.

1.1 Recent Advances in Hyperthermia Heating Systems

Hyperthermia treatment systems employ many different heating methods and devices. Typical power sources include microwaves, ultrasonic waves, radiofrequency (RF) waves, infrared (IR) waves and conductive-convective modalities (Field and Franconi 1987). Microwave energy can be delivered by apertures, horns, aperture phased arrays, monopole interstitial radiators set both singly and in arrays and dipole microstrip arrays. Radiofrequency devices vary depending upon whether the power source is radiative, distributed E-field, H-field radiative, magnetic dipole, and inductive or capacitive currents. Treatment devices include but are not limited to RF electrode arrays, helix radiators, distributed current dipoles, distributed magnetic dipoles, helixes, distributed current sheets, ferromagnetic thermoseed arrays and direct-contact electrodes. Ultrasonic sources include single or multiple focused, unfocused stationary or scanned transducers and electrically focused and scanned arrays. An example of an infrared source is an infrared lamp. Conductive-convective sources include warm saline perfusion, warm blood perfusion and skin direct-contact methods such as warm water or wax baths or heat boxes with warm air or radiant surfaces (Field and Franconi 1987).

In recent years a second generation of hyperthermia heating systems has evolved which have the capability to vary the geometric pattern of the power application. Investigations of these second generation systems which employ microwave applicators include studies of a fixed-position, multiple-element surface-heating system (Hand, Cheetham and Hind 1986) and a study of a fixed-position multiple antennae/electrode system for heating at depth (Trembly 1985; Trembly et al. 1986). Lee et al. (1986) reported on the clinical application of scanned, single-applicator second-generation microwave systems. Investigations of second generation ultrasonic systems include the systems described by Ogilvie (1986) or ter Haar and Hopewell (1985). For heating at depth, Lele and Parker (1982) and Hynynen et al. (1987) describe scanned focused ultrasonic systems, while Doss (1985) discusses a localized current field system. Clearly, these second generation hyperthermia heating systems have greater flexibility when required to apply power to a given spatial domain. In order to take advantage of this greater flexibility, however, one must employ an improved control system which is more sophisticated in its ability to control the spatial deposition of the power.

1.2 Hyperthermia Control Systems Literature Survey

In the past, hyperthermia control systems were simplistic in nature as were the heating systems. One temperature sensor was used to control one amplitude of a single applicator. As second generation heating systems were being developed, more advanced control systems were proposed and evaluated. A review of recent hyperthermia control

systems literature not only gives one an understanding of why a sophisticated advanced control system is necessary but also shows why adaptive control systems were selected for this study.

1.2.1 Knudsen and Overgaard

Knudsen and Overgaard (1986) designed a microcomputer based feedback controller for a hyperthermia heating system which employs an inductive RF heater and a water bag for surface cooling. They control the temperature in one dimension (collinear with the direction of propagation of the power below the applicator) at the two boundaries of a tumor using applied power and cooling water temperature as their inputs. The control parameters were determined in two ways. First, a one-dimensional thermal model was developed using the transient bioheat transfer equation and second, a stochastic discrete time model was used with either a least-squares or Markov estimator. From twenty-four treatments with six patients they made the following important conclusions. Tissue blood perfusion variations have a considerable effect on the model parameters and as a result, theoretically determined parameters may contain significant error. An identification in each treatment based on experimental data is thus required and because blood perfusion changes as a function of time and temperature an adaptive controller is necessary.

1.2.2 Knudsen and Heinzl

Knudsen and Heinzl (1986) considered the same control problem as Knudsen and Overgaard (1986). They wished to control the

temperature in one dimension at two tumor boundaries below an inductive RF power applicator. They also used applied power and cooling bath temperature as their inputs. They estimated the controller parameters during a warm-up phase and then employed a self-tuning feedback controller. They experimentally evaluated their controller using a perfused phantom. A perfused phantom consists of an appropriate absorbing medium with embedded tubes to simulate blood vessels. The choice of absorbing medium depends upon the heating modality, e.g., microwave, ultrasound, radiofrequency, or others; however, the medium's energy absorption and thermal properties are selected to match those of tissue. (For an example of the design of a perfused phantom refer to Baish, Foster and Ayyaswamy 1986.) Knudsen and Heinzl's experimental results indicate that the control system works for homogeneous as well as inhomogeneous tissue as long as the specific system input bounds were not exceeded. The controller was always able to obtain a temperature maximum between the two controlled temperatures (that is, in the imaginary tumor of the phantom), however, the exact location and magnitude of the maximum temperature could not be controlled. It should be noted that Knudsen and Heinzl's control system can only control temperature beneath the applicator. Other dimensions must be controlled by applicator placement. Their final recommendation was to improve control by relating it to an estimated complete temperature field.

1.2.3 Knudsen and Hartmann

Knudsen and Hartmann (1986) designed a control system for a hyperthermia heating system consisting of a phased array of four RF applicators surrounding a cylindrical tissue model. The control system was designed to control seven temperatures using the four power amplitudes and the three independent phases as inputs to a self-tuning optimal control algorithm. Their control model was a linearized first order transfer function for the effect of each input (4 amplitudes, 3 phases) on each output (7 temperatures). The controller was made self-tuning by using a step-function test signal for each amplitude or phase and observing the transient response of each output. The gain and time constant for the first order transfer function relating each of the outputs to each of the inputs was determined from the form of the transient responses. Control was implemented with an optimal control algorithm employing a quadratic performance index with cost function consisting of all of the states and inputs. The control system was tested on two-dimensional simulations (circular cylindrical coordinates) of patient treatments. From these tests Knudsen and Hartmann concluded that their control algorithm worked. One significant problem was that the self-tuning phase took too long (approximately 50 min) for clinical implementation. They recommended that a priori information be used to improve the speed of the self-tuning phase. In addition, they concluded that an adaptive controller (which could change the control locations or change the set-point temperatures) would be useful. They also recommended that the controller use estimated temperatures for information at locations not measured.

being heated. The five region controller added a central octagonal path (generally measuring 1 cm from face to face) which was considered as one region monitored by a temperature sensor placed within the interior of the smaller octagon. The nine region controller had eight control regions of equal length along the outer octagonal path with one control region for the central octagonal path. They determined that the control system was generally able to bring the temperature in each region to or above the desired set-point temperature. The controller was not able to keep normally perfused regions which were adjacent to highly perfused regions from becoming too hot because of energy transported from the highly perfused region to the normally perfused region. This could potentially cause the temperature in normal tissue to exceed safe levels. They recommended using estimated temperatures to control unmonitored locations.

1.2.6 Babbs, Vaguine and Jones

Babbs, Vaguine and Jones (1986) developed a theoretical control scheme for a general hyperthermia heating system which might employ multiple surface and/or interstitial applicators using various power sources. Multiple applicators are equivalent to a scanned system capable of rapid scanning and control of power versus location. Their controller uses a predictive-adaptive algorithm that infers the applied power and the effective perfusion from the responses of multiple temperature sensors (located where desired within the controlled region) as each of the multiple power applicators is briefly turned off. Using the estimated values of applied power and

local perfusion, the optimal allocation of power which would generate the most uniform intratumoral temperature with a desired spatial mean can be determined.

The control algorithm consists of three stages. First, the applied power density and effective perfusion are estimated. Second, the optimal partitioning of the total power among the various applicators is determined, and third, the total power is scaled to achieve the desired mean. Applied power density is determined from the change in the transient temperature slope at a particular monitored location when the power to each applicator is turned off. Similarly, "effective perfusion" (see Roemer, Fletcher and Cetas 1985 for a definition of effective perfusion) is determined from the transient temperature decay at each monitored site when all power to all applicators is briefly turned off. The time required to determine these parameters is approximately 30 seconds. This is short when compared with the total time for a typical treatment which usually lasts from 30 to 60 minutes. This cycle, called the diagnostic cycle, is continuously repeated because blood perfusion varies with time. To determine the optimal partitioning of the total power between each applicator, Babbs, Vaguine and Jones assume that the net power from multiple applicators is a linear combination of the powers generated by the individual applicators. The power generated by an individual applicator is in proportion to its fraction (σ) of the total power allocation. The intratumoral mean squared temperature deviation about a desired temperature can thus be determined as a function of the σ

values. The partial derivatives of this function with respect to each σ are set equal to zero and the resulting set of simultaneous linear equations is solved for the unique set of σ's yielding a minimum intratumoral temperature variation. Finally, the total power is scaled by a multiplier to make the actual temperature rise equal to the desired temperature rise. The σ's partition the power for uniformity of temperature and the multiplier scales the power for the desired temperature rise.

Babbs, Vaguine and Jones (1986) tested their algorithm by controlling a one-dimensional computer model based on the transient bioheat transfer equation. The first test was a simple case with two applicators heating two uniformly perfused bands of tumor tissue. To simulate noise and limited thermocouple precision a random number generator added errors between $\pm$ 0.05 °C to each temperature and then each value was rounded to the nearest 0.1 °C. (Typical noise and precision for clinical hyperthermia temperature measurement instrumentation.) The control algorithm worked, distributing the power equally between both regions and bringing each controlled temperature to the desired set-point temperature. The second test had the same geometry as test one but perfusion was varied as a function of temperature. The algorithm worked again, keeping the controlled temperatures to within $\pm$ 1°C of the set-point temperature despite more than a six-fold increase in perfusion over the temperature range tested. Without control the temperatures diverged.

Future algorithms could improve this technique in two major areas. First, the present algorithms measure "effective perfusion" at

the sample locations, whereas, future algorithms could estimate the perfusion field based on some treatment model. This is a significant improvement since the effective perfusion includes the effects of energy transport due to conduction as well as perfusion (see Roemer, Fletcher and Cetas, 1985). Second, the present algorithms control temperatures at only the measurement locations, whereas, future algorithms could control unmeasured locations by employing a state estimation routine.

1.2.7 Summary Comments

Several other investigators have worked on control of second generation hyperthermia heating systems. For example, Lele and Parker (1982) and Dar and Lele (1984) suggest varying the power deposition as a function of position. Nikawa et al. (1986) discuss a control system for a direct-contact microwave applicator. Ogilvie et al. (1986) and Rude et al. (1987) present results for commercially available multipoint controllers for RF and ultrasonic heating systems, respectively.

Throughout most of the papers reviewed, two major improvements in control systems for second generation hyperthermia heating systems were suggested. These were: 1) to employ a state estimation routine to estimate temperatures at unmeasured locations thus providing the control system with more information than simply what is measured, and 2) to provide some form of adaptive control which uses knowledge of the spatial and temporal variation of the perfusion. In light of these recommendations and for other reasons, this dissertation

discusses the design of three adaptive schemes for control of second generation hyperthermia heating systems. Each of these three algorithms is made adaptive by continually estimating the perfusion distribution with respect to space and time. All of these algorithms utilize the estimated perfusion field to determine the tissue temperature at unmeasured locations, however, each algorithm uses the estimated temperature field in a different manner. (An excellent reference on the techniques of adaptive control is Landau 1979.) The adaptive control schemes developed in this dissertation use state and parameter estimation techniques to determine the unknown perfusion field and unmeasured temperatures. To do this, the adaptive control schemes require a model of the energy transport in the tissue during a treatment. For this model, the transient bioheat transfer equation proposed by Pennes (1948) is assumed to govern the energy transport within the treated tissue region. Since this equation is a partial differential equation, the resulting control system is defined to be a distributed parameter system.

1.3 Distributed Parameter Control

In the past two decades, much work has been done concerning control and parameter estimation for distributed parameter systems. (See, for example, Ray and Lainiotis 1978, Buhler and Franke 1980, Teo and Wu 1984, Leondes 1986, Tzafestas 1982.) Because this theory is applicable to the control systems described in this dissertation, a brief discussion of distributed parameter control systems is included here.

Ray and Lainiotis (1978) define a distributed parameter system as a system whose processes vary in space and time. Generally, this is a system with a state equation that is a partial differential equation or an integral equation. Just as partial differential equations are classified as parabolic, hyperbolic and elliptic depending upon their basic form, so are distributed parameter control systems. The transient bioheat transfer equation is parabolic and the steady-state bioheat transfer equation is elliptic. There are several methods for solving the governing partial differential equation and using the results for control. For example one could make both the time and space variables discrete, apply numerical analysis techniques and solve the equations on a digital computer. Tzafestas (1982) lists other solution techniques which include reducing the partial differential equation to an ordinary differential equation by using functional transforms (this is the method used in this dissertation), the method of characteristics, power series methods, Monte Carlo methods and others.

Distributed parameter systems are more complex than lumped parameter systems. Control system design for distributed parameter systems requires not only more complex models but also introduces new problems in satisfying controllability, observability and optimality conditions. For example, a given state will respond to controls applied anywhere on or in a system domain. As a result, controllability and optimality must be concerned with both surface and volume controls. Sensor locations could be a function of space and

time, therefore, observability must consider which variables to observe as well as what sensor locations are appropriate. System identification and control techniques, like those developed for control and estimation of lumped parameter systems, such as optimal control, parameter identification, state estimation, and stochastic control exist for distributed parameter systems. The interested reader is referred to the listed references for further information.

CHAPTER 2

METHODS

First generation hyperthermia heating systems are only capable of varying the power deposition as a function of time. Second generation hyperthermia heating systems are capable of varying power as a function of space and time. This dissertation discusses the design of three adaptive control schemes for control of second generation hyperthermia heating systems. Each of these three schemes is made adaptive by continually estimating the perfusion distribution with respect to space and time. All of these schemes utilize the estimated perfusion field to determine the tissue temperature at unmeasured locations; however, each of the schemes uses the estimated temperature field in a different manner. All three adaptive control schemes are compared to a multiregion proportional-integral-derivative (PID) control scheme described in detail later in this chapter. Each of the schemes is assigned an acronym and described briefly. The first adaptive control scheme (AD1) uses the PID algorithm as its main core but estimates an optimal set of set-point temperatures. The second adaptive control scheme (AD2) uses the PID algorithm as its main core but it controls unmeasured locations by employing an observer. The third adaptive control scheme (AD3) again uses the PID

algorithm as its main core but controls unmeasured locations using an observer. It also estimates an optimal set of set-point temperatures.

2.1 Block Diagram of the Control Algorithms

The three adaptive control schemes are similar and can thus be represented by the single block diagram shown in Figure 2.1. The name, input and output of each block in Figure 2.1 is summarized in Table 2.1 for the PID and for each of the adaptive controllers. The input and output of each block in Figure 2.1 and a brief description of the workings of each block is presented in the following sections. More detailed information about the more involved blocks will follow.

2.1.1 Block Q

For AD1 and AD3, block Q is a Gaussian estimation routine which optimizes the magnitudes of the spatial distribution of the specific power to yield a temperature distribution which approximates a desired temperature distribution to a specified tolerance for some preselected cost criterion. It is through this optimization that control schemes AD1 and AD3 control the "entire" temperature field ("entire" meaning the entire modeled field at each node). The input to block Q is the desired temperature distribution at all points in space and time. In general, the desired distribution is constant with respect to time. A typical desired temperature distribution, and one which will be used henceforth throughout this dissertation, is the ideal distribution of therapeutic temperature in the tumor tissue (43 °C) and arterial

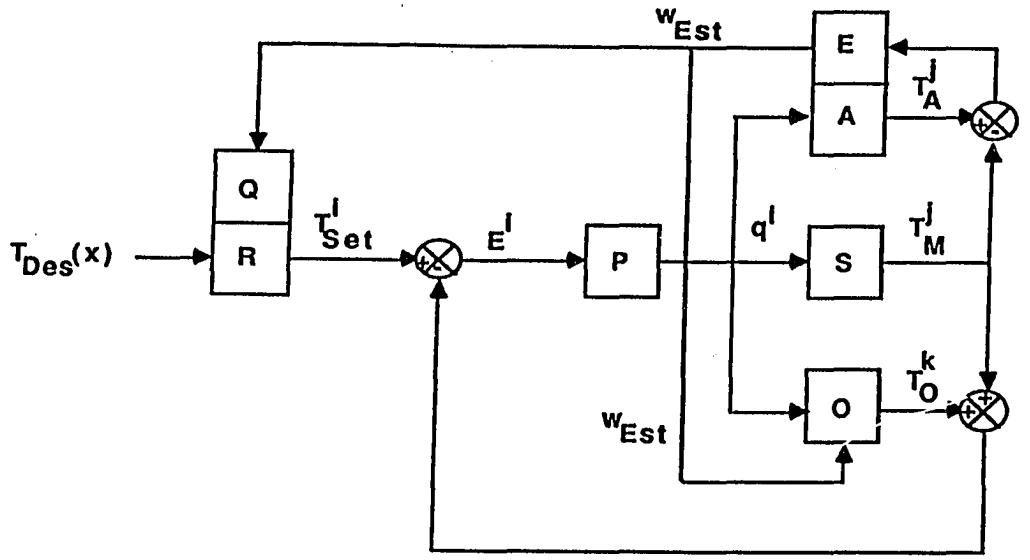

Legend

M = Number of sensors
N = Number of power (control) regions
i = Index for number of power regions in the control algorithm (1 → N)
j = Index for number of measured temperatures i.e. sensors (1 → M)
k = Index for number of estimated temperatures (M+1 → N)
Note: When N = M the observer is not used thus index i and index j cover the same range and index k is not needed.

x = Spatial vector of all nodes
T_{Des} = Desired temperature distribution at all nodes
T_{Set} = Set point temperatures at N locations: [M sensors + (N-M) Observed]
T_A = Model temperatures at M sensor locations
T_M = Measured temperatures at M sensor locations
T_0 = Estimated temperatures at (N-M) nodal locations

$$E^I = \text{Error at N locations} = \begin{cases} T_{Set}{}^j - T_M{}^j & j = 1 \rightarrow M \\ T_{Set}{}^k - T_0{}^k & k = M+1 \rightarrow N \end{cases}$$

q^I = System specific power in N regions (W/m^3)
q_{Est} = Estimated specific power vector in N regions (W/m^3)
w_{Est} = Estimated perfusion vector in W regions (kg/m^3-s) (The number of perfusion regions is unrelated to the number of power regions or the number of sensors)

Figure 2.1. Block Diagram Illustrating the Structure of all Three Adaptive Control Schemes.

Table 2.1

Block Diagram Information

Type	Q	R	P	S	E	A	O
N=M PID	1	Filter	PID	System	-	-	-
In	$T_D(x)$	$T_D(x)$	E^I	q^I			
Out	$T_D(x)$	$T_{Set}{}^I$	q^I	T^J			
N=M ADI	Power Estimator	Model q Variable	PID	System	Perfusion Estimator	Model w Variable	-
In	$T_D(x)$	w_{Est}, q_{Est}	E^I	q^I	$(T_M-T_A)^J$	q^I	
Out	q_{Est}	$T_{Set}{}^I$	q^I	T^J	w_{Est}	$T_A{}^J$	
N>M ADI	1	Filter	PID	System	Perfusion Estimator	Model w Variable	Observer
In	$T_D(x)$	$T_D(x)$	E^I	q^I	(T_M-T_A)	q^I	q^I
Out	$T_D(x)$	$T_{Set}{}^I$	q^I	T^J	w_{Est}	$T_A{}^J$	$T_O{}^K$
N>M ADI	Power Estimator	Model q Variable	PID	System	Perfusion Estimator	Model w Variable	Observer
In	$T_D(x)$	w_{Est}, q_{Est}	E^I	q^I	$(T_M-T_A)^J$	q^I	q^I
Out	q_{Est}	$T_{Set}{}^I$	q^I	T^J	w_{Est}	$T_A{}^J$	$T_{O_I}{}^K$

temperature in the normal tissue (37 °C). This temperature distribution is impossible to obtain in reality so the purpose of the Gaussian estimation routine is to optimize the spatial distribution of the specific power to achieve a temperature distribution as close as possible to this ideal. When this optimization is complete the output of block Q is the estimated optimal power magnitudes. Block Q is not used in the PID or AD2 algorithms. For these schemes, the input to block R is the same as the input to block Q.

2.1.2 Block R

For the PID and the AD2 schemes block R acts as a simple filter which selects those points from the complete desired temperature distribution which will be used as control locations. For a simple PID controller these points would correspond to the locations of the actual temperature sensors. For the AD2 scheme these points would correspond to the actual sensor locations as well as to unmeasured locations whose states are being observed.

For the AD1 and AD3 schemes block R is a reference model of the energy transport in the tissue regions being treated. This model contains all the significant thermal parameters including the tissue properties. The estimated perfusion field and the optimized spatial power distribution are inputs to this block. The output is the set of set-point temperatures which correspond to the optimal power distribution from block Q and the estimated perfusion field from block E. For

AD1 these temperatures correspond to the locations of the actual temperature sensors, whereas, for AD3 this set corresponds to the locations of the actual temperature sensors as well as to unmeasured locations whose states are being observed. One way to view this optimal set of set-point temperatures is to consider the following. For a standard PID controller, the set-point temperature will be either 43 °C or 37 °C depending upon whether the temperature sensor in question is located in cancerous tissue or healthy tissue. For the adaptive schemes AD1 and AD3 the set-point temperatures will be perturbed from these values in order to control the entire temperature field. For example, a sensor located in the tumor tissue but adjacent to the normal healthy tissue might have a set-point temperature equal to 41 °C as a compromise between the 43 °C desired in the tumor and the 37 °C desired in the normal tissue. The idea being to achieve an overall temperature distribution (even at unmeasured locations) which more closely approximates the desired ideal temperature distribution by perturbing the inputs to a standard PID control scheme.

2.1.3 Block P

Block P is the same for all control schemes. It is the standard proportional-integral-derivative control algorithm central to all of the adaptive schemes. The particular algorithm selected is the velocity algorithm described in Bibbero (1977). This algorithm is designed for implementation in a digital control system. The velocity algorithm was selected for its anti-windup and bumpless control characteristics. The input to block P is the error signal calculated

by taking the difference between the set-point temperatures obtained from block R and the measured temperatures for those points corresponding to the locations of actual temperature sensors or the observed temperatures for unmeasured points. The output from block P is the magnitude of the power for each control region.

2.1.4 Block S

Block S is the same for all control schemes. This block represents the system being controlled by the controller. It includes the heating system as well as the heated system. The heating system is the scanned focused ultrasonic system described in Hynynen et al. (1987) for actual treatments or a model of a general heating system capable of changing power with respect to space in the case of treatment simulations. The heated system also varies depending upon whether a treatment or a simulation of a treatment is being used. For actual treatments the heated system would be a patient. For treatment simulations the heated system is a patient model based upon the transient bioheat transfer equation. For this research, a perfused phantom was developed for experimentally evaluating the control schemes. These results are presented in Appendix A.

2.1.5 Block E

Block E functions as the adaptation mechanism for the adaptive control schemes. It consists of a Gaussian estimation algorithm which estimates the spatial distribution of the perfusion field which gives agreement between the temperature decay following a power-off

transient as predicted by a treatment model and the actual temperature decay measured by temperature sensors located in the treated tissue. (When treatment simulations are done, "measured temperatures" are taken from the treatment model at simulated sensor locations.) The input to block E is the error calculated as the difference between the predicted model temperatures and the temperatures measured by the actual temperature sensors (or the difference between predicted model temperatures and treatment model temperatures when treatment simulations are used). The output of block E is the estimated perfusion field. Block E would not appear in a simple PID scheme.

2.1.6 Block A

Block A is the adjustable model used by the Gaussian estimation routine (block E) to predict the tissue temperatures following a power-off transient for each adaptive control scheme. This model contains all significant thermal parameters including the tissue properties and the spatial boundaries of the perfusion field. The trial perfusion field from block E and the actual spatial power distribution calculated by block P are inputs to this block. The output is the predicted temperature field for the temperature decay following a power-off transient. Block A would not appear in a simple PID scheme.

2.1.7 Block O

Block O functions as an observer for the temperatures at unmeasured locations. An observer serves to provide a control scheme with states that are either unmeasured or that cannot be measured. An observer generally employs a model of the controlled system. For the control schemes developed herein, the observer is simply a model of the energy transport in the treated tissue which contains all significant thermal parameters including the tissue properties, the actual spatial and temporal power distribution and the estimated spatial and temporal variation of the perfusion field. Block O is not used in a simple PID scheme or in the adaptive scheme AD1. For these schemes each control region has a temperature sensor and thus no observed temperatures are necessary. For AD2 and AD3, however, the number of control regions exceeds the number of actual temperature sensors and thus an observer is required to estimate the temperatures at the unmeasured locations. It is through the observer that control scheme AD2 controls more of the entire temperature field than the standard PID scheme. The input to this block is the estimated perfusion field from block E and the actual spatial power distribution calculated by block P. The output from this block is the predicted temperature field during the treatment.

2.2 Perfusion Measurement

Thermal energy transport in normal biological systems is dominated by conduction and blood perfusion. During a hyperthermia treatment, when uniform temperatures are desired, blood perfusion is

the dominant mechanism for energy removal. Perfusion varies significantly depending upon tissue type (see, e.g., Table 2.2 from Lehmann 1982). In addition, perfusion can vary with respect to time as shown by Waterman et al. (1987) in Figure 2.2. All three adaptive control schemes developed herein use a model of the thermal energy transport in the treated region either to determine an optimal set of set-point temperatures or as an observer or both. Because these models require knowledge of the spatial and temporal variation of the perfusion field, the possibility of using thermal techniques to directly measure the perfusion at specified locations and times was investigated.

2.2.1 Direct Measurement of Perfusion

Presently several direct perfusion measurement techniques are employed, which are based on thermal phenomena. Representative examples of approaches previously developed are presented below, then the possibility of using each approach in an adaptive control scheme is evaluated.

Chen and Holmes (1980) used a heated thermistor with a pulse-decay technique. The thermistor is placed in the tissue at the location where perfusion is to be estimated. It is allowed to reach thermal equilibrium and is then given a short pulse of power. The temperature quickly rises to a maximum and then decays at a rate dependent on the local perfusion. The temperature decay curve can then be analyzed to determine the local perfusion magnitude. Parker (1981) suggested using the same technique but proposed heating the

Table 2.2

Typical Resting Perfusion Rates of Various Tissues and Organs

Tissue	Anatomical Location and Qualifications	Perfusion (kg/m^3-s)
Skin	Foot -- dorsal (normal resting flow)	2.38 ± 0.43
	Calf "	1.77 ± 0.22
	Thigh "	1.63 ± 0.43
	Arms "	1.40
	Hands "	3.34
	Abdomen "	1.44
	Thorax "	1.08
	Head "	7.15
	Face "	11.72
Subcutaneous Fat	Thigh -- adipose tissue 11mm thick	0.93
	" 20mm "	0.33
	" 43mm "	0.15
	Abdomen -- adipose tissue 10-29 mm	0.51 ± 0.35
	" 30-39 mm	0.36 ± 0.20
	" >40 mm	0.31 ± 0.12
Muscle	Anterior calf (resting flow)	0.46 ± 0.11
	Anterior thigh "	0.43 ± 0.17
	Forearm "	0.53 ± 0.23
Joint	Knee -- average value for skin T=30°C	0.22
	" " T=35°C	0.47
Bone	Range of flow in marrow	0.08 ± 0.03
Organ	Brain	9.00
	Liver	9.62
	Heart	14.00
	Kidney	70.00
Tumor (Examples)	Brain	8.30
	Liver Carcinoma	2.00
	50% all tumors (average)	0.20 + 3.33

Source: Therapeutic Heat and Cold, edited by Lehmann (1982)

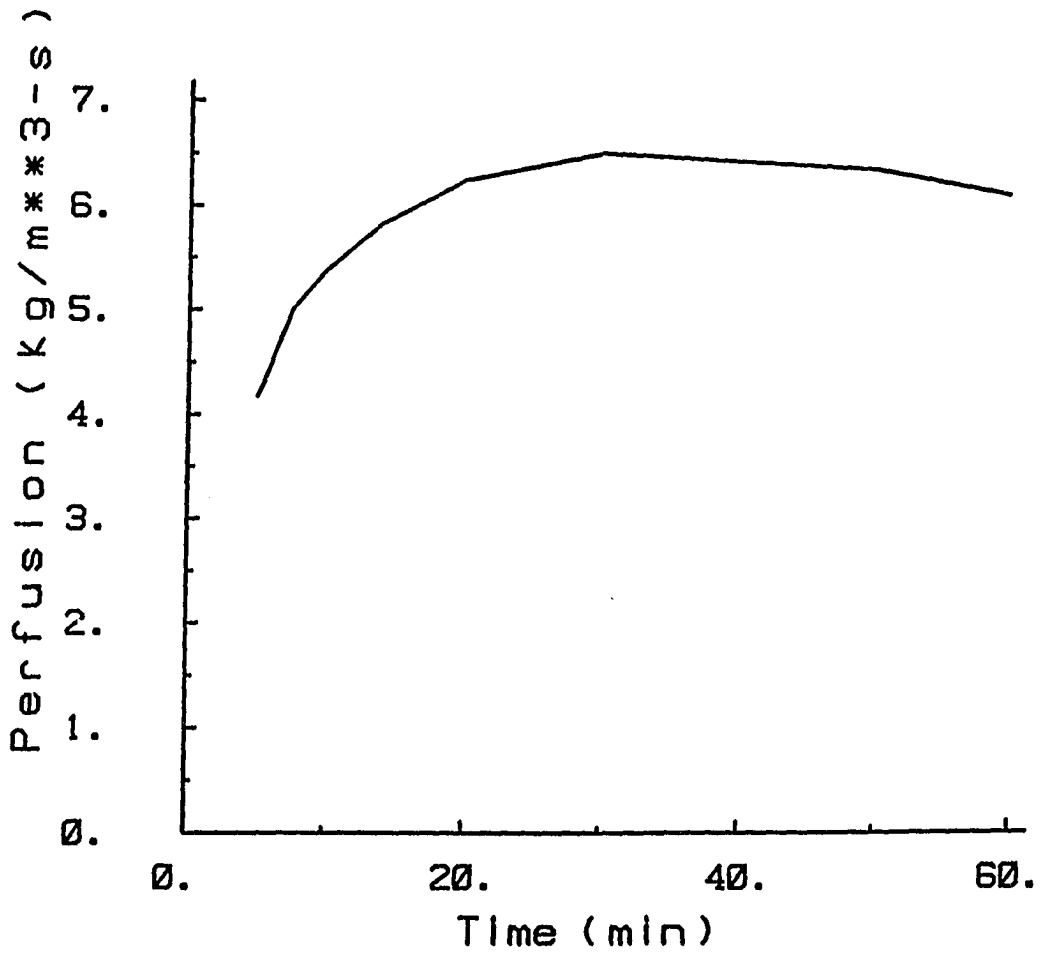

Figure 2.2. Variation of Perfusion with Respect to Time for a Human Tumor During a Hyperthermia Treatment. Temperature = 43.7 °C, from Waterman et al. (1987).

tissue surrounding a thermocouple using a focused ultrasonic transducer. Heating the tissue with a focused ultrasonic transducer would produce, approximately, a two-dimensional Gaussian power deposition pattern whose dimensions would depend upon the radius of curvature, size, and frequency of the transducer, and the absorption of sound in the tissue.

Johnson, Abdelmessih and Grayson (1979) developed a spherical probe which is operated in a constant power mode. The probe starts in thermal equilibrium with the surrounding tissue, the power is switched on, and the temperature rises to a steady state. Both the transient temperature rise and the steady-state temperature are functions of the local perfusion magnitude.

Valvano, Allen and Bowman (1984) recently improved the thermal diffusion technique developed by Balasubramanian and Bowman (1974), an approach which uses a spherical thermistor probe operated at a constant temperature. The probe starts in thermal equilibrium with the surrounding tissue, the power is switched on, and the temperature rises to a preset value. A feedback controller adjusts the power so that the probe temperature remains at the preset value. Perfusion is estimated from the steady-state power which is obtained by extrapolating the measured transient power data to steady-state conditions. Patera, Mikic´ and Bowman (1978) have also studied the possibility of using a cylindrical probe (having a circular cross section) with this method. These techniques have power as the dependent variable. For a more complete survey, Eberhart,

Shitzer and Hernandez (1980) have recently reviewed a variety of perfusion measurement techniques.

Each of these techniques is a viable perfusion measurement method. Each technique estimates perfusion in an entirely different manner, which impacts the accuracy and range of applicability of the technique. The goal of this investigation was to develop a common method for comparing these different techniques and to determine if these techniques could be used in the adaptive control schemes being studied.

2.2.2 Comparative Method for Direct Measurement Techniques

In order to determine which, if any, of the perfusion measurement techniques would be applicable to the adaptive control schemes, it was necessary to model each technique and to determine the sensitivity of the modeled signal to perfusion variations.

Thermal energy transport in biological systems is a complex process involving many variables. In general, however, blood perfusion and conduction are the major contributors to the transport of thermal energy in tissues. In the vicinity of large arteries or veins or during a hyperthermia treatment when tissue temperature is constant (43°C), blood perfusion accounts for most of the thermal energy transport. The flow of blood varies in both magnitude and direction on a microscopic scale. To model these variations would require complicated models such as those developed and studied in Weinbaum, Jiji and Lemons (1984), Weinbaum and Jiji (1985), Jiji, Weinbaum and Lemons (1984), Dagan, Weinbaum and Jiji (1986), and Song,

Weinbaum and Jiji (1987). These models include the effects of arterial temperature variation in space and blood flow directionality. Using these models, however, requires detailed a priori knowledge of the modeled tissues and solving these models requires relatively large amounts of computer time. Considering the computing power and imaging capability available in present-day hyperthermia clinics, both of these requirements pose insurmountable problems for implementation of these models in an adaptive control scheme for hyperthermia heating systems. Instead, an engineering approach must be taken, whereby one selects a model that may not be perfect in all respects but can yield information adequate for a particular application. Such a model for implementation in an adaptive control scheme for hyperthermia treatment systems is the bioheat transfer equation of Pennes (1948). It is given by the following partial differential equation:

$$\nabla\bullet(k\nabla T) - wc_b(T - T_{ART}) + q + q_{MET} = \rho c \frac{\partial T}{\partial t} . \qquad (2.1)$$

In equation (2.1), T is temperature in (°C), T_{ART} is the arterial temperature in (°C), t is time in (s), ∇T is the temperature gradient with units of (°C/m), k is the tissue thermal conductivity (W/m-°C), $\nabla\bullet$ is the divergence, w is the specific blood perfusion (kg/m^3-s), c_b is the blood specific heat (J/kg-°C), ρ is the tissue density (kg/m^3), and c is the tissue specific heat in (J/kg-°C). The first term in equation (2.1) represents the energy transport due to conduction, the second term models energy transport due to the blood perfusion, the third term is the applied power (q), the fourth term represents the metabolic energy (q_{MET}) and the fifth term is the energy storage.

All of the perfusion measurement techniques can be modeled with the bioheat transfer equation and the applicability of each technique to measuring low perfusions can be determined. This analysis is presented in Kress and Roemer (1987). The analysis of the pulse-decay technique is presented here.

The pulse-decay technique determines tissue blood perfusion by comparing the temperature decay measured by an implanted thermistor which has been rapidly heated with a short pulse of power to the temperature decay predicted by a model containing blood perfusion as a parameter. If one assumes that the tissue is homogeneous and isotropic, that the applied power is much greater than the metabolic power, that the arterial temperature is uniform over space and time and that there is a constant and uniform initial temperature equal to the arterial temperature, then, in nondimensional form, the bioheat transfer equation is given by:

$$\nabla^2 u - \gamma u + q^* = \frac{\partial u}{\partial \tau} \, . \qquad (2.2)$$

In equation (2.2) the variable u is the dimensionless temperature defined as $u_{PD} = (T - T_0)/(T_1 - T_0)$ for the pulse-decay technique, where T_0 is the initial temperature before the power pulse is applied (generally equal to T_{ART}) and T_1 is the maximum temperature (reached at the end of the power pulse), or as $u_{SH} = (T - T_0)/(q_M a^2/k)$ for the step heating technique (See Appendix B). Here, q_M is the maximum specific power (W/m^3), a is the characteristic heated region size (m) and k is the tissue thermal conductivity (W/m-°C). The dimensionless parameter γ is defined as $wc_b a^2/k$, where w is the specific blood

perfusion rate (kg/m^3-s) and c_b is the blood specific heat (J/kg-°C). The normalized power function q^* is determined by dividing the spatial and temporal power distribution $q(\tau,R,Z) = q_M p(\tau)S(R,Z)$ by the maximum specific power, q_M. The dimensionless radial variable R is defined as (r/a), the dimensionless axial variable Z is defined as (z/a), and τ is the dimensionless time ($\alpha t/a_r^2$ if a_r is defined or $\alpha t/a_z^2$ if it is not defined). For an infinitesimally short power pulse, such as an idealized, limiting pulse-decay technique, the time function for the applied power is represented by the Dirac delta function; that is, $p(\tau) = \delta(\tau)$. The space function, S(R,Z), varies with the heated region geometry. When power is applied in reality, it must be applied over a nonzero period of time. As shown in Kress and Roemer (1987), for a short time period, Δt, temperature gradients are small and thus conduction heat transfer is unimportant and the temperature at any location in the heated region will rise in proportion to the local applied power. Therefore, when a short pulse of power is applied, the spatial distribution of temperature will be the same as the spatial distribution of power. The temperature will subsequently decay from this distribution after the pulse is stopped.

In an infinite, uniformly perfused medium the tissue temperature will approach arterial temperature as the distance from the treated region increases. Thus, in circular cylindrical coordinates the following symmetry and boundary conditions hold:

$$\frac{\partial u(0,\tau)}{\partial R} = 0 \qquad (2.3)$$

$$\lim_{R\to\infty} u(R,\tau) = 0 \ . \qquad (2.4)$$

For the spherically heated region (simulating a thermistor), the initial condition for the temperature decay after the power pulse is

$$u(R,0) = \begin{cases} 1 & R \leq 1 \\ 0 & R > 1 \end{cases} . \qquad (2.5)$$

The system of equations (2.2 - 2.5) (with q^* set equal to zero) can be solved for the decay of the nondimensional temperature. The solution uses the transformation $u = u'e^{-\gamma\tau}$ to give the new set of equations:

$$\nabla^2 u' = \frac{\partial u'}{\partial t} \qquad (2.6)$$

$$\frac{\partial u'(0,\tau)}{\partial R} = 0 \qquad (2.7)$$

$$\lim_{R\to\infty} u'(R,\tau) = 0 \qquad (2.8)$$

$$u'(R,0) = \begin{cases} 1 & R \leq 1 \\ 0 & R > 1 \end{cases} . \qquad (2.9)$$

Using Laplace transforms, I have evaluated the solution at R = 0 to be

$$u'(0,\tau) = \operatorname{erf}\left[\frac{1}{2\sqrt{\tau}}\right] - \frac{1}{\sqrt{\pi\tau}} e^{-1/4\tau} \ . \qquad (2.10)$$

Therefore,

$$u(0,\tau) = \left[\operatorname{erf}\left[\frac{1}{2\sqrt{\tau}}\right] - \frac{1}{\sqrt{\pi\tau}} e^{-1/4\tau} \right] e^{-\gamma\tau} \qquad (2.11)$$

The solution was evaluated only for R = 0 since this point was selected to represent the entire probe temperature.

A pulse-decay system using a focused ultrasonic transducer to noninvasively supply power would have a power deposition pattern approximated by a two-dimensional Gaussian

$$q(R,Z,\tau) = q_M \, e^{-R^2} \, e^{-(Z/AR)^2} \, \delta(\tau), \qquad (2.12)$$

where AR is the aspect ratio defined as the ratio of the 1/e relaxation length in the axial direction to the 1/e relaxation length in the radial direction. This power deposition pattern would yield the following initial condition at the end of a short pulse of power:

$$u(R,Z,0) = e^{-R^2} \, e^{-(Z/AR)^2}. \qquad (2.13)$$

With this initial condition, the temperature decay after the power pulse can be determined using a Green's function solution following the solution method of Parker (1985). For the center point of the two-dimensional Gaussian, this solution is

$$u(0,0,\tau) = \left(\frac{1}{1 + 4\tau}\right) \sqrt{\frac{1}{1 + 4\tau(1/AR)^2}} \; e^{-\gamma\tau} \, . \qquad (2.14)$$

The temperature decay solutions for other heated geometries can be obtained in a similar manner and are presented in Appendix B. A unified method is needed to compare the performance of the heated thermistor pulse-decay technique to the performance of a pulse-decay technique using a noninvasive power source. This method is based on a time window approach which is developed in the following section and Appendix B.

2.2.3 Time Window Analysis for the Pulse-Decay Technique

The dimensionless temperature at the probe center (R = 0) versus dimensionless time is shown for the spherical heated geometry pulse-decay technique for zero blood perfusion (conduction only, denoted as u_k) and nonzero blood perfusion (conduction plus blood perfusion, denoted as u_{k+w}) in Figure 2.3. The conduction-plus-blood flow solution (u_{k+w}) simulates the expected in vivo conditions, while the conduction only solution (u_k) simulates zero flow conditions. The difference between the two solutions is an estimate of the contribution of blood perfusion to the simulated total in vivo signal (u_{k+w}). Both u_k and u_{k+w} start at 1.0 and decrease to a steady-state value of zero. The conduction-only decay and the conduction-plus-low flow decays are both initially slow until a temperature gradient is established near the center. When the difference between the two decays reaches 10% of the original temperature ($u_k - u_{k+w} = 0.1$), blood perfusion is said to make a significant contribution. This is the beginning of the time window which is used to quantify the efficacy of the various techniques. Later, when the conduction-plus-blood flow decay curve approaches steady state, that is, to within 10% of its complete decay and $u_{k+w} = 0.1$, the signal is deemed too low to distinguish from noise and the time window is closed. Clearly, the time window size is a function of heated region size, blood perfusion, thermal properties, arterial temperature, and heating technique.

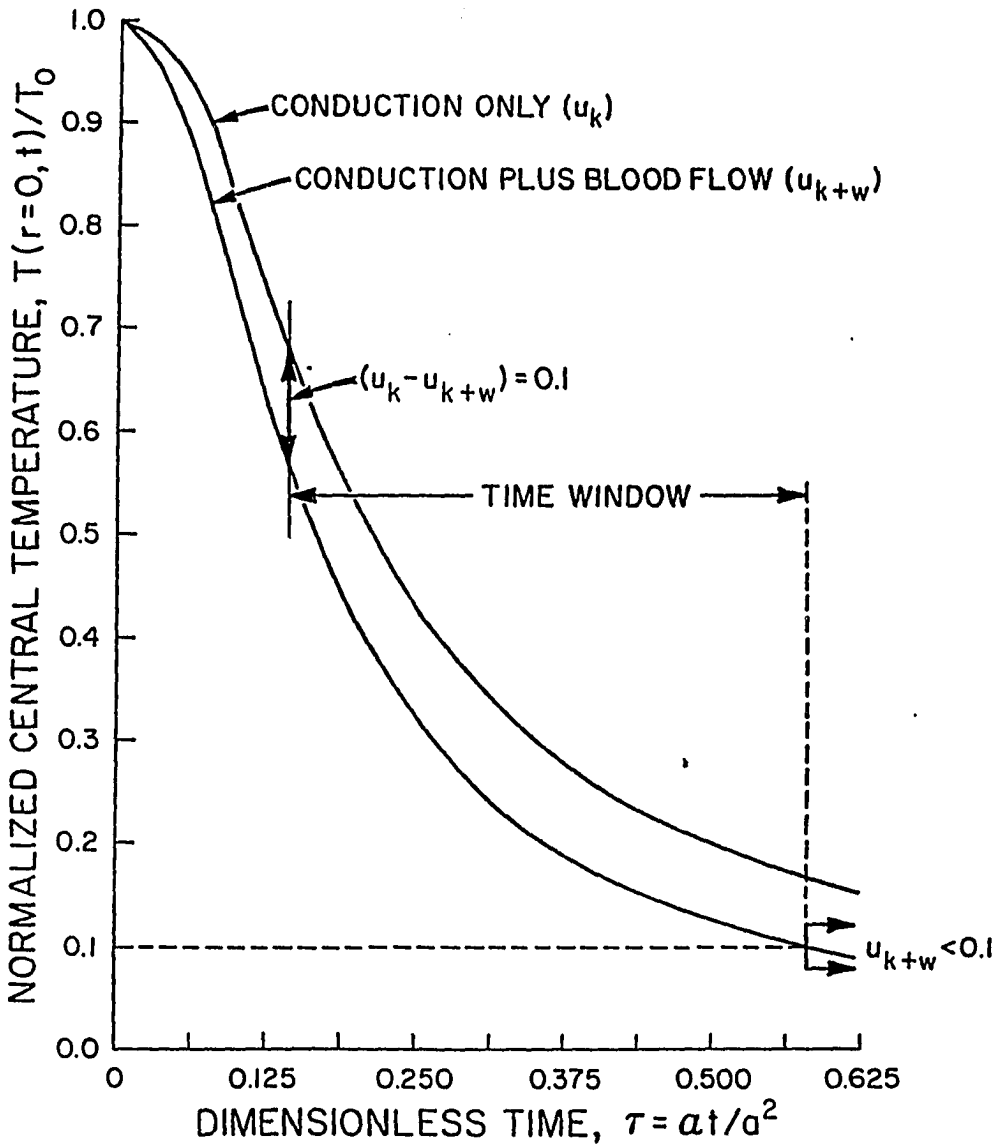

Figure 2.3. Normalized Center Temperature versus Dimensionless Time for Pulse-Decay Technique with Spherical Heated Geometry.

Figure 2.4 gives an example of the time window size versus heated region size and blood flow for fixed tissue properties. Each contour line in Figure 2.4 represents a specified value of the time window length. The solid lines are for a 10% time window criterion (described above) and the dotted lines are for a 1% criterion. For example, a heated radius of 3 mm and a blood perfusion of 10 kg/m^3-s (typical of liver or brain, see Table 2.2) has a time window of approximately 30 seconds for the 10% criterion. For a heated radius of 6 mm and blood flow of 10 kg/m^3-s, the time window is approximately 100 seconds. Each contour line is a dual-valued function of blood flow for a given heated radius. For example, consider a radius of 6 mm, a 10% criterion, and a 100-second time window. Below the lower part of the 100-second line, perfusion is very low, and thus the window opens late because of the length of time required for a 10% difference to appear between the conduction-only and the conduction-plus-blood flow curves. Due to this late opening, there is insufficient time for a 100-second window to develop, since the conduction-plus-blood flow signal falls below the 10% noise level before 100 seconds have elapsed. Above the upper part of the 100-second line, there is also insufficient time for a 100-second window. The perfusion is large, and thus a 10% difference will occur quickly between the conduction-only and the conduction-plus-blood flow decay, however, because of the high perfusion, the conduction-plus-blood flow decay falls below the noise level before 100 seconds, resulting in a time window of less than 100 seconds.

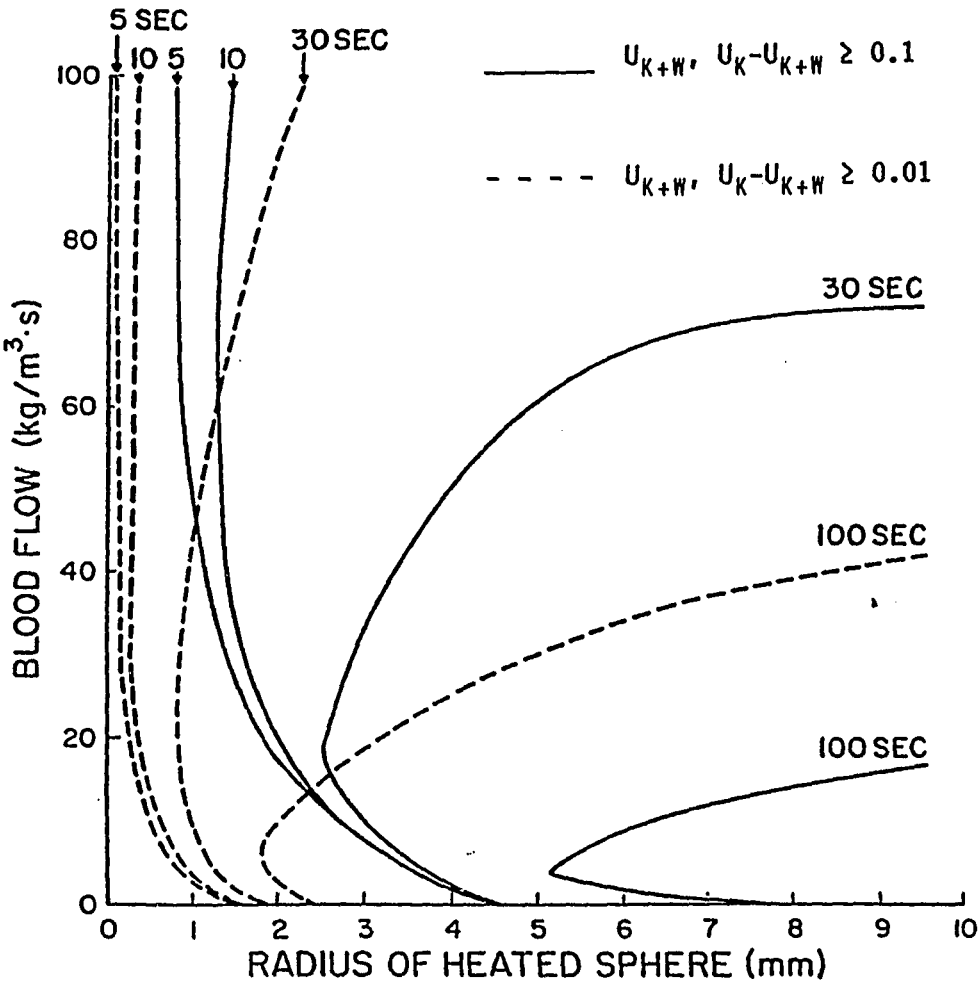

Figure 2.4. Length of Time Window Contour Plot for the Pulse-Decay Technique with Spherical Heated Geometry.

The difficulty in trying to measure perfusion magnitudes typically encountered in treated tissue is evident in Figure 2.4. For resting muscle or fat, Table 2.2 shows that perfusion is on the order of 1 kg/m^3-s. A large but reasonable-sized heated thermistor of radius 1 mm has a negligible time window, less than 5 s even for the 1% criterion. Thus, a large heated region is required in order to obtain a reasonable time window.

In order to compactly present the results for the spherically heated case, consider the nondimensional graph of Figure 2.5. This figure is a plot of the dimensionless blood perfusion variable γ (defined as $wc_b a^2/k$) versus the dimensionless time τ (defined as $\alpha t/a^2$). This figure includes the contents of Figure 2.4 but in dimensionless form. Consider $\gamma = 1.25$ as shown in Figure 2.5. As τ increases, the point where the $\gamma = 1.25$ line first intersects the 10% limit curve is that dimensionless time when the difference between the conduction-only decay and the conduction-plus-blood flow decay is equal to 10% of the initial rise, that is, $u_k - u_{k+w} = 0.1$. This is the start of the time window for this case and is denoted τ_i. The point where the line again intersects the 10% limit curve represents that time when the conduction-plus-blood flow decay comes to within 10% of steady state, that is, $u_{k+w} = 0.1$. This is the end of the time window for this case and is denoted as τ_f. The dimensionless time window length is $\tau_f - \tau_i$. As as example, suppose one wished to determine an appropriate probe size to estimate a given perfusion. The $\gamma = 1.25$ line gives a normalized time window of $\Delta\tau \simeq 0.3$.

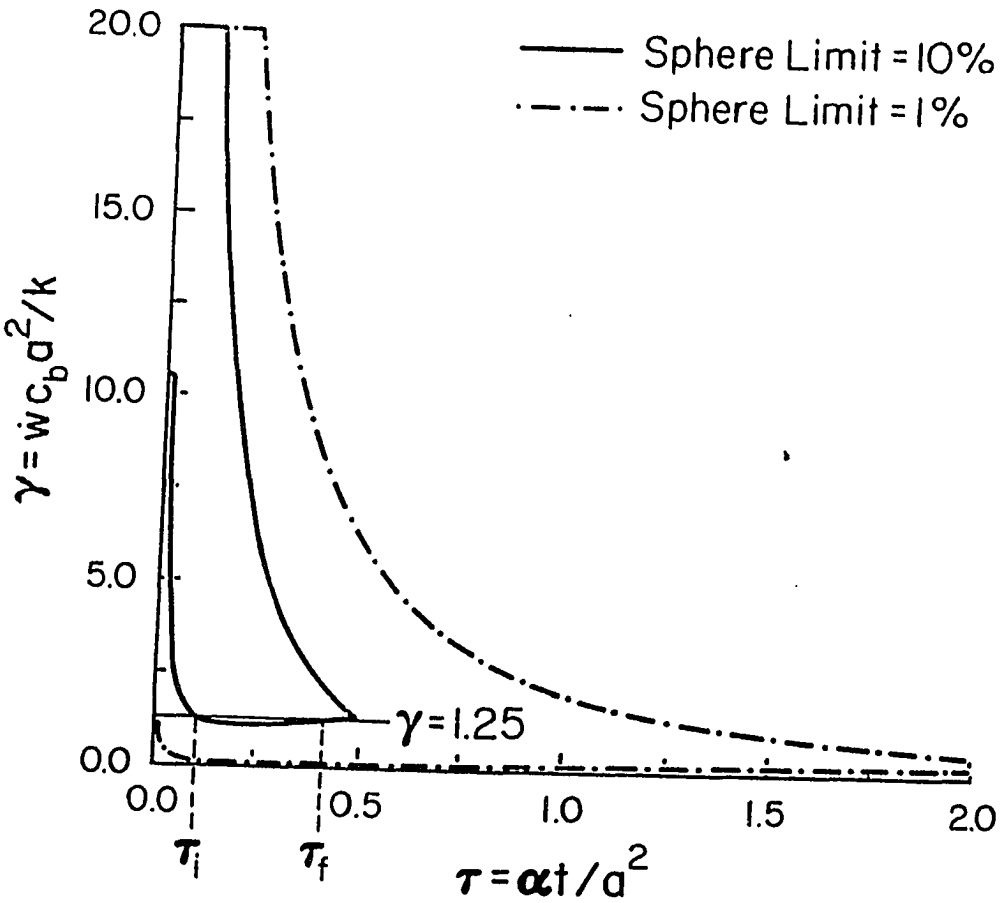

Figure 2.5. Dimensionless Time Window Results for Pulse-Decay Technique with Spherical Heated Geometry.

This could be acceptable, depending on the perfusion level. If γ ($=wc_b a^2/k$) = 1.25 and the perfusion was, say, 2 kg/m^3-s, then for typical tissue properties, the heated radius, a, is calculated to be 8.6 mm. This gives t_l = 60 seconds and t_f = 250 seconds, which yields a 190-second time window. This would be an acceptable time window in which to estimate perfusion, however, an 8.6-mm-radius probe would be impractical for a heated thermistor system. A noninvasive power deposition system would be appropriate in this case. Even the noninvasive system could experience problems because a heated region with diameter of almost 2 cm is likely to contain numerous blood vessels, possibly large arteries or veins, and possibly even different tissue types.

Since the γ line tangent to the lower limit curve has $\Delta\tau$ = 0, the time window length is 0 seconds for this line. Thus, the tangent line determines the lowest perfusion that can be measured with a given probe size. In Figure 2.5, the $\gamma \simeq 1$ line is tangent to the lowest 10% limit curve. Thus, for example, for a probe with a radius of 8.6 mm, in principle the minimum measurable blood perfusion would be slightly above 1.6 kg/m^3-s, with an almost zero time window. For a probe with a radius of 2 mm, the minimum measurable blood perfusion would be slightly above 30 kg/m^3-s, again with an almost zero time window. Referring to Table 2.2, it is evident that 30 kg/m^3-s is a larger perfusion than any tissue with the exception of the kidney. In addition, Figure 2.5 shows that the starting time of the time window is also a function of perfusion (e.g., compare $\tau_l \simeq 0.1$ for γ = 1.25

to $\tau_1 \simeq 0.05$ for $\gamma = 2.5$). Clearly, this would be a difficult technique to use for measuring perfusion in most tissues.

These same analysis techniques are applied to the other heated region geometries (Gaussian, two-dimensional Gaussian and cylindrical) and to each of the other heating techniques (constant power and constant temperature) in Appendix B. The results presented there show that none of the geometries and none of the techniques are applicable to perfusion measurement for any reasonable range of perfusions. Preliminary experiments in dog thighs with the pulse-decay technique demonstrated the expected difficulty with measuring low perfusions. Other techniques are available for measuring blood perfusion (e.g. xenon clearance or radioactive microspheres). These techniques are applicable to measuring low perfusions, however, they are expensive and complicated to use. As a result, the decision was made to use estimation techniques to determine blood perfusion.

2.3 Perfusion Estimation

It has been noted in Knudsen and Overgaard (1986), Johnson et al. (1987), Babbs, Vaguine, and Jones (1986) and Winget et al. (1986) that for temperature control during hyperthermia treatments, blood perfusion is the dominant unknown parameter. One way to determine the local blood perfusion at many locations is to employ state and parameter estimation techniques. These techniques adjust unknown parameters in a treatment model of a perturbed tissue region. When the modeled temperatures agree with measured temperatures to a desired

tolerance the parameters are believed to represent those in the actual treated region. These techniques have been previously applied to biological systems.

2.3.1 Parameter Estimation During Hyperthermia

Winget et al. (1986) employed a two-dimensional finite element transient bioheat transfer equation-based model to estimate the complete temperature field in tissue undergoing a hyperthermia treatment. They used a modified Levenberg-Marquardt scheme (for information on the Levenberg-Marquardt scheme see Beck and Arnold 1977) to optimize the following: power, convective heat transfer coefficient at the skin, and blood perfusion. They represented the blood perfusion distribution as five regions of uniform perfusion. When this algorithm was applied to clinical data, the predicted perfusions were within expected ranges for the tissues tested. Winget et al. (1986) recommended improving the results by using an improved bioheat transfer equation or by representing the blood perfusion as a continuous function.

Clegg and Roemer (1985a, 1985b) and Clegg, Roemer and Cetas (1985) have investigated the use of unconstrained optimization techniques for estimating the complete temperature field using steady-state and transient bioheat transfer equation-based models with blood perfusion distribution as the unknown parameter. Clegg, Roemer and Cetas (1985) used a transient optimization algorithm based on the Gauss method. A brief description of the Gauss method is presented in Appendix C. The algorithm was tested using a one-dimensional bioheat

transfer equation-based tumor model with seven regions of uniform perfusion. The effects of perfusion distribution, sensor location, number of sensors and model mismatch were investigated. A brief summary of some of their important conclusions follows. 1) Using transient power-off decay data provides the best convergence results. 2) Depending upon the magnitude and spatial distribution of the perfusion, sensor placement, and the noise level associated with the measured temperatures, it is possible to accurately estimate more unknown perfusions than the number of temperature sensors. 3) The Gauss method is the best estimation technique for this problem. For more information on parameter estimation see Beck and Arnold (1977).

2.3.2 Perfusion Estimation Routine

Following the recommendations of Clegg, Roemer, and Cetas (1985) it was decided to use transient power-off data and a transient Gaussian estimation algorithm to estimate the perfusion distribution within the tissue regions of interest.

The transient temperature data are collected at each sensor location following the power-off transient. The number of sensors does not have to be equal to the number of parameters to be estimated (the number of perfusion magnitudes), however, in general the greater the ratio of the number of parameters to the number of sensors the less the likelihood of the estimation to converge.

The transient Gaussian estimation algorithm, described in Appendix C, requires a model of the energy transport in the treated region. Besides containing all significant thermal properties

(k,ρ,c,c_b) and boundary and initial conditions, the model must also have knowledge of the temporal and spatial distribution of the specific power delivered by the heating system. In addition, the model must have an adjustable perfusion distribution. In order to keep the model simple, some assumptions must be made about the spatial distribution of the perfusion. For this dissertation, the perfusion will be modeled as distinct regions of uniform (but not necessarily equal) perfusion. This was the spatial perfusion distribution assumed in Clegg, Roemer and Cetas (1985). The perfusion regions are fixed in space. Their boundaries are not changed by the Gaussian estimation algorithm. Only the magnitude of the perfusion in each region is varied by the estimation algorithm. The boundaries of the perfusion regions are determined from a priori knowledge such as CT scans or ultrasonic images. The perfusion region boundaries are placed where significant variations in tissue perfusion are expected; e.g., between major organs, between muscle and fat, between skin and underlying tissue, where major blood vessels are present, etc. In addition, perfusion is assumed to remain constant in time over an estimation interval. That is, the power-off transient will be shorter than the time required for a significant change in the local tissue perfusion. The Gaussian estimation algorithm adjusts the magnitudes of the perfusion distribution until: 1) the difference between the modeled and measured transient temperatures is less than a preset tolerance (least-square error over space and time), or 2) the modeled and measured transient temperatures agree as well as possible, that is, the new perfusions do not change significantly between iterations.

The perfusion estimation routine has two significant parameters which affect its convergence properties. The first is the length of the transient decay time. Too long a decay will cause the treatment temperatures to fall below a therapeutic limit thus making the treatment ineffective. Too short a decay time will not allow sufficient time for information to be transported from regions without temperature sensors to regions containing temperature sensors. The second significant parameter is the decay sample interval. A small sample interval will yield too much data which can cause the estimation routine to take an excessive amount of time to converge. Too large of a sample interval and there will be insufficient data to make an accurate estimation (especially in the limit when one has an ill-posed problem in which there are fewer data points than parameters). To be effective for use in an adaptive control algorithm, these parameters must be optimized for an accurate but fast estimation of the perfusion field.

2.4 Power Estimation

The power estimation routine uses state and parameter estimation techniques to determine the specific power field which will minimize the difference between the modeled steady-state temperature distribution and a prespecified ideal temperature distribution. Just as in the perfusion estimation, a Gaussian estimation algorithm is employed, however, only a steady-state algorithm is required since the resulting optimal temperature distribution is a steady-state distribution. The power estimation is very similar to the perfusion

estimation except that the perfusion estimation compares modeled temperatures to data (or simulated data), whereas the power estimation compares modeled temperatures to a desired ideal temperature distribution.

The steady-state Gaussian estimation algorithm, also described in Appendix C, requires a model of the energy transport in the treated region. Besides containing all significant thermal properties (k, c_b) and boundary conditions, the model must also have knowledge of the spatial distribution of the perfusion field. In addition, the model must have an adjustable specific power distribution. For the controllers designed in this dissertation, the specific power will be modeled in a similar manner as the blood perfusion was modeled, that is, with distinct regions of uniform power with variable magnitudes and fixed boundaries. The power region boundaries are determined from a priori knowledge just as were the perfusion region boundaries. In fact, the power region boundaries should be related to the perfusion region boundaries as well as to the tumor boundaries. The Gaussian estimation algorithm adjusts the magnitudes of the specific power distribution until: 1) the difference between the modeled and the desired steady-state temperature distributions is less than a preset tolerance (at all modeled locations, and not just at measured locations), or 2) the modeled and desired steady-state temperature distributions agree as well as possible, that is, the computed power distribution does not change significantly between iterations.

The power estimation routine has one significant parameter which affects its convergence properties. It is the time between estimations. In other words, how long should the treatment continue before a new estimation is required? If the interval is too short the treated region does not reach steady-state. This is bad from a treatment standpoint because the cancerous tissue has not had sufficient time to reach a therapeutic temperature. If the interval is too long, the controller is not updating the power on a timely basis because perfusion changes with respect to time and so will the optimal power distribution. Presently, the control algorithms update at a fixed interval which is selected to be long enough to allow the treated region to reach steady-state but short enough to catch significant temporal variations in the perfusion.

In closing it is important to note that the perfusion estimation employs a model with known powers for which the Gaussian estimation routine varies perfusion, whereas, the power estimation employs a model with known perfusions for which the Gaussian estimation routine varies the power. Clearly, the model and the Gaussian estimation routine can be the same for both of these applications, only the implementation of and interactions between the model and the Gaussian estimation routine will change.

2.5 PID Control Algorithm

The heart of each adaptive control scheme is a proportional-integral-derivative (PID) controller. The PID controller works as follows. The operator divides a desired treatment region into

separate subregions and assigns a temperature sensor or an observer output to each subregion. Given a heating system capable of varying power over space and time and given the desired sensor or observer output assignments, the PID controller varies the power delivered to each subregion according to a PID algorithm using the temperature history from the sensor or observer output associated with that subregion. The particular algorithm selected is the velocity algorithm described in Bibbero (1977). In discrete-time form it is given by:

$$\Delta q_n = K_P(e_n - e_{n-1}) + K_I\, e_n \Delta t_s + \frac{K_D}{\Delta t_s}(e_n - 2e_{n-1} + e_{n-2}) \ , \quad (2.15)$$

where Δq_n is the incremental change in power at time n, e_n is the error signal at time n, Δt_s is the controller sample interval, K_P is the proportional gain constant, K_I is the integral gain constant, and K_D is the derivative gain constant. For this incremental power change, the new power in each subregion is given by:

$$q_{n+1} = q_n + \Delta q_n \ , \quad (2.16)$$

where q_{n+1} is the power at time n+1 and q_n is the power at time n. A new power is calculated for each of the subregions at each sample interval.

For the scanned focused ultrasonic hyperthermia treatment system for which the adaptive control algorithms were designed, the PID controller is implemented in the following manner. The operator divides a desired treatment region into separate subregions and

assigns a temperature sensor or an observer output to each subregion. The PID controller varies the power delivered to each subregion according to a PID algorithm using the temperature history from the sensor or observer output associated with that region. The power is changed in a given subregion when the focus of the scanned transducer (or transducers) crosses the boundary into that subregion. Power is altered by varying the duty cycle, defined as the ratio of the amount of time that the transducers are at full power to the total cycle time (usually 20 ms). For a more detailed description of the mechanics of the control system as applied to the scanned focused ultrasonic hyperthermia treatment system refer to Johnson (1987).

2.6 Numerical Model for Adaptive Control Algorithms

All the adaptive control algorithms utilize a model or models of the treated region. Each of these models is based on the bioheat transfer equation. For the complicated spatial and temporal distributions of perfusion and power that are encountered in a typical hyperthermia treatment, analytical solutions are out of the question. The bioheat transfer equation must be solved numerically on a digital computer. Clearly, if the adaptive control schemes are to work at all, the numerical method selected to solve the bioheat transfer equation must be fast as well as accurate. Standard numerical techniques such as explicit methods can require hours of CPU time to accurately solve for a perfusion field when used with a Gaussian estimation routine. Thus, a more sophisticated numerical technique was used to solve the bioheat transfer equation for

implementation in the adaptive control schemes. This technique, referred to as a spectral method, is described in the following sections.

2.6.1 Introduction to Spectral Methods

Spectral methods involve seeking the solution to a differential equation in terms of a series of known, smooth functions. In the past few years spectral methods have emerged as a viable alternative to finite difference and finite element methods for the solution of partial differential equations, particularly since the development of fast transform algorithms such as the fast Fourier transform of Cooley and Tukey (1965). Spectral methods are presently used in numerical weather prediction, numerical simulation of turbulent flows, turbulent transition studies, ocean dynamics, and many other applications where high accuracy is desired for complicated problems. The advantage of the spectral technique used herein lies in its inherent ability to achieve high spatial accuracy with a limited number of terms by representing the spatial distribution of the temperature as a series of orthogonal functions. If the number of terms is properly selected then the time required for a solution with desired accuracy can be reduced over a more conventional numerical solution using finite differences or finite elements. The faster, more accurate solution is a result of the rapid convergence of a series of orthogonal functions to a desired functional distribution. The rate of convergence, however, depends upon the continuity of the desired functional distribution.

The problem considered here is of the form:

$$\frac{\partial u(x,t)}{\partial t} = L(x,t)u(x,t) + f(x,t), \quad x \in D, \; t \geq 0, \tag{2.17}$$

with the following boundary and initial conditions:

$$b(x)u(x,t) = 0, \quad x \in \partial D, \; t > 0, \tag{2.18}$$

$$u(x,0) = g(x), \quad x \in D . \tag{2.19}$$

In equations (2.17) through (2.19), D is a spatial domain with boundary ∂D, $L(x,t)$ is a linear (spatial) differential operator and $b(x)$ is a linear (time-independent) boundary operator. It is assumed that for each t, $u(x,t)$ is an element of a Hilbert space H with inner product $(*,*)$ and norm $||*||$. For each $t > 0$, the solution $u(x,t)$ belongs to the subspace B of H consisting of all functions $u \in H$ satisfying $bu = 0$ on ∂D. It is not required that $u(x,0) = g(x) \in B$ but only that $u(x,0) \in H$.

The spectral method will consist of forming a semi-discrete approximation to the governing equation. This approximation takes the form:

$$\frac{\partial u_N(x,t)}{\partial t} - L_N u_N(x,t) + W_N(x,t)\, u_N(x,t) - f_N(x,t) = R_N(x,t), \tag{2.20}$$

where, for each t, $u_N(x,t)$ belongs to an N-dimensional subspace B_N of B, R_n is a residual, and $L_N = P_N L P_N$, where P_N is a projection operator of H onto B_N and $f_N = P_N f$. It is assumed that $B_N \subset B_{N'}$ when $N < N'$ and that $u_N(x,0) = P_N u(x,0)$.

2.6.2 Formulation of the Spectral Method

Formulation of the spectral method involves two steps: 1) choosing the approximation space B_N and 2) choosing the projection operator P_N. Three general formulations are presently used: 1) the Galerkin approximation, 2) the Tau approximation, and 3) the collocation or pseudospectral approximation. With blood perfusion varying with respect to time, the bioheat transfer equation has a nonconstant coefficient, thus the collocation approximation is most appropriate because of its ability to efficiently handle the product of perfusion and temperature in physical space (Gottlieb and Orszag 1977, p. 117).

The collocation approximation starts by selecting N points interior to the domain D referred to as collocation points. With $\phi_n(x)$ $(n = 1,\ldots,N)$ as a basis for the approximation space B_N (assume that $\det[\phi_n(x_i)] \neq 0$) then for each $u \in H$ the projection operator P_N is defined as:

$$P_N u = \sum_{n=1}^{N} a_n(t)\ \phi_n(x)\ . \tag{2.21}$$

Collocation is characterized by the condition that:

$$R_N(X_i,t) = 0\ , \tag{2.22}$$

for $i = 1,\ldots,N$ and $P_N u \in B_N$. Also note that the approximation results will depend upon both the collocation points x_i and the basis functions

ϕ_n for n = 1,...,N.

The choice of basis functions depends upon the governing equation and its boundary conditions. Some examples of basis functions are: complex exponentials, sines, cosines, Chebyshev, Legendre, Laguerre and Hermite polynomials. In general it is desirable to choose basis functions which are eigenfunctions of a singular Sturm-Liouville problem because of their good convergence properties (Gottlieb and Orszag 1977, p. 33). However, if the functions to be approximated satisfy certain special boundary conditions, other basis functions may also exhibit good convergence properties. In particular, if the boundary conditions are periodic, sines, cosines and complex exponentials make good basis functions. For this choice of basis functions, the projection operator P_N is the finite Fourier transform of a function. As a result, these functions are advantageous for use with collocation techniques because the fast Fourier transform routines allow for efficient determination of forward and inverse Fourier transforms. Because of the structure of present Fourier transform routines, the grid points must be evenly spaced and the number of points must be a power of 2. For the solution of the transient bioheat transfer equation in cartesian coordinates with temperature equal to zero on each of the boundaries and with perfusion varying with respect to time, collocation with sine basis functions will be used. Thus, the following basis functions and collocation points are selected for an N mode system:

$$\phi_n(x) = \sin \frac{n\pi x}{L_x} \qquad n = 1,\ldots,N \qquad (2.23)$$

$$x_i = \frac{iL_x}{N+1} \qquad i = 1,\ldots,N\ . \qquad (2.24)$$

The collocation equations

$$\sum_{n=1}^{N} a_n \sin \frac{n\pi i}{N+1} = u(x_i)\ , \qquad i = 1,\ldots,N \qquad (2.25)$$

can be solved by using the relation

$$\sum_{i=1}^{N} \sin \frac{n\pi i}{N+1} \sin \frac{m\pi i}{N+1} = \frac{N+1}{2} \delta_{nm} \qquad (2.26)$$

valid for $0 < n,m < N+1$, to obtain

$$a_n = \frac{2}{N+1} \sum_{i=1}^{N} u(x_i) \sin \frac{n\pi i}{N+1}\ , \ n = 1,\ldots,N\ . \qquad (2.27)$$

With the definition of a_n above, the Fourier sine transform of the temperature is given by:

$$P_N u(x,t) = \sum_{n=1}^{N} a_n(t) \sin \frac{n\pi x}{L_x}\ , \qquad (2.28)$$

and the Fourier sine transform of the power is given by:

$$P_N f(x,t) = \sum_{n=1}^{N} q_n(t) \sin \frac{n\pi x}{L_x}\ , \qquad (2.29)$$

and the Fourier sine transform of the perfusion term $w_N(x,t)u_N(x,t)$ is given by:

$$P_N w(x,t)u(x,t) = \sum_{n=1}^{N} b_n(t) \sin \frac{n\pi x}{L_x}\ . \qquad (2.30)$$

Note that the b_n's of equation (2.30) are like the a_n's of equation (2.28) except instead of being the coefficients of the Fourier sine transform of $u(x,t)$, the b_n's are the coefficients of the Fourier sine transform of the product of $w(x,t)$ and $u(x,t)$. Finally, the Fourier sine transform of the conduction term is given by:

$$P_N L P_N u(x,t) = \sum_{n=1}^{N} c_n(t) \sin \frac{n\pi x}{L_x} , \qquad (2.31)$$

where for the one-dimensional case:

$$c_n(t) = - \frac{n^2 \pi^2}{L_x^2} a_n(t) \quad \text{for} \quad L = \frac{\partial^2}{\partial x^2} . \qquad (2.32)$$

Using equations (2.28) through (2.32), the transient bioheat transfer equation becomes (Note: The time dependence of a_n, b_n, c_n and q_n has been removed for clarity.), for $i = 1,\ldots,N$:

$$\sum_{n=1}^{N} (kc_n - c_b b_n + q_n) \sin \frac{n\pi x}{L_x}\Big|_i = \rho c \sum_{n=1}^{N} \frac{da_n}{dt} \sin \frac{n\pi x}{L_x}\Big|_i . \qquad (2.33)$$

Since perfusion and power are both generally complicated functions of time, b_n and q_n are also complicated functions of time. Therefore, equation (2.33) must be solved using a numerical integration routine. Note that these equations illustrate only the one-dimensional case. Two- and three-dimensional cases are a logical extension, with two dimensions having a double Fourier series (thus the coefficient set will be doubly subscripted) and three dimensions having a triple Fourier series (the coefficient set will be triply subscripted). See Appendix E for the three-dimensional equations. For more detailed

information on spectral methods refer to Gottlieb and Orszag (1977) or Voigt, Gottlieb and Hussaini (1984).

2.6.3 Implementation of Spectral Method for Transient Solution

The spectral method has now been formulated, meaning that the basis functions and projection operator have been selected and applied to the bioheat transfer equation. Next a technique must be selected to efficiently solve the resulting system of ordinary differential equations (2.33) for time varying power and perfusion. This technique is the pseudospectral technique. Figure 2.6 illustrates how the pseudospectral technique is implemented. The collocation points are selected as an initial step. Then the product of perfusion and temperature is formed at all grid locations. Next the temperature, the product of perfusion and temperature, and the power are forward Fourier transformed with a fast Fourier transform (FFT) algorithm to yield a_n, b_n and q_n respectively. If perfusion changes slowly with time (e.g., as in Figure 2.2), it can be assumed to be constant for a short time period, thus making b_n in equation (2.33) a constant. Now, the truncated series of equation (2.33) represents a set of ordinary differential equations for a_n. This set is:

$$-ka_n \left\{ \frac{n^2\pi^2}{L_x^2} \right\} - c_b b_n + q_n = \rho c \frac{da_n}{dt} \quad , \text{ for } n = 1,\ldots,N \quad (2.34)$$

The set of ordinary differential equations (2.34) can be solved for one small time step. The temperature is then inverse Fourier transformed (IFT) with a fast Fourier transform algorithm and the product of perfusion and temperature at each collocation point is

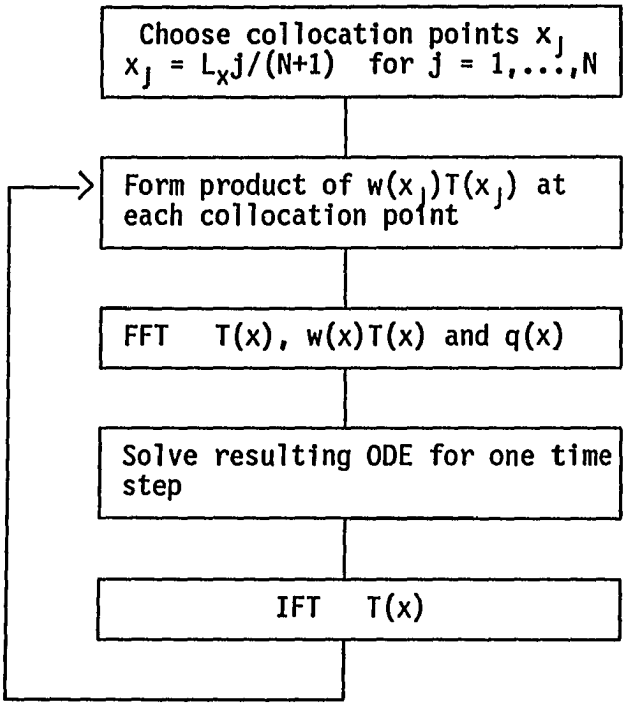

Figure 2.6. Flow Chart Illustrating the Implementation of the Pseudospectral Technique for Solving the Transient Bioheat Transfer Equation.

formed at the new time. The cycle is then repeated. When the routine is operating with variables on the spatial grid, it is said to be working in physical space, and when the routine is operating on the Fourier coefficients, it is said to be working in spectral space. The pseudospectral technique has numerous advantages. First, it is faster to compute the inverse Fourier transform of the temperature, form the product of temperature and perfusion at all grid points in physical space, and then forward transform the product than to form the product of temperature and perfusion in spectral space since this would involve taking the product of two Fourier series. For one-dimensional problems, the pseudospectral technique would require $2N\log_2 N$ operations for the perfusion-temperature product compared to N^2 operations when working in spectral space alone. For three-dimensional problems this would be $(2N\log_2 N)^3$ operations compared to N^6 operations. Second, the pseudospectral technique works well with models having time and/or temperature dependent perfusion since the temperature is always known in physical space at each time step and the perfusion is never required in spectral space. This is also good for output of the temperature, for example when the models are used as observers, since the temperature is always available in physical space at each time step. The pseudospectral technique also has disadvantages, the major one being aliasing.

Aliasing is an error which occurs when a function consisting of an infinite number of functional modes is approximated by a finite series of functional modes. Fourier modes which assume identical

values at the points of a discrete grid create the phenomenon called aliasing when Fourier transform algorithms are used. For example, consider a nine point grid spanning the range 0 to L_x. (Nine points implies eight modes since the value of the function at L_x is periodic and equal to the value of the function at 0.) The values of $\sin(2\pi x/L_x)$ and $\sin(18\pi x/L_x)$ are the same at each of the grid points $iL_x/8$, for $i = 0,1,2,\ldots,8$. In fact, $\sin[(2+j16)\pi x/L_x]$ assumes the same values at these grid points as $\sin(2\pi x/L_x)$ for any value of j. (In general, $\sin(n\pi x/L_x)$ is the same as $\sin[(n+j2N)\pi x/L_x]$ for all j on an N+1 point (N mode) grid given by iL_x/N, for $i = 0,1,2,\ldots,N$.) Because these higher frequency modes can not be distinguished from the lower frequency modes on the finite grid, their contribution to the function is included in the coefficients of the lower frequency modes. The coefficients of the higher frequency modes generally have a smaller magnitude, consequently, when a forward Fourier transform is completed, the relative error in the coefficients is larger as frequency increases. In other words, when a given function is forward Fourier transformed the higher-frequency-mode coefficients contain a greater relative error due to aliasing than do the lower-frequency-mode coefficients. Since the temperature distribution consists of an infinite number of functional modes, aliasing error occurs whenever the temperature field is forward Fourier transformed. The same error occurs when the perfusion distribution and power distribution are Fourier transformed.

To solve the problem of aliasing, dealiasing is done. In this technique, the function to be transformed is defined on a 2N+1 point grid. The forward Fourier transform is then done for 2N modes (yielding 2N coefficients) recognizing that the latter coefficients, those running from N+1 to 2N, contain the greatest aliasing error. The new coefficients are determined by the governing ordinary differential equation in spectral space but only for the lower frequency modes, 1 to N. The higher frequency coefficients are necessary because the inverse transform is required at 2N+1 points thus the higher frequency coefficients are set equal to zero (this is adding no error) and the inverse Fourier transform done at 2N+1 points. Of course this means that the function is only being represented by N modes but the representation is more accurate than using the full 2N modes containing the coefficients with aliasing error. For three dimensions, the original function needs to be known on a $(2N+1)^3$ grid for N modes in each direction.

The set of ordinary differential equations (2.34) is solved by a numerical integration routine. Many different integration routines, for example Euler's method, are applicable. Gottlieb and Orszag (1977, p. 108) have shown that Crank-Nicolson time differencing is unconditionally stable for the standard diffusion equation (perfusion equal to zero). For the models in the adaptive control routines, perfusion is not zero and varies with time. Because perfusion is a function of time, the b_n of equation (2.34) is unknown at all future times. The Crank-Nicolson technique uses a future time step in its difference formulation, as a result the Crank-Nicolson technique can

only be applied to the conduction term. The perfusion term must be handled explicitly. This modified Crank-Nicolson technique leads to the following difference equations for uniform perfusion, w_u and uniform power, q_u:

$$-k\omega_n^2(a_n^{i+1} + a_n^i)\frac{1}{2} - c_b w_u a_n^i + q_u = \rho c \frac{1}{\Delta t}(a_n^{i+1} - a_n^i), \quad (2.35)$$

for $1 \leq n \leq N$, where ω_n is defined as $n\pi/L_x$ and $a_n{}^i$ is the n-th coefficient at time i. Solving for the coefficients at the new time, i+1, one obtains:

$$a_n^{i+1} = \frac{\left[1 - \Delta t\left(\frac{\alpha\omega_n^2}{2} + \frac{c_b w_u}{\rho c}\right)\right] a_n^i + \frac{q_u \Delta t}{\rho c}}{\left(1 + \Delta t \frac{\alpha\omega_n^2}{2}\right)} \quad (2.36)$$

where Δt is the time step and α is the thermal diffusivity. The set of equations (2.36) can be solved for the coefficients at the next time step and an inverse Fourier transform done to obtain the temperature at the new time. For the time differencing to be stable, the coefficients must not grow without bound. For this to be true, the ratio of the coefficient's magnitude at the new time to that at the old time must be less than one. This is expressed mathematically by setting the absolute value of $a_n{}^{i+1}/a_n{}^i < 1$ which gives:

$$\Delta t < \frac{2\rho c}{c_b w_u}, \quad (2.37)$$

for the stability limit on the time step. Without using the modified Crank-Nicolson technique the stability limit is:

$$\Delta t < \frac{2}{\alpha\omega_N^2 + \frac{c_b w_u}{\rho c}} , \tag{2.38}$$

which is a much more restrictive limit considering Δt from equation (2.38) is O(0.1) for a typical grid (N=32) and Δt from equation (2.37) is O(100). (Note in equation 2.38 that ω_N is $N\pi/L_x$ where N is the total number of modes.) These limits are applicable to one-, two- or three-dimensional models, with the proper definition of ω_N used in equation (2.38). See Appendix E.

2.6.4 Implementation of Spectral Method for Steady-State Solution

When the spectral approximation was applied to the transient bioheat transfer equation, the original partial differential equation was reduced to a set of ordinary differential equations in time. When the spectral approximation is applied to the steady-state bioheat transfer equation, the original ordinary differential equation is reduced to a set of algebraic equations.

The steady-state bioheat transfer equation is:

$$\nabla\cdot(k\nabla T) - wc_b(T - T_{ART}) + q + q_{MET} = 0 . \tag{2.39}$$

For the implementation of the spectral method on the steady-state bioheat transfer equation it is convenient to use complex Fourier series to efficiently handle the product of perfusion and temperature. The following definitions hold for temperature:

$$T = \sum_{-N/2}^{N/2-1} a_n e^{i\omega_n x} , \tag{2.40}$$

for perfusion:

$$c_b w = \sum_{-N/2}^{N/2-1} b_n e^{i\omega_n x} , \tag{2.41}$$

and for the specific power:

$$q = \sum_{-N/2}^{N/2-1} q_n e^{i\omega_n x} , \tag{2.42}$$

where ω_n is defined as $2n\pi/L_x$. These complex series are equivalent to standard Fourier sine and cosine series (Haberman 1983 or Ferziger 1981). Equations (2.40) through (2.42) can be substituted into equation (2.39) to obtain:

$$-k \sum_{-\frac{N}{2}}^{\frac{N}{2}-1} \omega_n^2 a_n e^{i\omega_n x} - \sum_{-\frac{N}{2}}^{\frac{N}{2}-1} \sum_{-\frac{N}{2}}^{\frac{N}{2}-1} a_n b_m e^{i(\omega_n + \omega_m)x} + \sum_{-\frac{N}{2}}^{\frac{N}{2}-1} q_n e^{i\omega_n x} = 0 . \tag{2.43}$$

Noting that $\omega_k = \omega_{k+j} + \omega_{-j}$ and dividing out the $e^{i\omega x}$ terms yields the following matrix equation:

$$Ma = q , \tag{2.44}$$

where the (i,j) entry of the matrix M ($M \in R^{NXN}$) is given by:

$$m_{i,j} = \begin{cases} 0 & \text{for} \quad i-j < -N/2 \\ b_{i-j+N+1} & \text{for} \quad -N/2 \le i-j < 0 \\ b_1 + k\omega^2_{i-N/2-1} & \text{for} \quad i-j = 0 \\ b_{i-j+1} & \text{for} \quad 0 < i-j \le N/2-1 \\ 0 & \text{for} \quad N/2-1 < i-j \end{cases} \tag{2.45}$$

and the vectors **a** and **q** (**a** and **q** ϵ R^{NX1}) are defined as:

$$\mathbf{a} = [a_{-N/2} \quad a_{-N/2+1} \cdots a_{N/2-1}]^T, \tag{2.46}$$

$$\mathbf{q} = [q_{-N/2} \quad q_{-N/2+1} \cdots q_{N/2-1}]^T. \tag{2.47}$$

Note that "T" denotes transpose. The elements of **M** and **q** are known; thus a linear equation solver can be used to obtain the vector **a** in equation (2.44). The method used for this work is Gaussian elimination with partial pivoting and the routine is from Yakowitz and Szidarovszky (1986).

Steady-state solution in three dimensions proceeds in a similar manner. The only difference is that the coefficient set is now triply-subscripted (a_{IJK} versus a_n). Thus, the matrix **M** is now N^3 X N^3 and the vectors **a** and **q** are now N^3 X 1. It is important to note that since the matrix **M** is N^3 X N^3, the solution of the linear system is very slow for large numbers of modes.

The transient and steady-state spectral method routines were verified by comparing their solutions to numerous analytical solutions. Different boundary and initial conditions were tested as well as different perfusion and power distributions. Verifications were done with test problems ranging in complexity from single perfusion-only decays to three-dimensional transient problems with conduction, perfusion and power. For the simple test problems, analytical solutions were obtained directly and for the complex test

problems, solutions were taken from Carslaw and Jaeger (1980) and modified to include perfusion. Properties, test problem lengths, perfusion and power magnitudes and distributions were all varied. The accuracy of the spectral method solution varied, depending upon the particular test problem and the implementation of the spectral technique. Typical midpoint errors for a three-dimensional verification with uniform perfusion and sinusoidal power were less than 0.01% at a time equal to one time constant. The spectral technique was always able to at least match the performance of an explicit routine and in many cases improved the execution time by several orders of magnitude.

CHAPTER 3

RESULTS

All of the adaptive control schemes discussed in Chapter 2 were tested on one-dimensional simulations of patient treatments. It was assumed that the treatment system contained a heating system capable of varying power in space and time. Following the one-dimensional simulations, the adaptive control scheme AD1 was tested experimentally. AD1 was selected for further testing because it was simplest in design and performed as well as the other adaptive schemes in the one-dimensional tests.

3.1 Basic Controller Parameters

Prior to using any of the adaptive routines, the Gaussian estimator parameters, the spectral method model parameters and the PID control algorithm parameters needed to be determined. These parameters, referred to as basic controller parameters, were determined in preliminary tests and were kept fixed for all subsequent investigations.

3.1.1 Estimator Parameters

In Clegg and Roemer (1985a) several different optimization methods are applied to the problem of estimating temperature fields during hyperthermia treatments. Their recommendation is that the

Gauss method is best because it converged fastest and was most robust (converged most often). This is the reason why the Gauss method was selected for both the perfusion estimation and the power optimization (where applicable). An improvement to the Gauss technique is to use Tikhonov regularization. Groetsch (1984) and Appendix C discuss this theory. Tikhonov regularization of order zero was used to improve the perfusion estimation but was not needed for the steady-state power optimization. Work is still in progress to determine a proper value for the regularization parameter since it has been found to depend on many variables including perfusion. In the present work a value of 10 was used. The Gauss technique requires a number of other parameters for its operation. These include the gradient step size used for calculating the Jacobian of the temperatures with respect to the perfusions, the convergence criteria used to determine when the estimates have converged, and the minimum and maximum values that bound the estimates. Table 3.1 summarizes the parameters used for the Gaussian estimation routines. Note that there are two ways for the estimation to converge: first, the measured and calculated temperatures at all measurement locations and at all times could agree using some preselected norm, in this case the Least-Square Error (LSE) defined as the square root of the sum of the squares of the differences between the measured and calculated temperatures at each location at each time divided by the total number of measurements; or second, the change in the estimates between iterations (ΔB) can become small. Thus there are

Table 3.1

Parameters for Estimation Routines

B	Gradient Step Size	Tikhonov Parameter	Convergence Criteria		B* Minimum	B* Maximum
			LSE on T	ΔB*		
$w_{Est.}$	0.1	10	0.01°C	0.001	-0.1	10
$q_{Est.}$	0.1	NA	0.10°C	1	0	10^6

*Units are: Perfusion estimation (kg/m^3-s)

Power estimation (W/m^3)

two convergence criteria listed in Table 3.1, LSE and ΔB respectively. The minimum and maximum perfusions are appropriate for the tissue types being considered and the minimum and maximum specific powers are appropriate for a typical hyperthermia heating system. The perfusion convergence criteria were selected from direct case tests, that is, tests where perfusions are predicted using data from a simulated treatment with no mismatch (boundary, regions or properties) between the estimator model and the treatment simulation model. The criteria were selected to achieve a good balance between the speed of convergence and the accuracy of the estimates. The convergence criteria for the power optimization were selected for speed of convergence. (Convergence was always by ΔB).

The perfusion estimation uses a transient technique in which the treated region is heated to steady-state, the power is turned off and the temperatures are allowed to decay for a specified length of time. The transient decay data are then used in the Gaussian estimation routine. To achieve an accurate estimation in a reasonable time period using transient data requires the determination of three more parameters: the length of time and the sample interval used to collect decay data (referred to as decay time and sample interval) and the amount of time to heat the treated region in order to achieve steady-state (referred to as update interval). Collecting too much transient data can cause the estimation to take too long, however, too little data causes the estimation to be inaccurate. Too small a sample interval or too long a decay will yield too much data; too large a sample interval or too short a decay will yield too little

data. Not allowing the temperatures to reach steady-state can lead to significant errors in the perfusion estimation because of the assumption of steady-state temperatures as an initial condition in the perfusion estimation routine.

Direct case tests were used to determine the best combinations of decay time and sample interval for the perfusion estimation. The treatment model contained 33 nodes with seven regions of perfusion. The simulated temperatures started from steady-state and were allowed to decay for different time lengths with data collected at various intervals. Table 3.2 describes the treatment model and the location of the modeled temperature sensors used to obtain the simulated transient data. The Gaussian estimation routine used a model with the exact regions and properties as the treatment model to estimate the perfusion distribution (Convergence criteria and all other parameters were as discussed above). The root mean square (RMS) error defined as:

$$\text{RMS Error} = \sqrt{\frac{1}{7}\sum_{i=1}^{7}\left(w_{i_{Est}} - w_{i_{Actual}}\right)^2}\ , \qquad (3.1)$$

was used as a measure of the accuracy of the estimation. Figure 3.1 has contours showing different values of the RMS error as a function of decay time length in minutes and sample interval in seconds. Figure 3.2 shows contours of the CPU time (seconds an a VAX 8600) required to complete the perfusion estimation as a function of decay time length in minutes and sample interval in seconds.

Table 3.2

Tumor Model for Decay Time/Sample Interval Study

Region	1	2	3	4	5	6	7
Perfusion	1	1	2	0	2	1	1
Nodes	1-4	5-9	10-14	15-19	20-24	25-29	30-33
Sensor Locations	3	7	12	17	22	27	31

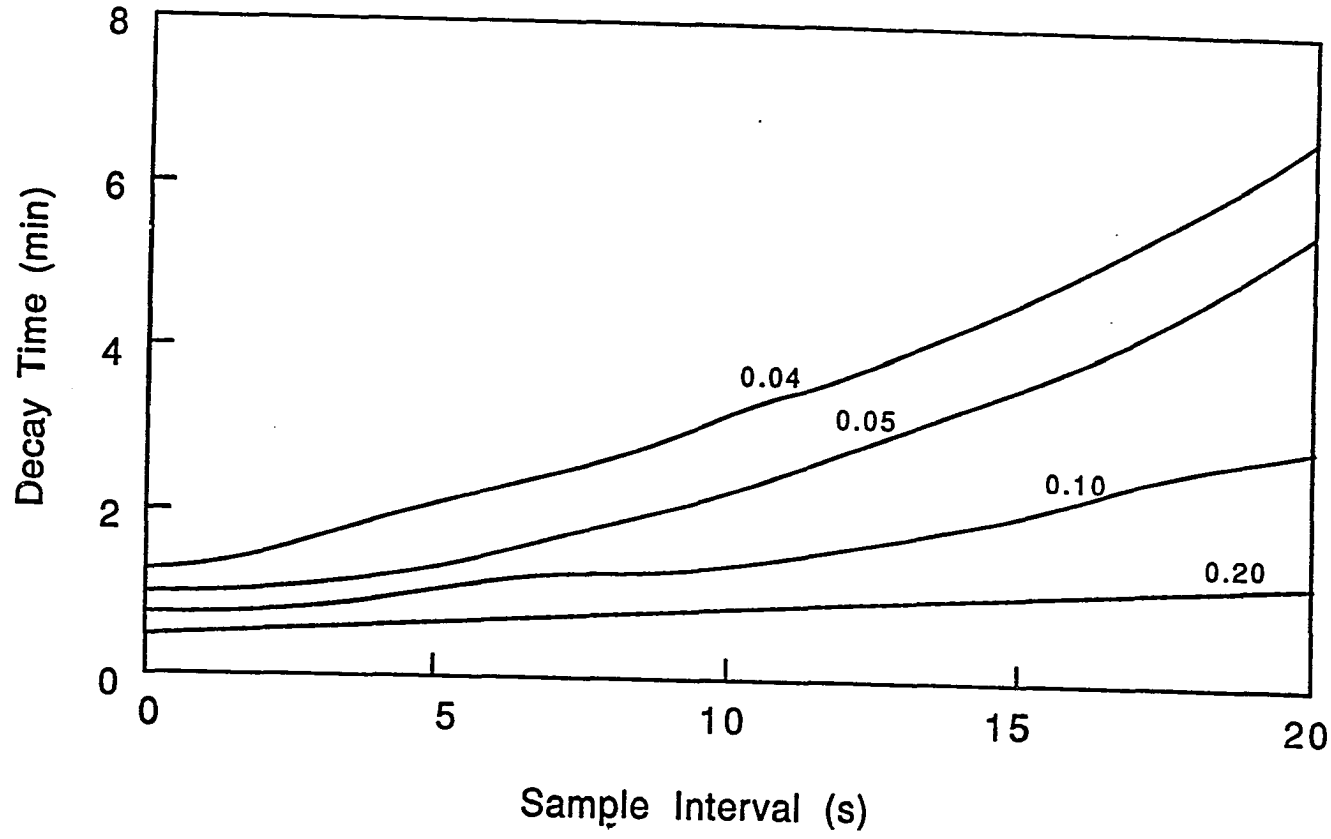

Figure 3.1. RMS Error in Perfusion Estimation as a Function of Decay Time and Sample Interval

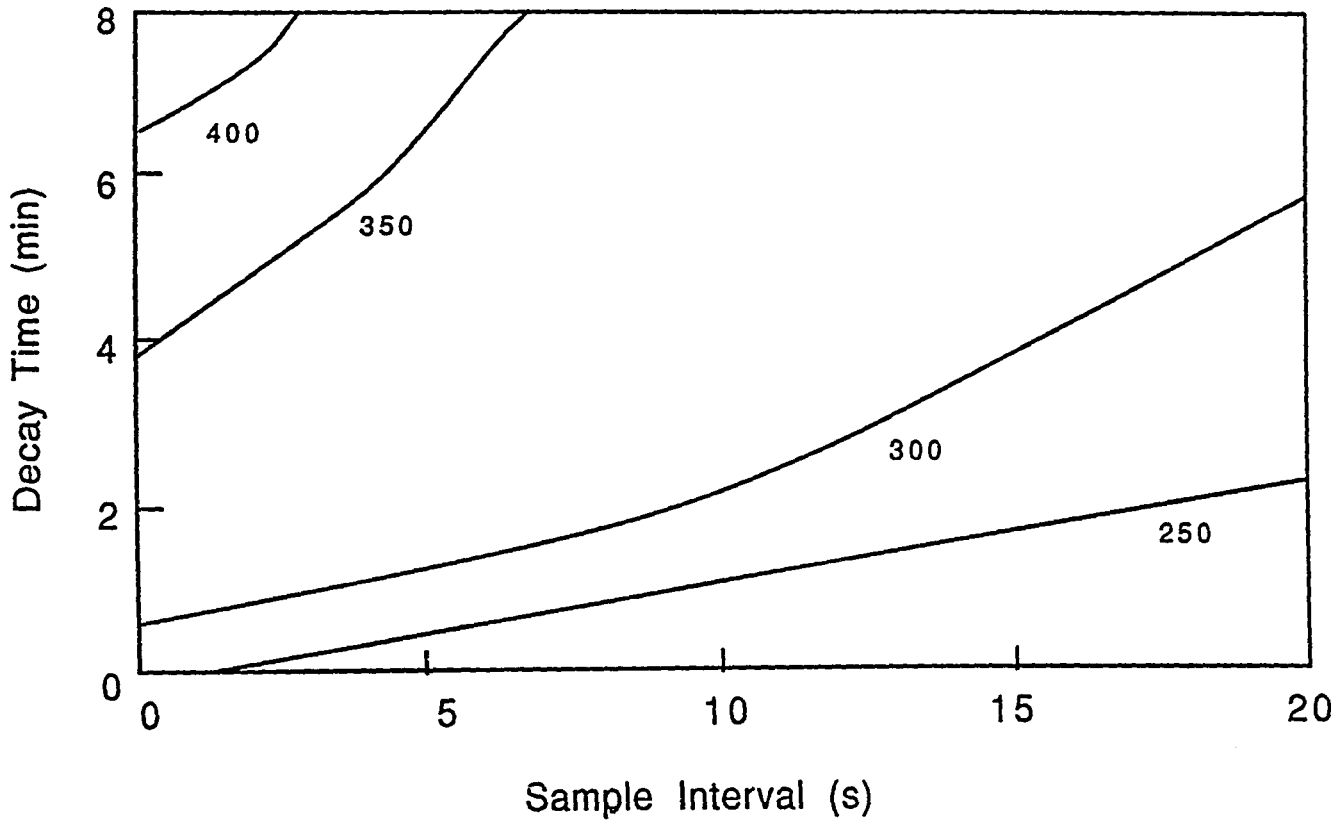

Figure 3.2 CPU Time (Seconds) Required to Complete Perfusion Estimation on VAX 8600 as a Function of Decay Time and Sample Interval

A decay time of 4 minutes and a sample interval of 15 seconds were selected for use in all of the adaptive control schemes.

Once the decay time and sample interval had been determined, the update interval was studied. In this case, the simulated temperature decay did not start from steady-state but rather from the temperature distribution obtained after the PID controller was operated for a fixed length of time (update interval). Figure 3.3 is a plot of the RMS error versus the update interval. An update interval of 5 minutes was selected for use in all of the adaptive control schemes.

The perfusion estimation routine must know the power delivered by the PID controller. The power varies at each control calculation (every 15 s) and in many cases it switches between zero and some power, thus it was important to determine how the average power delivered by the PID routine was to be calculated. Clearly, taking the most recent value could cause a significant error. By using direct case simulations and trying several averaging intervals, I found that averaging over the four most recent powers was best. In any case, it was imperative that an even number of powers be used in the calculation.

The decay time, sample interval, update interval and average time selected were by no means optimal values. They were simply values which worked well for the treatments simulated for this dissertation. Optimal values of these parameters are certainly a function of many variables such as the estimation routine, the

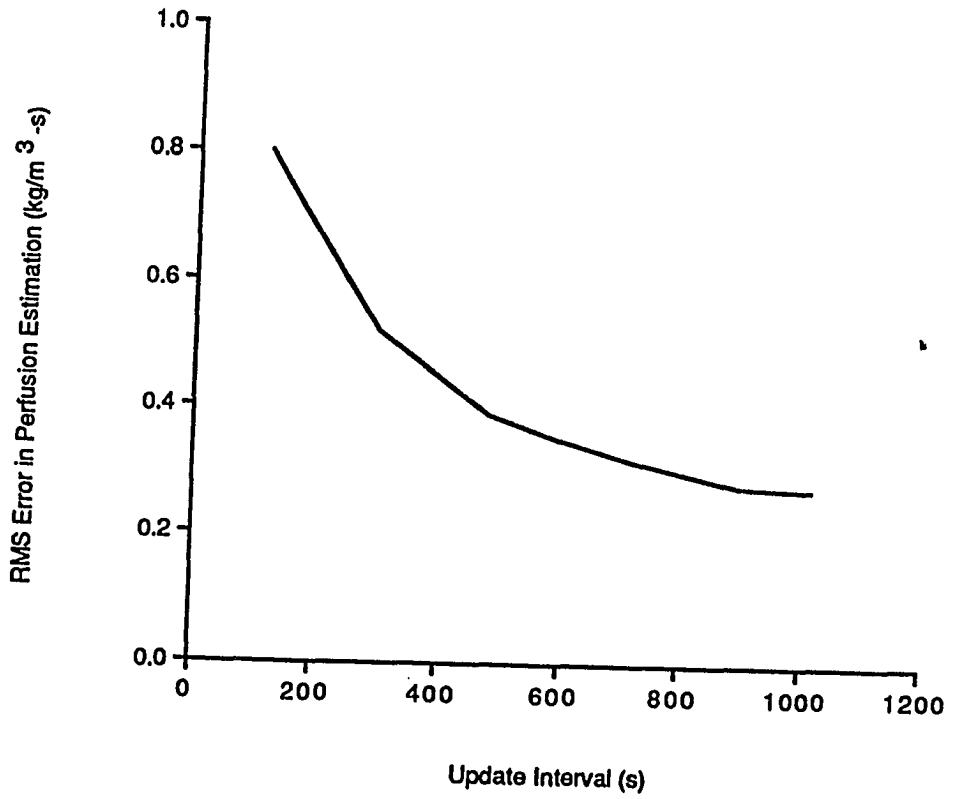

Figure 3.3. RMS Error in Perfusion Estimation versus Time of of Power-On Prior to Estimation (Update Interval).

treatment model, the solution technique, the modeled region size and properties, the actual treated region size and properties, and perfusion.

3.1.2 Model Parameters

All three adaptive routines employ a model of the treated region. Each of these models is based on the bioheat transfer equation and is solved by the spectral technique outlined in Chapter 2. There are several parameters that are associated with the physical model and the governing equation (2.1). Since tissues are comprised mostly of water, the values used for thermal conductivity, density, blood specific heat and tissue specific heat in the treatment models are selected to be equal to water properties. Thus, thermal conductivity is 0.583 W/m-°C, density is 1000 kg/m^3 and the specific heats are 4200 J/kg-°C. A length of 0.1 m was selected as reasonable for modeling hyperthermia treatments. This is sufficiently long to include most treatable tumors and is not so long that it would exceed the bounds of a normal sized patient. The number of nodes was selected to give a node spacing of approximately 3 mm. Typical probe spacing in experimental hyperthermia treatments is 10 mm. The number of Fourier modes was selected based on two criteria. First, it is important to be able to represent complicated temperature distributions by the Fourier expansion and the greater the number of modes, the better the representation, except at certain "pathological" points such as discontinuities (Haberman 1983, p. 75). Second, for an effective adaptive control

scheme the model must be capable of being solved quickly. A large number of modes makes the solution slow. If the spectral method model takes too long to solve the bioheat transfer equation, the treatment will be over before any adaptation can be done; however, if the estimates are too inaccurate, the adaptation is not effective. Consequently, a balance must be achieved between speed and accuracy. When results from the spectral method routine were compared to exact analytical solutions for the one-dimensional case, 32 modes were found to be sufficient to represent a typical parabolic temperature distribution that would be produced by uniform power with fixed arterial temperature at the boundaries. When results from the steady-state spectral method routine were compared to exact analytical solutions for the three-dimensional model, even 9 nodes in each direction were found to be inaccurate and took too much real time to solve. The time step (Δt) in equation (2.36) had to be selected to achieve a balance between speed and accuracy of the temperature solution. The time step also had to satisfy the stability criterion analogous to equation (2.37). One second met all of these constraints for the one-dimensional transient model.

3.1.3 PID Controller Parameters

The proportional, integral and derivative gain constants, K_P, K_I, and K_D, respectively, needed to be determined for the PID control algorithm used in all of the adaptive control schemes. The results of the theoretical study of Appendix D were used as an initial guide in determining the range of gains to study.

The PID controller was first studied with a computer model of a treatment based on the effective perfusion form of the bioheat transfer equation shown in Appendix D. For this study, the controller gains were varied as follows: K_P (10^4,10^5,10^6), K_I (10^3,10^4,10^5,10^6) and K_D (10^4,10^5,10^6). The values of effective perfusion used were (1,2,10,20 kg/m^3-s). The temperature started at arterial temperature (37 °C) and was controlled to 43 °C. The percent overshoot, the rise time and the 2% settling time were studied for all combinations of these parameters. The results indicated that $K_P = 10^6$, $K_I = 10^5$ and $K_D = 10^4$ were best at reducing rise time, settling time and percent overshoot. However, it was felt that a better model was needed to make a final decision.

Next, the PID controller was studied using a numerical model of the treatment based on the one-dimensional bioheat transfer equation. For this study, the proportional and derivative gains were varied over a wider range; K_P was varied from values of 10^5 to 10^9 and K_D from 10^3 to 10^7. The integral gain was kept relatively low compared to the proportional and derivative gains based on the results of the theoretical study presented in Appendix D. The integral gain was varied from 10^1 to 10^3. Blood perfusion was modeled as uniform throughout the entire treated region and was varied from 1 to 10 kg/m^3-s. The tumor was heated as one complete region and was considered to be the middle third of the 0.1 m modeled length. Besides studying the percent overshoot, the rise time and the 2% settling time, two other measures of the controller

performance were added: the time to the peak temperature and the steady-state error. When the parameter study was complete, the gains which minimized percent overshoot, rise time, 2% settling time, and steady-state error were selected. The values chosen were: $K_P = 5X10^6$, $K_I = 5X10^2$ and $K_D = 5X10^6$. The PID controller was also found to be quite insensitive to blood perfusion when these gains were used, as is shown in Table 3.3.

The sample interval for the PID routine was selected to be 15s based on the results presented in Johnson et al. (1987). This was found to be fast enough to give effective control.

3.2 One-Dimensional Results

All three adaptive control schemes were tested on one-dimensional spectral-method simulations of a patient being treated with a second generation hyperthermia heating system. In addition, the multiregion PID control scheme, whose integral-only version was described in Johnson (1987), was simulated, tested, and used as a bench mark for evaluating the performance of the adaptive routines. Table 3.4 summarizes the one-dimensional models used to test the control schemes. Each of the models has a "tumor" which has a necrotic core (perfusion equal to 0) and a highly perfused periphery surrounded by normal tissue (perfusion equal to 1).

Table 3.3

PID Controller Performance Criteria versus Perfusion

Perfusion (kg/m^3-s)	Percent Overshoot	Time to Peak (s)	Rise Time (s)	Settling Time (s)	Steady-State Error (°C)
1	0.1793	30	28	28	0.006970
5	0.3705	30	30	28	0.002311
10	0.7331	32	32	30	-0.002270

Table 3.4

Summary of One-Dimensional Tumor Models

Region		1	2	3	4	5
Nodes		1 → 9	10 → 14	15 → 19	20 → 24	25 → 33
Perfusion	LFNTPC	1	2	0	2	1
	LFNTPFT	$1(2-e^{-t/\tau})$	$2(2-e^{-t/\tau})$	0	$2(2-e^{-t/\tau})$	$1(2-e^{-t/\tau})$
	HFNTPC	1	5	0	5	1
	HFNTPFT	$1(2-e^{-t/\tau})$	$5(2-e^{-t/\tau})$	0	$5(2-e^{-t/\tau})$	$1(2-e^{-t/\tau})$

LFNT = Low Flow Necrotic Tumor
HFNT = High Flow Necrotic Tumor
PC = Perfusion Constant
PFT = Perfusion Function of Time
τ = Perfusion time constant (720 s)

All perfusions in (kg/m^3-s)

3.2.1 Integral Square Error for One-Dimensional Simulations

Temperature as a function of location and time for the controller AD1 controlling the LFNTPC model of Table 3.4 is shown in Figure 3.4. This is a typical temperature distribution during a simulated treatment. It would be difficult to compare controller performance with such a figure, thus the measure of controller performance used to compare the control schemes in order to determine which scheme was more effective was the Integral Square Error (ISE) defined by:

$$ISE = \sqrt{\frac{1}{\tau}\,\frac{1}{L}\int_{t=0}^{\tau}\int_{x=0}^{L}\left[\,T(x,t) - T_{Des}(x,t)\,\right]^2 dx\,dt}\,, \qquad (3.2)$$

where τ is the total treatment time and T_{Des} is the desired temperature distribution as a function of space and time. Note that the ISE has dimensions of °C and that it includes power-off time. For the discrete time and discrete space used in a simulated treatment, equation (3.2) becomes:

$$ISE = \sqrt{\frac{1}{N\tau}\,\frac{1}{N+1}\sum_{j=1}^{N\tau}\sum_{i=1}^{N+1}\left(T_i^j - T_{Des\ i}^j\right)^2}\,, \qquad (3.3)$$

where $N\tau$ is the number of time steps in a treatment, that is, $\tau = \Delta t(N\tau)$, N+1 is the total number of nodes in the model (N modes in the spectral approximation) and T_i^j is the temperature at location $i\Delta x$ (node i) at time $j\Delta t$. Consider a temperature distribution which differs from the desired temperature distribution by ϵ at all nodes at all times. The ISE for this case would be ϵ. In this case, if the ISE for controller 1 was η more than the ISE for controller 2 for the

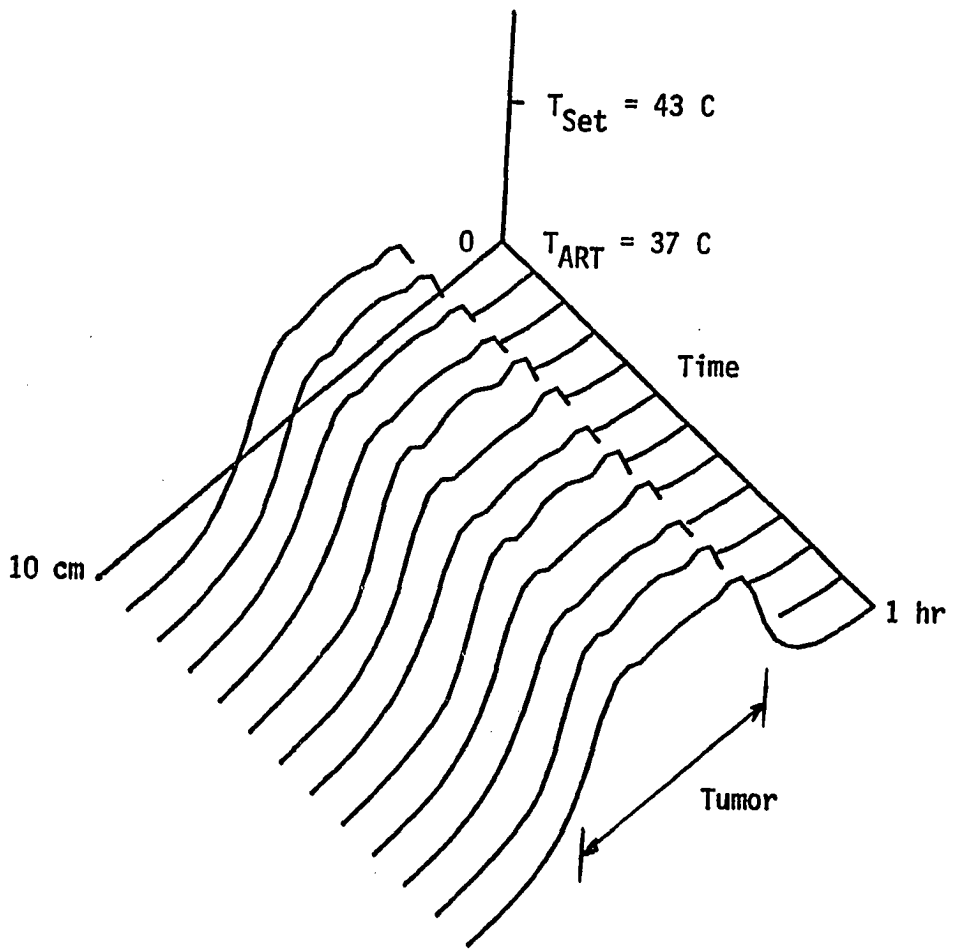

Figure 3.4. Temperature Contours for Simulated Treatment of Tumor Model LFNTPC with Adaptive Control Scheme AD1.

same test conditions, then controller 2 improved the control by η °C at all locations at all times. The ISE is a single number that can be used to quantify the performance of a particular controller for a given simulated treatment.

The first tests were done to examine different controller configurations for the PID and AD1 control schemes. The goal was to determine the effect of controller/model mismatch in perfusion regions and to determine if an adaptive control scheme could perform better than a standard PID scheme. The tumor boundaries were assumed to be known, supposedly from a priori information. The PID and AD1 controllers were tested on the treatment models of Table 3.4 with the controller power and perfusion region configurations shown in Figure 3.5. One hour treatments were simulated for all four models in Table 3.4 employing the PID and AD1 control schemes, using the controller parameters selected in the preliminary results. For each simulated treatment, the ISE (for PID and AD1) and the average CPU time to complete the estimation of perfusion and power (for AD1 on a VAX 8600) were determined as a function of controller configuration (Number of regions in the control model). Figure 3.6 compares the temperature profiles for the PID control scheme at steady-state to the AD1 control scheme before and after the perfusion estimation decay to the ideal desired temperature profile for 5 and 7 region controller configurations for the LFNTPC and HFNTPC tumor models.

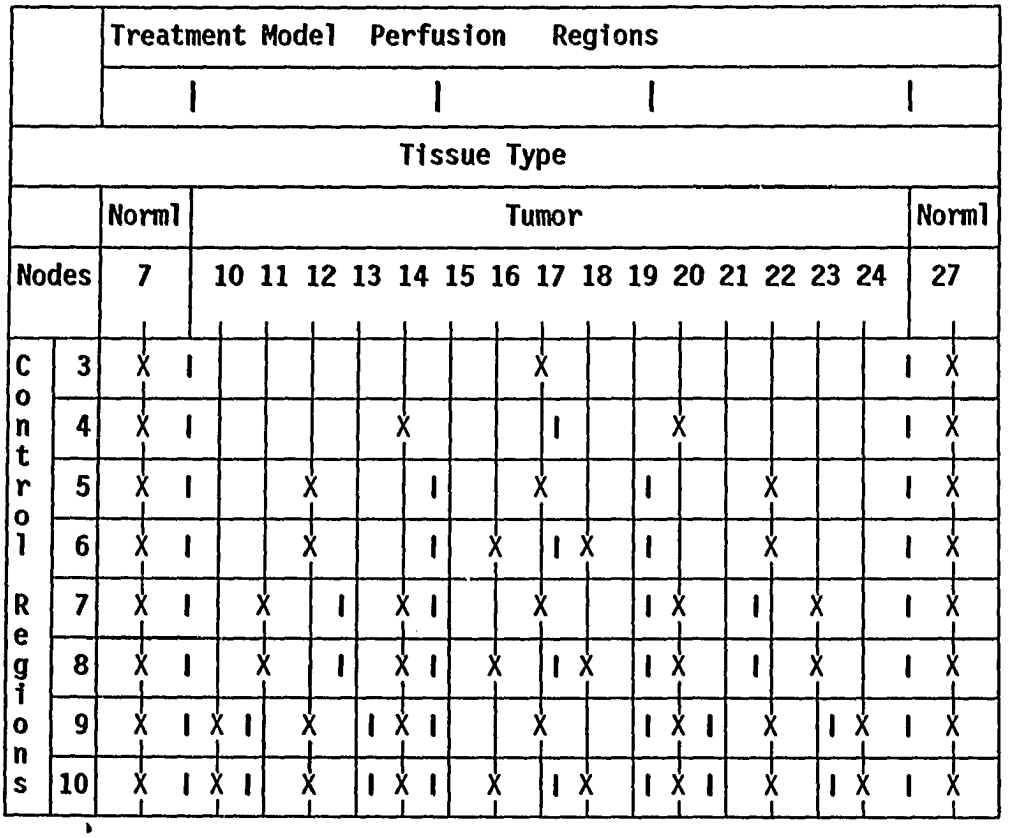

Legend

I Location of power region boundary (between nodes)

X Location of a simulated temperature sensor

All models have a total of 33 nodes.

Nodes not shown have no sensors or boundaries.

Figure 3.5. Control Model Power and Perfusion Regional Configurations for Tests of PID and AD1 Control Schemes.

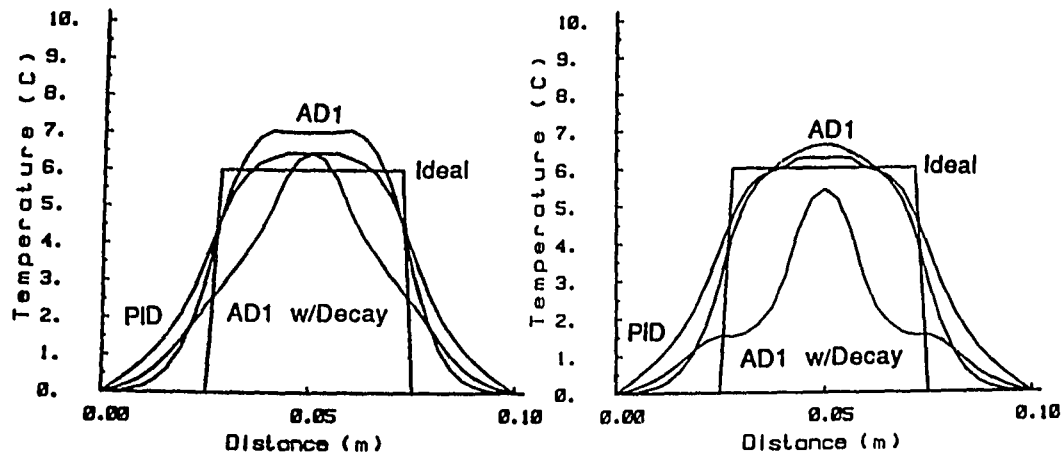

(a) LFNTPC 5 Regions

(c) HFNTPC 5 Regions

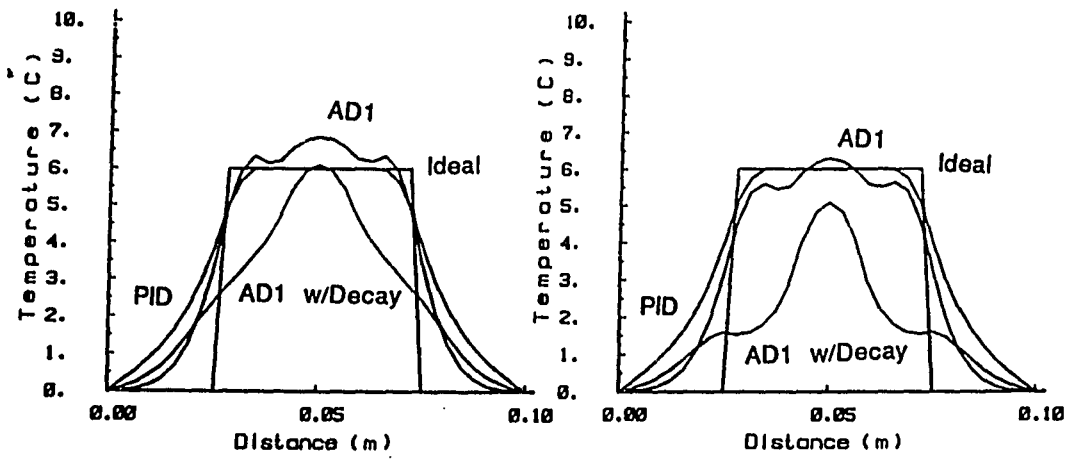

(b) LFNTPC 7 Regions

(d) HFNTPC 7 Regions

Figure 3.6. Temperature Profiles for PID and AD1 Control Schemes for LFNTPC and HFNTPC Tumor Models.

Figures 3.7 and 3.8 show the estimated perfusion and estimated power profiles, respectively, for the AD1 control scheme in 5 and 7 region configurations controlling the LFNTPC and HFNTPC tumor models. Figure 3.9 compares the PID and AD1 controller performance versus configuration for the LFNTPC tumor model. Figure 3.10 compares the performance of the AD1 control scheme versus controller configuration for the constant and variable perfusion tumor models LFNTPC and LFNTPFT. Figure 3.11 compares the performance of the AD1 control scheme versus controller configuration for the low-flow and high-flow tumor models LFNTPFT and HFNTPFT. These figures are examples of the variation of controller performance with respect to controller configuration. The other combinations of treatment models and control schemes exhibit similar trends. Table 3.5 compares the ISE versus controller configuration for all models for both control schemes. Note that Table 3.5 and Figures 3.9 through 3.11 have an ideal ISE indicated. This ideal was determined to be 0.48°C and was calculated by taking a 32 mode fast Fourier transform of the desired ideal temperature distributions. This is the best possible ISE that could have been obtained. Figure 3.12 shows the average CPU time required to complete the parameter estimation calculations for different controller configurations for the LFNTPC, the LFNTPFT and the HFNTPFT tumor models for control scheme AD1 (the PID scheme does not do any estimation). The HFNTPC model estimation times are similar to the LFNTPFT model values.

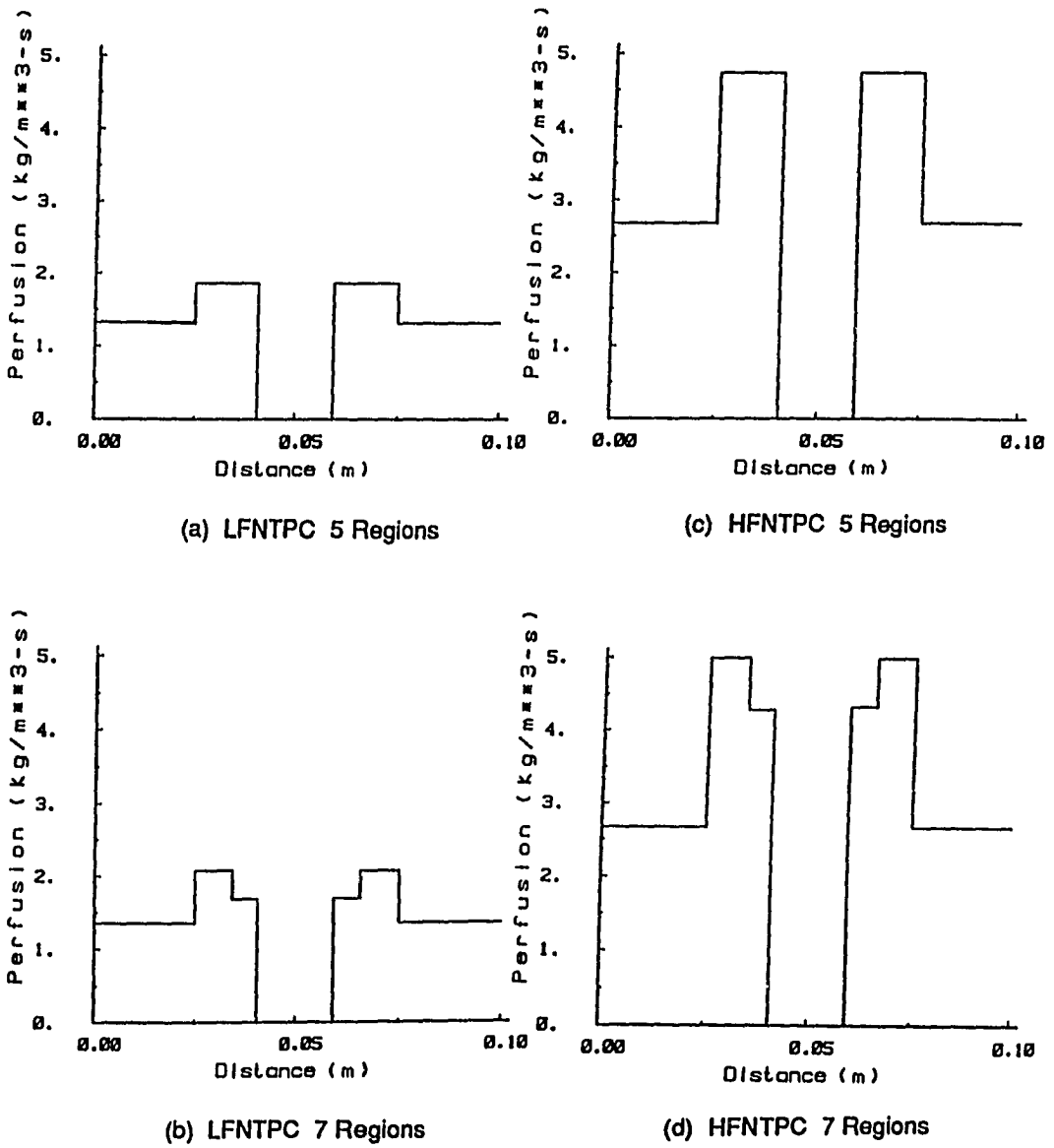

Figure 3.7. Estimated Perfusion Profiles for AD1 Control Scheme for LFNTPC and HFNTPC Tumor Models.

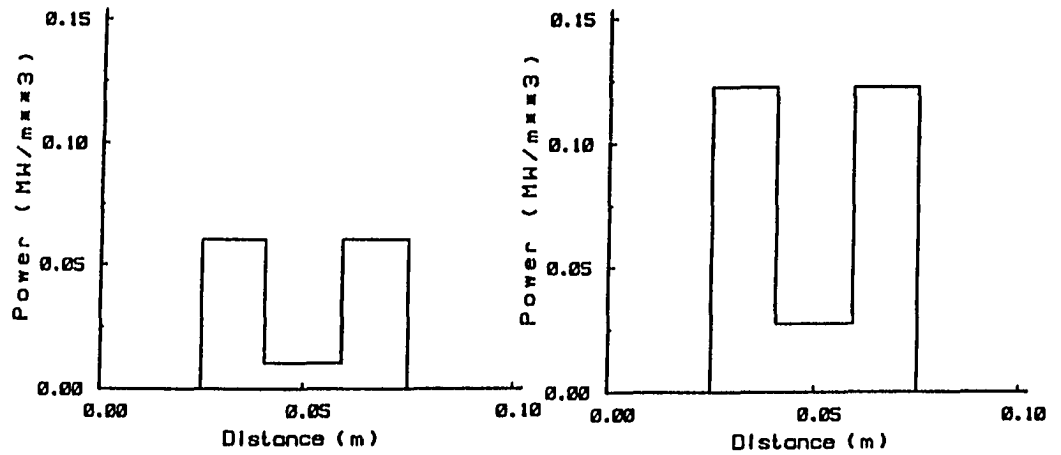

(a) LFNTPC 5 Regions

(c) HFNTPC 5 Regions

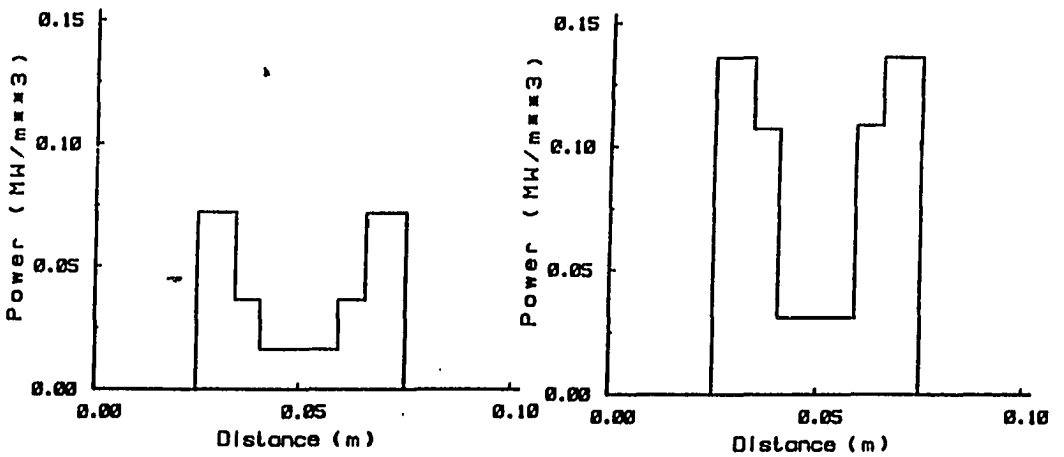

(b) LFNTPC 7 Regions

(d) HFNTPC 7 Regions

Figure 3.8. Estimated Power Profiles for AD1 Control Scheme for LFNTPC and HFNTPC Tumor Models.

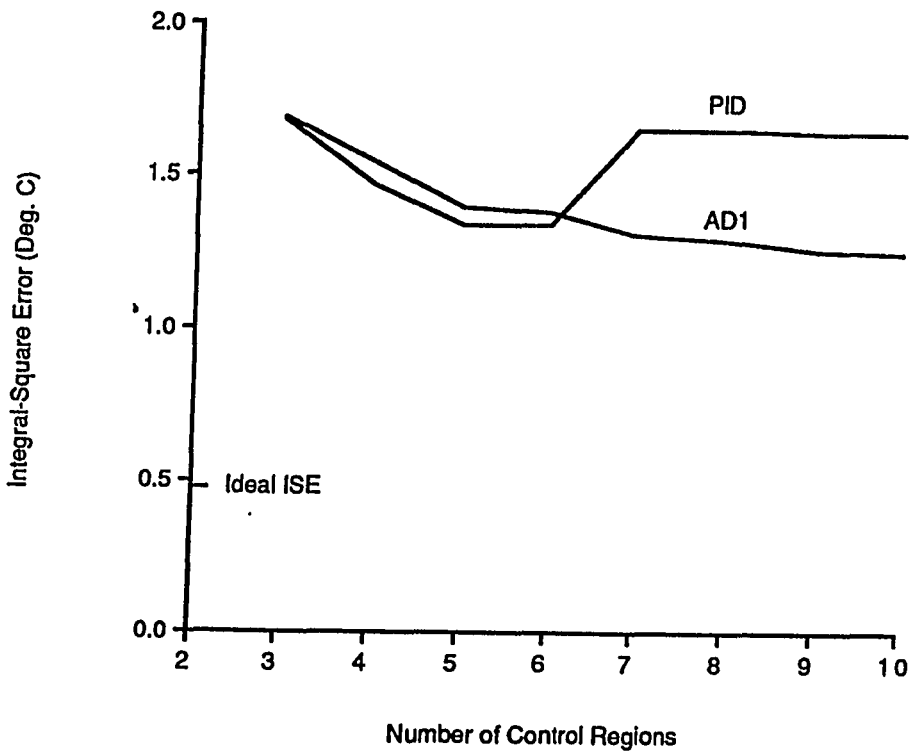

Figure 3.9. Comparison of Controller Performance for PID and AD1 Control Schemes for LFNTPC Tumor Model.

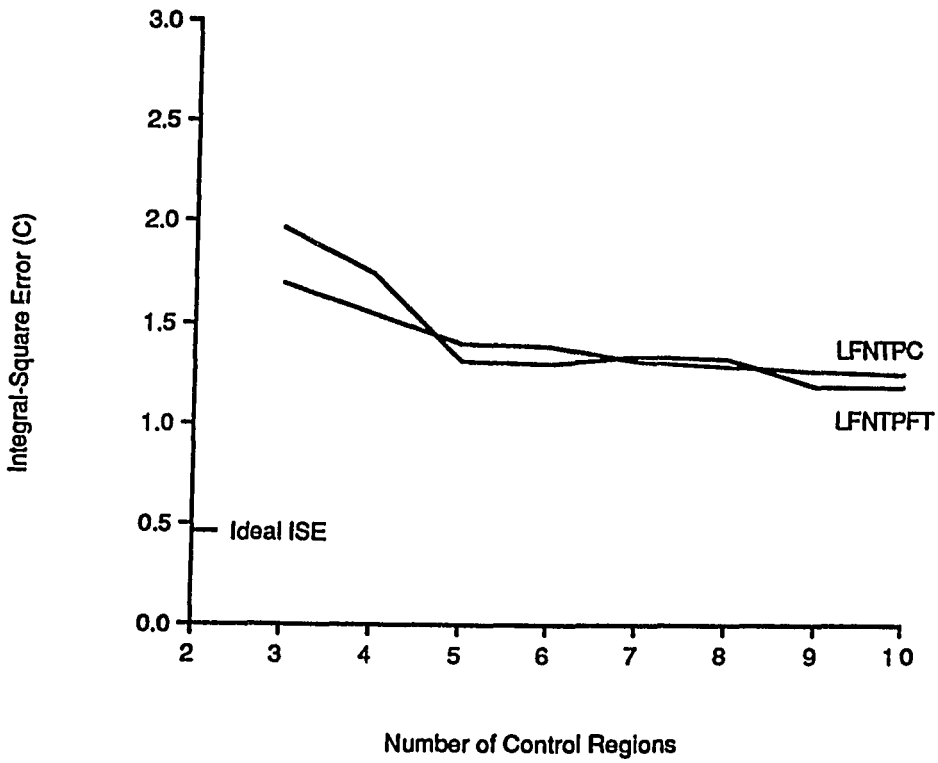

Figure 3.10. Comparison of Controller Performance for LFNTPC and LFNTPFT Tumor Models for AD1 Control Scheme.

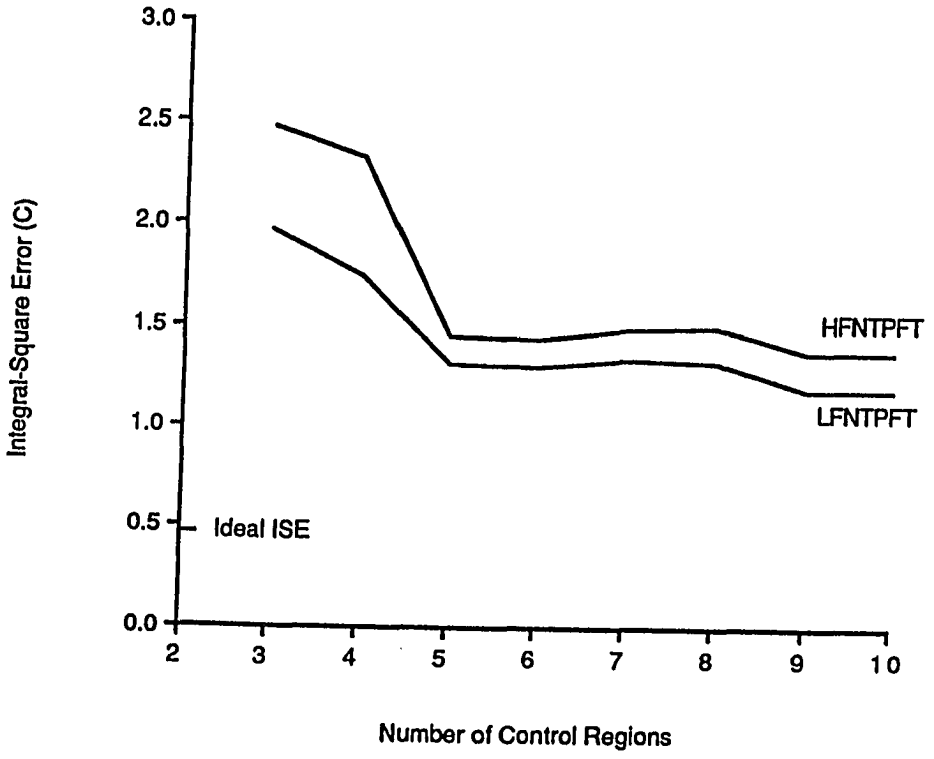

Figure 3.11. Comparison of Controller Performance for LFNTPFT and HFNTPFT Tumor Models for AD1 Control Scheme.

Table 3.5

Integral Square Error (°C) versus Number of Control Model Regions for Various Tumor Models using PID and AD1 Control Schemes

Model		LFNTPC		LFNTPFT		HFNTPC		HFNTPFT	
Controller		PID	AD1	PID	AD1	PID	AD1	PID	AD1
No. of Regions	3	1.687	1.697	1.936	1.969	2.102	2.173	2.399	2.478
	4	1.474	1.542	1.694	1.743	1.940	1.885	2.546	2.322
	5	1.338	1.395	1.166	1.310	1.366	1.449	1.195	1.442
	6	1.338	1.378	1.166	1.294	1.366	1.457	1.195	1.436
	7	1.649	1.307	1.428	1.333	1.637	1.407	1.410	1.484
	8	1.649	1.288	1.428	1.325	1.637	1.386	1.410	1.488
	9	1.648	1.257	1.428	1.188	1.636	1.284	1.412	1.367
	10	1.648	1.245	1.428	1.185	1.636	1.290	1.412	1.373

Notes: 1) Number of regions = number of sensors.

2) Ideal Integral Square Error calculated by a 32 mode Fast Fourier Transform of ideal temperature distribution is 0.48°C.

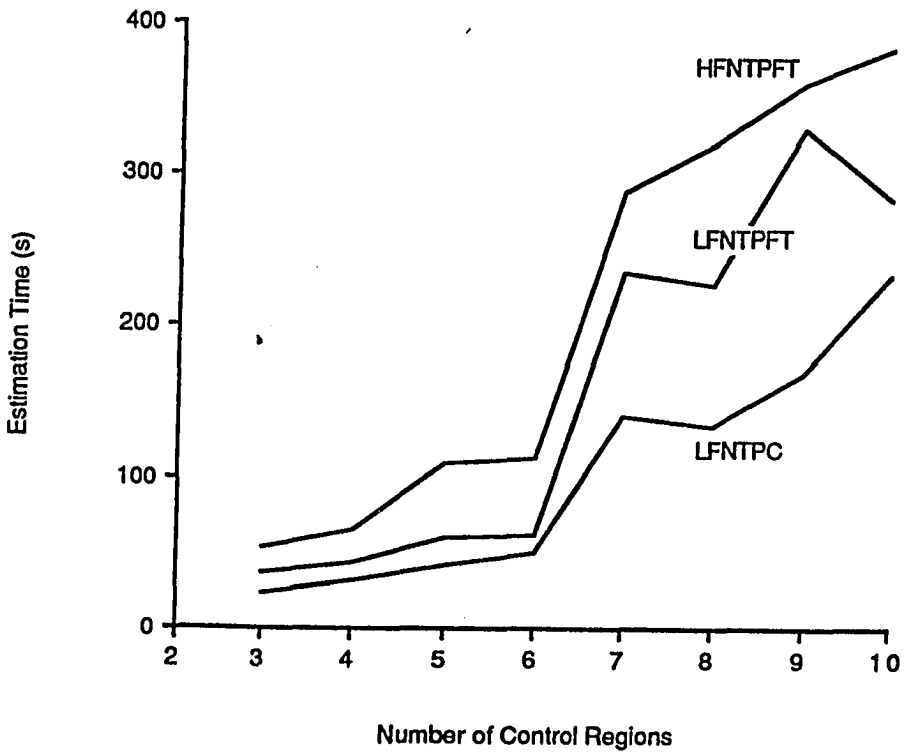

Figure 3.12. Comparison of CPU Time Required to Complete Both of the Parameter Estimations for LFNTPC, LFNTPFT and HFNTPFT Tumor Models for AD1 Control Scheme.

The second tests were done with the adaptive control schemes employing an observer (AD2 and AD3). For these tests, it was assumed that the treated region contained five temperature sensors and, as before, the tumor boundaries were known. With five simulated temperature sensors, the PID and AD1 schemes could have at most five control regions. The goal of these tests was to determine if the adaptive schemes AD2 and AD3 could improve the temperature control by using additional power regions in the controller. Control schemes AD2 and AD3 were tested for all four of the treatment models in Table 3.4 with the power region configurations shown in Figure 3.13. In all tests, five regions of perfusion were used in the control model. Only odd numbers of power regions were tested since the tests with the PID and AD1 schemes demonstrated that dividing the central power region made little or no difference in the controller performance. In addition, the three region controller configuration was not considered since five sensors were assumed to be available and it seemed imprudent to use a three region control scheme when a five region scheme was possible. Also eleven and thirteen region configurations were added for interest and because I felt that one might consider employing such a large controller configuration when an observer was used. Figures 3.14, 3.15 and 3.16 give examples of the variation of controller performance with respect to control scheme, treatment model and power region configuration for the AD2 and AD3 tests just as Figures 3.9, 3.10 and 3.11 did for the PID and AD1 tests.

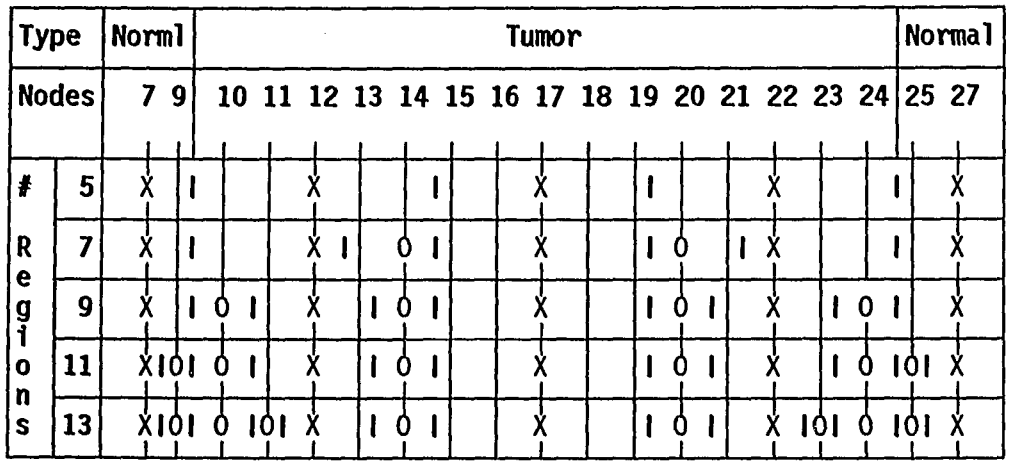

Legend

I Location of the boundary of the power region

X Location of a simulated temperature sensor

O Location of an observed temperature

All models have a total of 33 nodes.

Nodes not shown have no sensors or boundaries.

Figure 3.13. Control Model Power Regional Configurations for Tests of AD2 and AD3 Control Schemes.

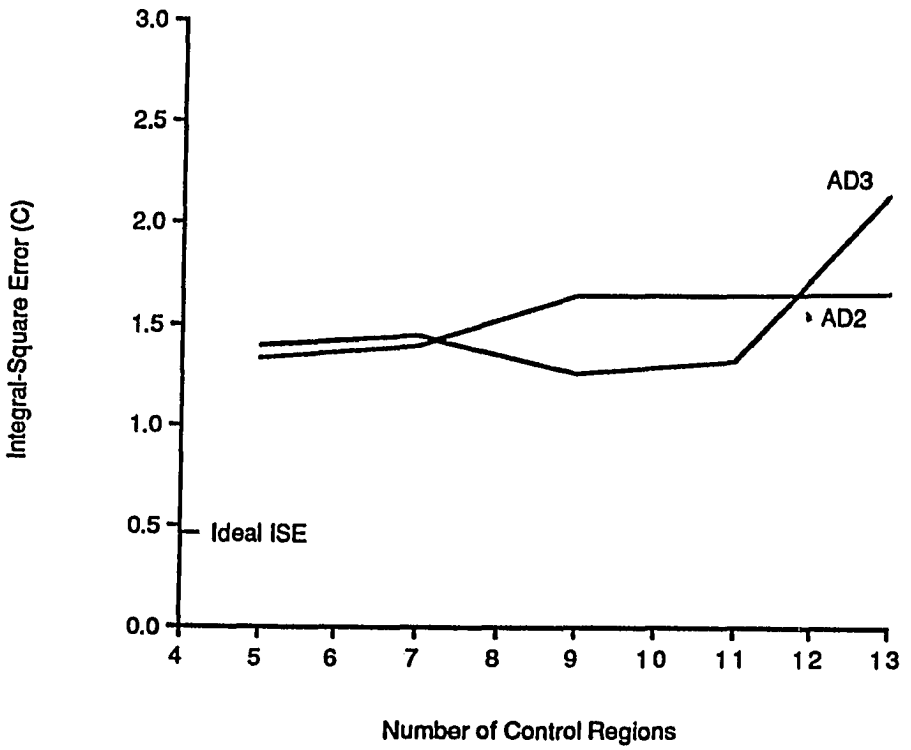

Figure 3.14. Comparison of Controller Performance for AD2 and AD3 Control Schemes for LFNTPC Tumor Model.

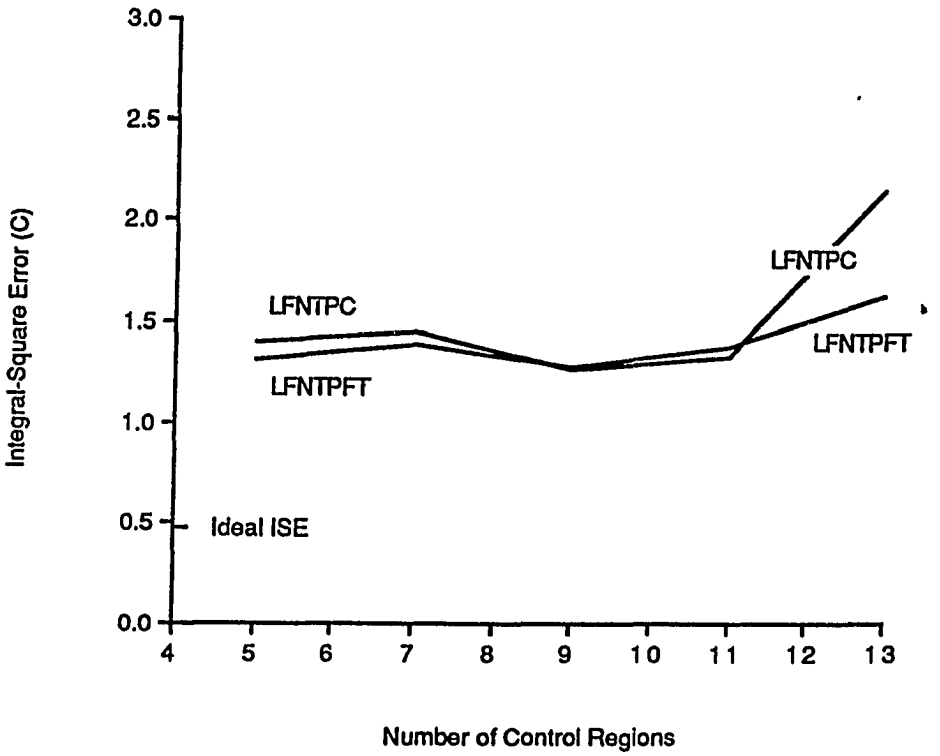

Figure 3.15. Comparison of Controller Performance for LFNTPC and LFNTPFT Tumor Models for AD3 Control Scheme.

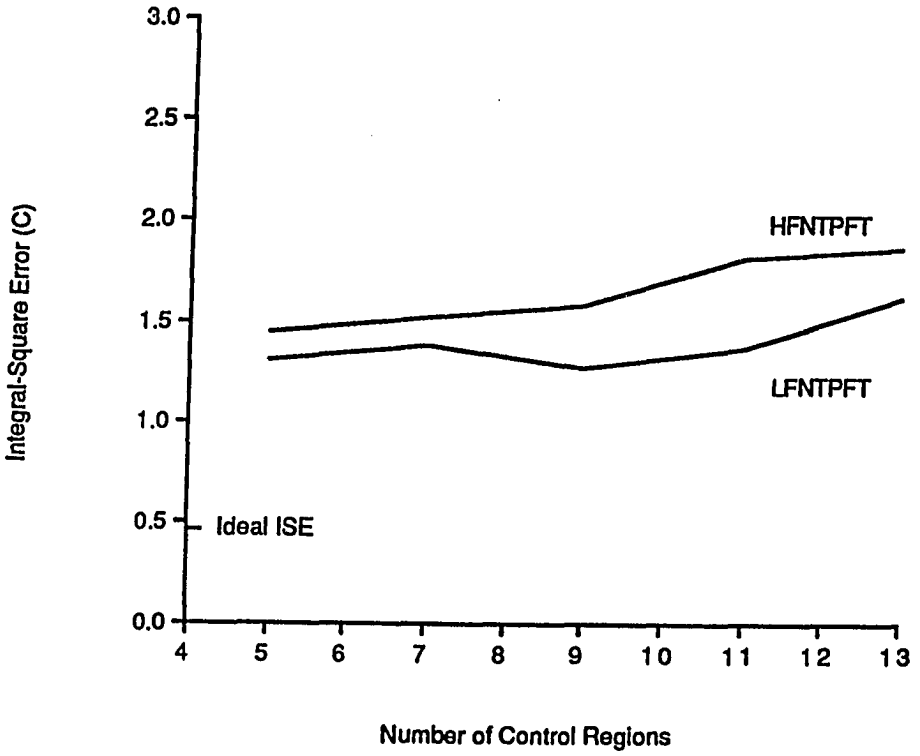

Figure 3.16. Comparison of Controller Performance for LFNTPFT and HFNTPFT Tumor Models for AD3 Control Scheme.

Table 3.6 contains the performance results of these tests for all the tumor models and for both control schemes. Table 3.7 compares the performance of all the control schemes for every tumor model. This table is based on a treatment model containing five simulated temperature sensors and shows the ISE and controller configuration which performed best and worst for each of the four models using the AD2 and AD3 adaptive control schemes. It also compares the performance of the AD2 and AD3 control schemes to the performance of the PID and AD1 control schemes when they are set in a five region configuration. Figure 3.17 compares the average CPU time required to complete the parameter estimation calculations for the AD2 and AD3 schemes versus power region configuration for the LFNTPC tumor model. Figures 3.18 and 3.19 compare the average CPU time required to complete the parameter estimation calculations for the AD2 and AD3 schemes, respectively, versus power region configuration for the LFNTPC, the LFNTPFT and HFNTPFT tumor models. The HFNTPC times are similar to the LFNTPFT times for both schemes.

3.2.2 Effect of Noise on Controller Operation

The next tests were done to determine if disturbances in the form of noise on the measured temperature signals would degrade the control schemes' performance. For these tests, noise was simulated by adding errors to the simulated temperature measurements. The error at each measurement was generated such that it was normally distributed with a zero mean and selected variance. The variances tested were 0 (no noise), 0.001, 0.005, 0.01, 0.05 and 0.1°C.

Table 3.6

Integral Square Error (°C) versus Number of Power Regions for Various Tumor Models using the AD2 and AD3 Control Schemes Employing Five Temperature Sensors

Model		LFNTPC		LFNTPFT		HFNTPC		HFNTPFT	
Controller		AD2	AD3	AD2	AD3	AD2	AD3	AD2	AD3
# Regions	5	1.338	1.395	1.166	1.310	1.366	1.449	1.195	1.442
	7	1.388	1.444	1.355	1.382	1.482	1.497	1.509	1.523
	9	1.646	1.262	1.444	1.264	1.747	1.418	1.607	1.577
	11	1.646	1.318	1.445	1.374	1.750	1.646	1.615	1.818
	13	1.653	2.143	1.485	1.616	1.730	1.689	1.633	1.872

Note: Since no temperatures are observed for five temperature sensors, AD2 with five regions is equivalent to the PID and AD3 with five regions is equivalent to AD1. (c.f. Table 3.5 with 5 regions.)

Table 3.7

Maximum and Minimum ISE (°C) and Number of Control Model Regions versus Controller Type for Various Treatment Models

Model			LFNTPC		LFNTPFT		HFNTPC		HFNTPFT	
Parameter			ISE (°C)	# Power Regions	ISE (°C)	# Power Regions	ISE (°C)	# Power Regions	ISE (°C)	# Power Regions
Controller		PID	1.338	5*	1.166	5*	1.366	5*	1.195	5*
		AD1	1.395	5*	1.310	5*	1.449	5*	1.442	5*
	AD2	Max. ISE	1.653	13	1.485	13	1.750	11	1.633	13
		Min. ISE	1.388	7	1.355	7	1.482	7	1.509	7
	AD3	Max. ISE	2.143	13	1.616	13	1.689	13	1.872	13
		Min. ISE	1.262	9	1.264	9	1.418	9	1.523	7

* By default the number of regions must be 5. The PID and AD1 schemes must have equal numbers of regions and measurement locations since they have no observer.

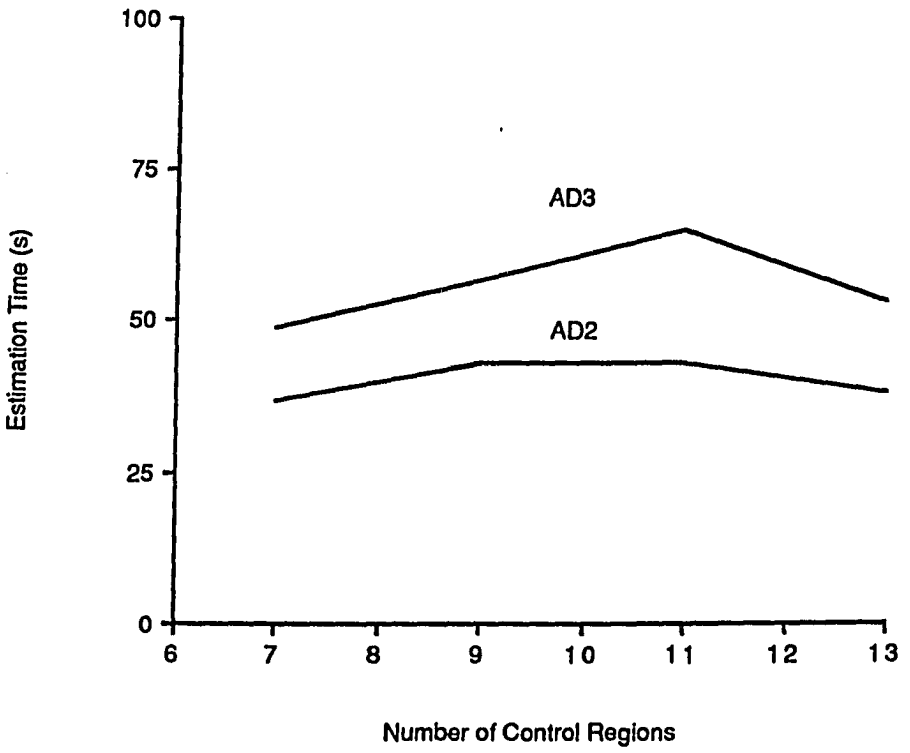

Figure 3.17. Comparison of CPU Time Required to Complete Both of the Parameter Estimations for AD2 and AD3 Control Schemes for LFNTPC Tumor Model.

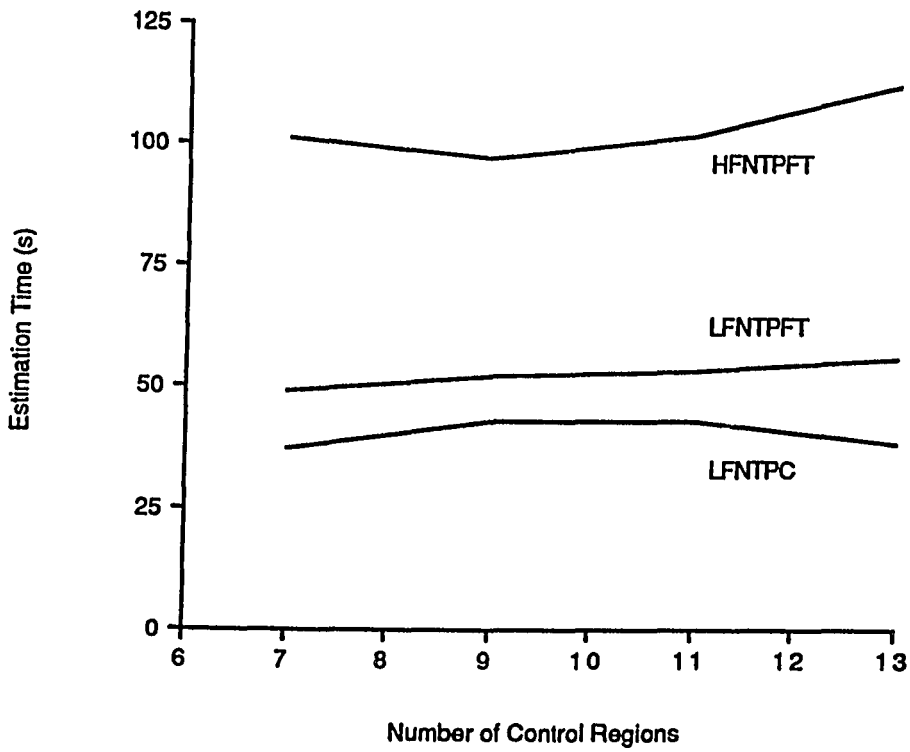

Figure 3.18. Comparison of CPU Time Required to Complete the Parameter Estimations for LFNTPC, LFNTPFT and HFNTPFT Tumor Models for AD2 Control Scheme.

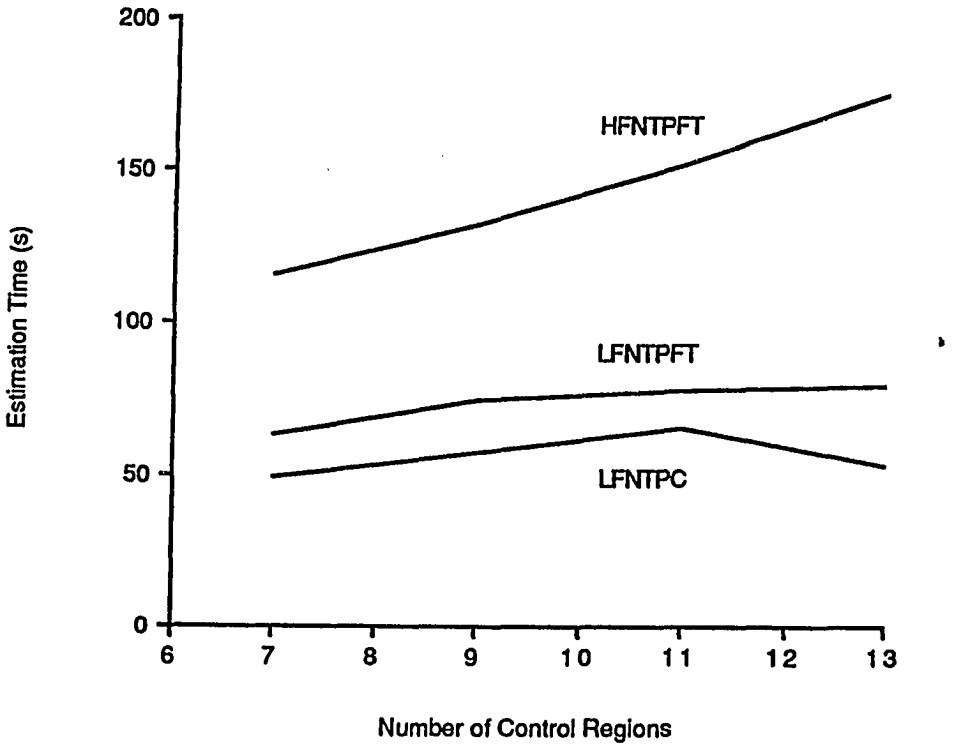

Figure 3.19. Comparison of CPU Time Required to Complete Both of the Parameter Estimations for LFNTPC, LFNTPFT and HFNTPFT Tumor Models for AD3 Control Scheme.

This accuracy is typical for a hyperthermia clinic. The method used to generate the errors is outlined in Abramowitz and Stegun (1970) on page 952. The particular algorithm used restricted the magnitude of the error to a range of three times the variance. The PID and AD1 schemes were used in a five region configuration and the AD2 and AD3 schemes used 5 perfusion regions and 7 power regions to control the LFNTPFT model of Table 3.4 with the six different noise levels added to the temperature measurements. The ISE and average estimation time (where applicable) were determined for each simulated treatment. For all tests, the addition of noise to the temperature measurements did not appreciably alter the control schemes' performance. (The ISE changed less than 1%.)

CHAPTER 4

DISCUSSION

The simulations of hyperthermia treatments employing the adaptive control schemes developed in this dissertation are by no means exhaustive but do indicate that the schemes are stable and are all capable of controlling the temperature field to a desired distribution with reasonable errors. The results indicate that an adaptive control scheme can be selected which will perform as well as or better than a standard PID for the model tumors tested. In addition, the results indicate that certain relationships exist between the performance of each adaptive control scheme and the control model configuration. These trends can be used as guidelines for developing new controller configurations.

4.1 Discussion of Basic Parameter Results

The preliminary tests to define the basic controller parameters produced predictable results. The square error versus decay time and sample interval contour plot results of Figure 3.1 indicate that as the amount of data increases, the perfusion estimation accuracy improves. The most accurate estimation should theoretically occur when the decay is longest (providing a measurable temperature signal

exists) and the sample interval is shortest, yielding the greatest amount of information. This is seen to be the case where the smallest value of the RMS error indicates the most accurate estimation of the perfusion. In actuality, because of errors resulting from added numerical computations required for larger data sets, the RMS error will increase when the sample interval becomes very small or the decay time becomes very large. As sample interval is increased for a fixed decay time, the RMS error increases again, indicating a less accurate estimation as expected. Also, as decay time is decreased for a fixed sample interval, the RMS error increases as expected.

The perfusion estimation time contour plot of Figure 3.2 follows expected trends. The greatest estimation time should be required for the largest data set. As stated above, this occurs for the longest decay and shortest sample interval. For a fixed decay time, increasing the sample interval decreases the data set size, thus decreasing the time required to complete the estimation. For a fixed sample interval, decreasing the decay time decreases the amount of data causing a corresponding decrease in estimation time. The decay time and sample interval values selected for use in the adaptive control routines (4 minutes and 15 seconds respectively) were chosen to provide an accuracy of approximately 5% and a new perfusion estimation in less than 5 minutes.

Figure 3.3 shows that the RMS error in the perfusion estimation decreases as the update interval (the time between successive estimations) increases. This is because when longer intervals are

used between estimations the temperature distribution is closer to steady-state when the new estimation begins. A developing temperature distribution in a hyperthermia treatment will have larger gradients throughout most of the treated volume than will a steady-state temperature distribution. Since the Gaussian estimation routine assumes that the decay starts from steady-state there will be an error introduced because of the incorrect initial condition. Heating for a longer period between estimations certainly reduces this error. A practical adaptive control scheme can not wait indefinitely for the temperature to equilibrate; in fact it might possibly never equilibrate because of the variation of perfusion with time in a treated subject. The update interval of 5 minutes was selected for the adaptive control schemes because, coupled with a 4 minute decay time and an expected estimation time of 5 minutes, it yields 3 or 4 adaptations during a one hour treatment. It was felt that this would be sufficient to provide reasonable perfusion estimations even during thermally induced perfusion increases such as those shown in Figure 2.2. In addition, the RMS error versus update interval curve ceased being linear after approximately 4 minutes and longer update intervals gave increasingly smaller improvements in the perfusion estimation accuracy because of the exponential approach to steady-state temperature.

The preliminary tests to define the basic controller parameters produced results which follow logical and predictable patterns. The results can thus aid the design of new controllers or the alteration of existing controllers. When changing the basic controller

parameters, certain guidelines must be followed. First, longer decay times and shorter sample intervals yield more accurate estimations, which require more CPU time, whereas shorter decay times and longer sample intervals give faster but less accurate estimations. A balance must be maintained between the desired accuracy and the time available for estimation. The time interval between estimations (update interval) must be long enough to allow the treated region to achieve a quasi-steady state. Again, a balance must be maintained between the number of adaptations (perfusion estimations) desired and the time available for heating between estimations. The sum of the decay time, the estimation time and the update interval must be small enough to allow for a few adaptations to take place during a typical treatment. Obviously, there is a practical limit to the number of adaptations, and, in addition, it is desirable to limit the number and lengths of the temperature decays to avoid lowering the temperature in the tumor below the toxic level. If the perfusion is anticipated to double during a typical treatment due to the patient's normal response, then three to four adaptations should suffice. This means that the sum of the decay time, the estimation time and the update interval should be below 20 minutes.

The treatment model and the associated model parameters are crucial to the operation of the adaptive controllers. The model is used numerous times by each estimation routine, therefore, any change in a model which alters its execution time will impact the adaptive control schemes' performance. If the treatment model is made slower

in any way, such as decreasing the time step or increasing the number of nodes, the resulting execution time increase could make the controllers inoperable, especially in the case of AD2 and AD3 where the treatment model is used as an observer. Any change in the model parameters must be made carefully and the impact of the change must be clearly defined.

The PID parameter studies yielded some useful information for establishing guidelines for potential changes in the controller gains. Changing the proportional gain had the strongest effect on the performance criteria (percent overshoot, time to the peak temperature, rise time, 2% settling time and steady-state error). Increasing the proportional gain increased the values of the performance criteria. Changing the derivative gain had the weakest effect on the performance criteria. Increasing the derivative gain tended to decrease the settling time; however, the effect of changing the derivative gain depended on the perfusion and is difficult to generalize. Changing the integral gain did little to most of the performance criteria with the exception of the steady-state error. Larger integral gains decreased the steady-state error as would be expected. The controller performance was not significantly altered by varying the perfusion from 1 to 10 kg/m^3-s. These trends apply only to the ranges of gains and perfusions studied and none should be extrapolated to untested values.

4.2 Discussion of One-Dimensional Simulations

The results of the one-dimensional simulated treatment studies showed that all the adaptive control algorithms worked in a qualitative sense. They were all able to control the tumor temperature to a therapeutic value while keeping the normal tissue near the safe arterial level. Figure 3.4 is an example of the good control provided by the schemes. It is clear that the performance of the adaptive schemes was not significantly degraded by the power-off decay periods necessary for the perfusion estimations.

The results of the one-dimensional treatment simulations show very clearly that the performance of any of the control algorithms is dependent upon the control model configuration relative to the treated region characteristics. Both the ISE and the average estimation time are strong functions of the number of control model regions and the particular simulated treatment. Low perfusion, high perfusion, both constant and variable, affected the controller performance.

The physical operation of the adaptive control routines can be described in four steps. First, each region is heated with power calculated by a PID scheme using a given set of set-point temperatures and temperature data from an actual sensor or observed temperatures from an observer. Second, the power is turned off and temperature is allowed to decay while data are collected from each sensor. Third, the perfusion is estimated using the decay data from each sensor and the average power from each region. Fourth, a new set of set-point temperatures is obtained by determining the power distribution

required to approximate a desired ideal temperature distribution considering the estimated perfusion field (AD1 and AD3 only). The cycle is then repeated.

Figures 3.6, 3.7 and 3.8 give a physical illustration of the operation of the adaptive controllers. Figure 3.6 shows temperature profiles that are very close to the desired ideal and that are symmetrical about the center point as expected. The temperatures for the AD1 scheme are lower in the normal tissue than the temperatures for the PID scheme for both the LFNTPC and HFNTPC models for both the 5 and 7 region configurations. The temperatures from the adaptive scheme AD1 were higher than those from the PID scheme over the entire tumor for the LFNTPC model and were higher only in the center of the tumor for the HFNTPC model. Thus the adaptive scheme AD1 is protecting the normal tissue better than the PID scheme. During the estimation decay, the temperature drops significantly, however, the ISE results (discussed later) indicate that this does not harm the overall performance. Seven power regions improve the steady-state profiles for both the AD1 scheme and the PID scheme. This figure also shows that AD1 is perturbing the set-point temperatures less than 1°C. Figure 3.7 shows perfusion estimates that are close to the actual perfusions. The estimates tend to be high in the normal tissue due to the adjacent highly perfused tumor tissues. The perfusion estimates do not change significantly after two estimations for any of the models or configurations. The seven region estimates are low adjacent to the necrotic core because of the lack of energy removal

due to the zero perfusion in the necrotic core. The fact that the perfusion estimations are in error is not disturbing when one realizes that the power estimation routine will provide a set-point temperature which is reasonably close to either 43°C or 37°C (depending upon the sensor location) regardless of the estimated perfusion. Figure 3.8 shows the estimated specific power corresponding to the estimated perfusions of Figure 3.7. As expected, the estimated power is highest in the regions of greatest estimated perfusion. Additionally, as expected, the estimated power is low in the necrotic core and zero in the normal tissue. The power estimates also do not change significantly after two estimations.

Referring to figures 3.9, 3.10 and 3.11 and Table 3.5 illustrates some general results concerning the differences between the PID and AD1 schemes. There always exists a controller configuration (number of power regions) which yields a best performance (minimum ISE). For the PID scheme, this was always a five region controller configuration corresponding to no boundary mismatch between the controller regions and the simulated treatment perfusion regions. For the adaptive control scheme AD1, the minimum ISE was always achieved with the largest number of control regions. This means that for the PID scheme to be most effective, it must be set up with little or no mismatch between its control region configuration and the perfusion regional structure. On the other hand, the adaptive control scheme AD1 did best when it was set up with the greatest number of control regions. A physician is likely to know the tumor

boundaries, the relative locations of major organs and tissues, and at best the locations of a few major arteries and veins. In almost all cases when a control model is established for an actual treatment there will not be exact agreement between the controller regions and the perfusion regions. For this reason alone, the adaptive scheme AD1 should tend to perform better than the PID. Table 3.5 shows that the adaptive control scheme AD1 could always be made into a configuration such that it performed as well as or better than the best performance of the PID routine. Table 3.5 also shows that because of symmetry, halving the central power region did not improve controller performance. (Compare the results for 5 and 6 or 7 and 8 regions for any model and controller.)

Figure 3.9 and Table 3.5 show an increase in the ISE of the PID control scheme when the number of regions is increased from 6 to 7. Since Figure 3.6 shows that the 7 region steady-state temperature profile is closer to the desired temperature distribution than the 5 region steady-state temperature profile, it must be concluded that the increase is due to the differences in the transient temperature profiles. The 7 region controller configuration has a power region in the tumor adjacent to the normal tissue which is controlled by a sensor placed closer to the normal tissue than in the 5 region configuration. As a result, the normal tissue will be warmed faster in the 7 region configuration since the power in the adjacent heated region will be larger due to the larger error signal resulting from the difference between the set-point temperature and the cooler sensor

temperature. Thus, the normal tissue spends a longer time at the elevated temperature, yielding a greater ISE.

In generating the results summarized in Table 3.5 it was found that adaptive controller configurations with small power regions adjacent to the tumor/normal tissue interface performed better than configurations using large regions extending into the simulated tumor tissue. The reason for the improved performance is that the important power variations occur near the tumor/normal tissue interface, as is indicated by Figure 3.8. Thus placing a small power region next to the interface allows the control scheme greater flexibility in varying the spatial power distribution between the tumor and normal tissue. The power can be gradually "stepped" from the center to the interface when numerous small regions are employed as opposed to the big change necessary when fewer large regions are used to span the entire tumor. Also, it was found that adding power regions in the normal tissue did not improve the controller performance because the optimal set-point temperature in these regions is, in almost all cases, 37 °C.

Controller performance was generally similar for variable or constant perfusion treatments. In particular instances, however, the control schemes performed better for the variable perfusion than for the constant perfusion. This is because the increasing perfusion in the normal tissue regions adjacent to the tumor helped to keep those regions cool. The control schemes performed much worse (higher ISE)

on the high perfusion models than on the low perfusion models for a small number of control regions.

The fact that the adaptive control scheme AD1 performs better than the PID scheme for constant perfusion models indicates that the adaptive control scheme is controlling the entire temperature field. If the perfusion does not vary, one might believe that an adaptive scheme is not necessary. However, AD1 optimizes the specific power distribution to yield the temperature distribution closest to the desired temperature distribution at all modeled locations at all times. Consequently, AD1 performs better than the PID scheme even when perfusion is constant with respect to time (cf. Table 3.5).

Turning now to the results of Figure 3.12 several general trends are evident. High flow simulations take longer for the parameter estimation than the low flow simulations. Variable perfusion simulations take longer for the parameter estimation than the constant perfusion simulations. In general, the average estimation times shown in Figure 3.12 are much shorter than the times shown in Figure 3.2. This is because the times in Figure 3.2 are for an estimation starting with an initial guess that is determined from fitting an exponential decay to the simulated temperature data. On the other hand, the average estimation times of Figure 3.12 include perfusion estimations which use the previous set of perfusions as an initial guess; consequently, convergence is much faster. This is also the reason that the variable perfusion simulations require more time for the parameter estimation. The initial guess in the perfusion

estimation is incorrect since the perfusion is varying with respect to time. (The perfusion estimation comprises anywhere from 80 to 95% of the total estimation time.)

Figures 3.14 through 3.19 and Table 3.6 show that, in general, the conclusions concerning the performance of the controllers for different simulations and different configurations, are the same for adaptive control schemes AD1, AD2 and AD3. That is, using the power optimization approach (AD3) improves the performance, the higher flow simulations are more difficult to control than the lower flow simulations and time-dependent perfusion is no more difficult to control than constant perfusion. Having a power region at every node or adding regions outside of the tumor did not improve the performance. Figure 3.17 shows that AD3 requires more time to estimate parameters than AD2. This is because the AD3 scheme also estimates the optimal specific power. The difference between the two curves is the time required to estimate the optimal specific power for the particular controller configuration. The average time to complete the parameter estimations is greater for the high-flow simulations than for the low-flow for both AD2 and AD3. Constant and variable flow estimation times are similar. Of course, control configurations with more regions required more estimation time.

Table 3.7 compares the performance of all the control schemes for a treatment which was assumed to have five temperature sensors. The best (minimum ISE) and worst (maximum ISE) configurations for AD2 and AD3 are compared to the PID and AD1 routines. The adaptive

schemes AD2 and AD3 can be configured such that they will perform as well as AD1 and maybe even slightly better, however, the improvement is only marginal. Since the particular configuration of the control schemes AD2 or AD3 which performs best is not consistent, it can not be predicted prior to a treatment. For this reason, one will not generally get better performance from control schemes AD2 and AD3 than from the AD1 scheme.

The results of the study where noise was added to the simulated temperature data indicate that the control schemes are all insensitive to the noise levels expected to be present in a typical hyperthermia clinic. Thus, any conclusions made from simulations done with no noise are applicable to a noisy environment. Certainly, larger noise levels could create problems so that any attempt to alleviate noise is important.

CHAPTER 5

CONCLUSIONS AND RECOMMENDATIONS

This dissertation details the development of three different adaptive control schemes for temperature control during hyperthermia treatments of cancer. These control schemes were developed with the particular heating system described in Hynynen et al. (1987) in mind, however, the approaches are applicable to any heating system with the ability to vary power as a function of location. The control schemes are not limited to application in hyperthermia treatments and, in fact, could be applied to any system with energy transport governed by an equation similar to the bioheat transfer equation.

5.1 Conclusions

The treatment simulations used in this study are by no means exhaustive. Many different simulations could be done to determine the characteristics of the adaptive control schemes and to determine the best control scheme for each tumor type. For example, treatment simulations including inhomogeneous tissues, randomly distributed perfusions and temperature dependent properties could be done. The controllers could also be tested on simulated treatments using models which include the heating system configuration and its interaction

with the tissue. Clearly, further experimental evaluation of the control schemes is necessary. Nonetheless, the simulations presented in this dissertation provide a basis for evaluating the different control schemes and illustrate some of the considerations that must precede the design of any control system for a second generation hyperthermia heating system.

Despite the limitations of the study, the conclusion can be made that the adaptive schemes can be made to perform better than the PID scheme for most simulated treatments even when perfusion is constant with respect to time. In the LFNTPC simulation, for example, using any configuration with more than 6 temperature sensors, the AD1 control scheme improved the performance of the PID scheme by an average of 0.4°C at all modeled locations at all times (See Table 3.5). This much improvement could be crucial to the success of a hyperthermia treatment. However, with some controller configurations in some simulated treatments, the adaptive control schemes performed only slightly better or even slightly worse than the PID scheme. In these instances nothing was lost by employing an adaptive control scheme because in no case did an adaptive control scheme perform significantly worse than the PID scheme. Since an adaptive control scheme performs at least as well as a PID scheme, and in many situations performs much better, and since the tumors encountered in a clinical situation are likely to encompass all ranges of perfusion distributions, it can be concluded that adaptive control schemes such as those developed herein would be superior to a standard PID scheme.

The decision to select an adaptive control scheme instead of a simpler PID scheme should be based upon many factors. Paramount among these should be consideration of the computer resources available. The model solutions and estimations necessary for the operation of these adaptive control schemes require a reasonably large computer. In addition, the skills required to implement these adaptive schemes are very different than those required to implement a standard PID scheme.

The three adaptive control schemes performed equally well in all the simulated treatments. The AD2 and AD3 schemes could generally be set in a configuration such that their performance was equal to the performance of the AD1 scheme. Adaptive control scheme AD1 is the simplest of the three schemes in both structure and implementation. Thus, unless different circumstances (such as a limited number of sensors) require otherwise, the AD1 scheme should be selected over the AD2 and AD3 schemes.

5.2 Recommendations

The adaptive control schemes designed in this dissertation could be improved. Some recommendations for future improvement follow. Using presently available technology, continuous functions, such as cubic splines and finite Fourier series, could be used to represent the spatial variation of the perfusion and specific power instead of the piecewise constant representation used in these implementations (smoothing techniques). With this change, the values of the coefficients in the continuous functions could be estimated instead of estimating the perfusion magnitudes in each region.

Besides providing a more realistic representation of the variation of the perfusion and specific power, representing the perfusion and specific power by continuous functions would improve the accuracy of the spectral simulations.

Using improved cost functions in the power optimizing routine is another presently available improvement. For example, the minimum tumor temperature and the maximum normal tissue temperature could be used to determine which power distribution is optimal. Another possibility would be to weight the errors according to location (see Appendix F), recognizing that some areas such as the tumor/normal tissue interface always have significant deviations from the ideal temperature distribution. Different cost functions might yield quite different relative performances for different controllers.

The latter two recommendations should be strongly considered before applying any of the adaptive control routines. Smoothing techniques would be a time-saving, accuracy-improving and presently implementable change. New cost functions must be tested before the adaptive routines are used. It is extremely important to determine what types of cost functions would yield the best performance.

For the future, new estimation routines could be developed. A routine could estimate the perfusion only one region at a time, thus the adaptation could continually proceed from region to region. In addition, several such routines could be implemented on a parallel processor and the perfusion in each region could be estimated simultaneously. This implementation could potentially yield much

faster estimations. Faster parameter estimation would also improve the control schemes' performance. More parameters such as thermal conductivity, surface heat transfer coefficient or arterial temperature could also be included in an advanced estimation routine.

A very desirable but difficult improvement would be to utilize the optimal specific power distribution as other than an intermediate value used to generate new set-point temperatures. If the power delivered by the heating system could be compared to the estimated optimal specific power, then the adaptation could be done on an "as-required" basis. That is, when the actual power being delivered by the heating system is no longer in agreement with the estimated optimal specific power distribution, then the control scheme could interpret this as an indication that perfusion has changed and that an adaptation is required. The control scheme would then be avoiding unnecessary temperature decays to estimate perfusion. It might eventually be possible to eliminate the PID portion of the adaptive control schemes altogether and simply allow the heating system to use the estimated optimal specific power distribution. This would greatly simplify the implementation of the control schemes by eliminating many temperature sensors; however, the adaptation on an "as required" basis could not be done. Two major developments must be made before this is possible. First, there must be a very good model of the treated region in order for the predicted temperature distribution to be a good indicator of the actual temperature distribution in the patient. If the model is bad, then the estimated optimal specific power

distribution is in error. Second, some way of relating the specific power calculated by the model to the specific power deposited in the treated tissue by the heating system must be developed. In general it is easy to measure (or calculate) the power (in W) delivered by the heating system, however, a model of the absorption of sound in the treated region is generally required to determine the specific power (in W/m^3) deposited in the tissue especially at unmonitored locations. Of course other instrumentation could be used to measure specific power but requiring these instruments would eliminate the advantage of a reduced number of temperature sensors. Finally, new adaptive control schemes could be developed which employ totally different approaches to the problem of control of the complete temperature field during a hyperthermia treatment.

APPENDIX A

EXPERIMENTAL INVESTIGATIONS

A.1 Kidney Model Perfused Phantom

Experimental conditions are difficult to control in vivo; consequently, the idea of employing a perfused phantom for evaluation of a thermal-biological system is very appealing. In Chapter 1, a perfused phantom was defined as a test device consisting of an appropriate absorbing medium with embedded tubes to simulate blood vessels. One advantage of a perfused phantom is that base temperature and perfusion could be controlled as desired. Attempts have been made to develop artificial perfused tissue phantoms using networks of tubes to represent arteries and veins such as the design presented in Baish, Foster and Ayyaswamy (1986). These have had limited success because they are difficult to make and because they do not do an adequate job of modeling the vasculature of an actual tissue. A more accurate phantom would have vasculature with dimensions and arrangement similar to those of actual tissue and with thermal properties that agree with those of actual tissue. One method of achieving this goal is to attach a surgically isolated organ to a perfusion apparatus. Valvano et al. (1984) used a freshly excised rat liver. Holmes et al. (1984) used an alcohol fixated kidney. Because the perfusion field in a

kidney varies significantly with position, because a kidney has a single supply artery, and because the fixated kidney can be stored and reused repeatedly, it was selected as the perfused tissue phantom for use in evaluating the proposed algorithms.

To use the perfused kidney model to evaluate the control algorithms, the apparatus of Figure A.1 was constructed. It consists of the following major elements: 1) a large water bath to simulate tissue; 2) a heat exchange system to maintain the bath temperature at 37 °C (not always used); 3) a variable-flow peristaltic pump to simulate blood perfusion; 4) a degasser for degassing the water bath; 5) a pressure and flow monitor for the perfusate (marked "P" and "F" in Figure A.1); and 6) a data acquisition system. Because degassed water is used, no bubble trap is necessary. Total blood flow to the kidney is measured with a graduated container and a stop watch. The kidney represents the treated region with perfusion varying as a function of position and the surrounding bath represents untreated tissue at arterial temperature. The entire unit, like a patient, can be placed on the scanned focused ultrasonic hyperthermia treatment system described in Hynynen et al. (1987) and used as a phantom with a treated region having total blood perfusion that can be controlled and measured. This phantom system has been used in previous control experiments in Johnson et al. (1987) and was very successful.

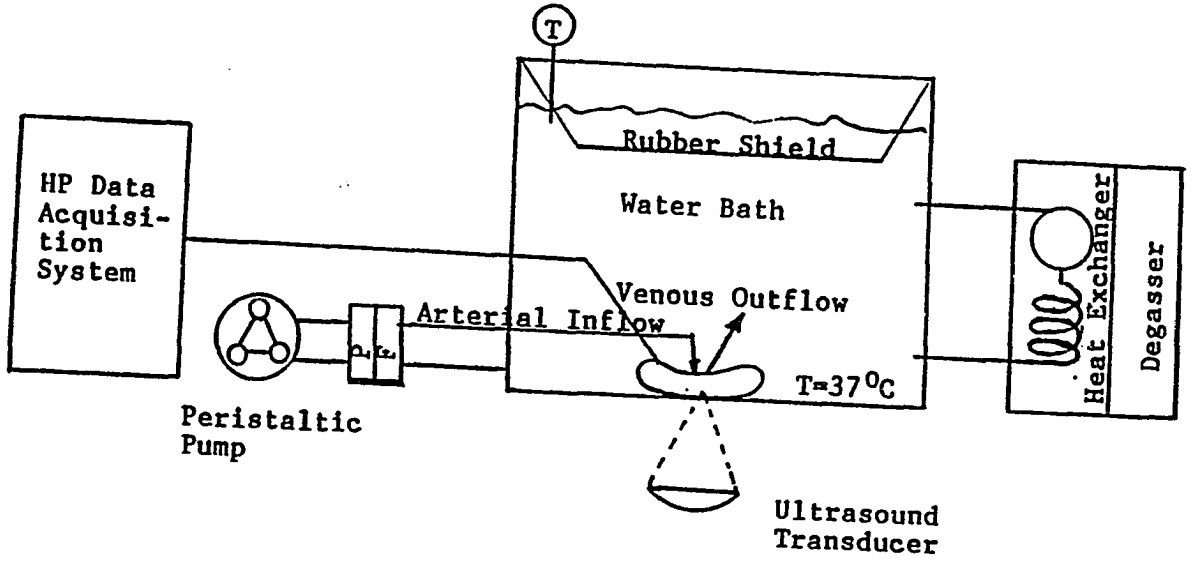

Figure A.1. Schematic of Kidney Model Perfused Phantom System

The preservation method of Holmes et al. (1984) consists of the following steps.

1) Purge the vasculature by perfusing with a saline plus 4% mannitol solution for 15 to 30 minutes.
2) Continue perfusing with 50% ethanol and water solution until the vasculature resistance lowers significantly. This usually takes about 30 minutes.
3) Leave the organ in 50% ethanol/water solution for 4 to 6 hours.
4) Perfuse the organ for 15 to 45 minutes with 80% ethanol/water solution.
5) Store the organ in 80% ethanol/water solution.

To use a previously preserved organ, the rehydration procedure is as follows.

1) Place the organ in 50% ethanol/water solution for 8 to 10 hours.
2) Place the organ in water for 8 to 10 hours.

To restore a rehydrated organ, repeat steps 2) through 5). In the above procedures, all solutions are mixed by weight and must be degassed to prevent filling the organ with gas. The perfusate pressure must always be kept below 120 mm Hg. To preserve a 60 g dog kidney, approximately 0.5 liter of each of the solutions was required for each of the perfusion steps.

The kidney model has some disadvantages which need to be noted. The organs can not be preserved indefinitely. With experiments in this dissertation and in Johnson et al. (1987), no kidney older than

one year was used. The vasculature may not remain intact and thus the perfusion field may not be as expected, however, it does vary with respect to position. The kidney is limited in size and the ultrasonic absorption is not good after preservation.

Regardless of the disadvantages enumerated above, the kidney model still proved useful. From several experiments the following additional comments can be made regarding the kidney model. The fluid in the box only needs to be degassed at the onset of the experiment. That is, continuous degassing is not necessary even for experiments lasting up to 24 hours, if the box is well sealed. Numerous thermocouple probes can be inserted into the kidney, however, catheters only slightly larger than the probes should be used. Probes fitting loosely into the organ create perfusion shunts and act as large "blood vessels" where most of the organ perfusion goes. Kidneys can be successfully represerved and rehydrated for several experiments.

A.2 Experimental Results

A limited number of experiments was performed utilizing the kidney model perfused phantom described earlier as a "patient" and the scanned focused ultrasonic treatment system described in Hynynen et al. (1987). The treatment system contains only a small microcomputer used for data acquisition, the memory of which is far too limited to be used for obtaining solutions of the bioheat transfer equation required for the estimation of perfusion and temperatures. In addition, the treatment system has no communications link to

the VAX 8600 used for the parameter estimations. Consequently, control schemes AD2 and AD3 could not be tested experimentally. However, since their performance was not a significant improvement over that of AD1, comparing only AD1 to the PID scheme should suffice.

Figure A.2 is a schematic illustration of a typical experiment. For this experiment, a 66 gram dog kidney was attached to the kidney model perfusion apparatus. Five seven-sensor thermocouple probes were inserted in the scan plane as shown. One centimeter separated the sensors on a given probe and one centimeter separated the probes. One seven-sensor probe was inserted vertically at the scan path in order to measure the temperature distribution along the sound transmission axis. The scan paths used are the two octagons shown. The outer (larger) octagon was traversed twice for every traverse of the inner (smaller) one. A nine region controller was established dividing the scan paths as shown in Figure A.3. The temperature sensor closest to the scan path in a given region was used to control the power delivered to that region as described in Chapter 2 and in Johnson (1987). In a normal kidney, the perfusion on the periphery is larger than the perfusion in the center. During the setup for this experiment, the two probes numbered 1 and 5 were inserted using large diameter catheters. Because the preserved kidney tissue is not as resilient as fresh kidney tissue, probes 1 and 5 did not fit snugly into the holes made by the large catheters. Consequently, the perfusate tended to stream out of the holes along probes 1 and 5.

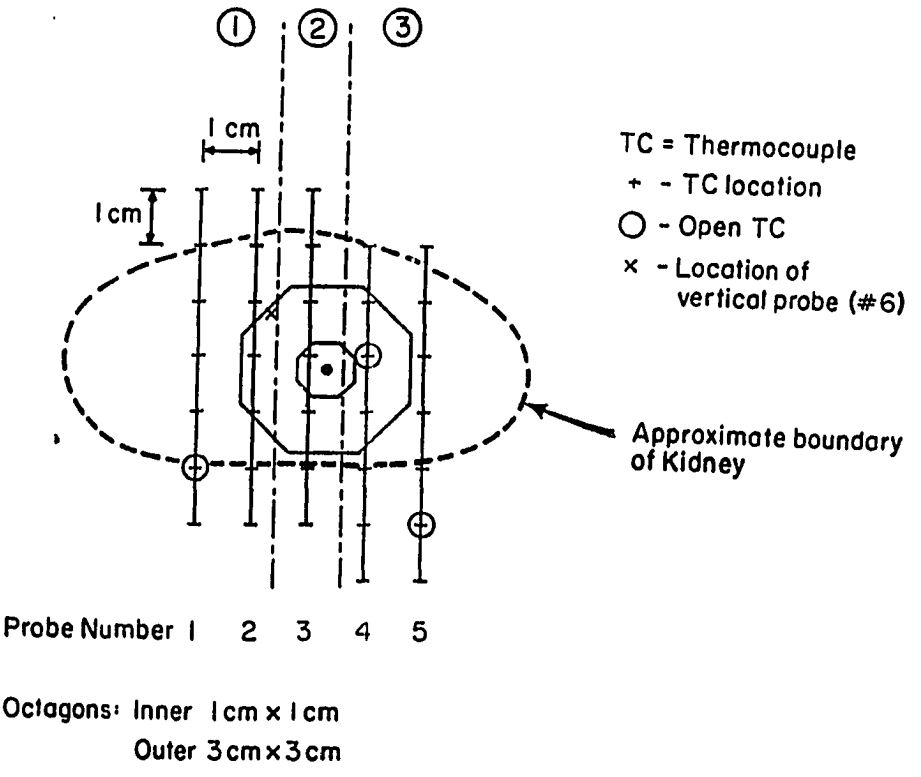

Figure A.2 Schematic of Typical Experimental Set-Up with Kidney Model Perfused Phantom.

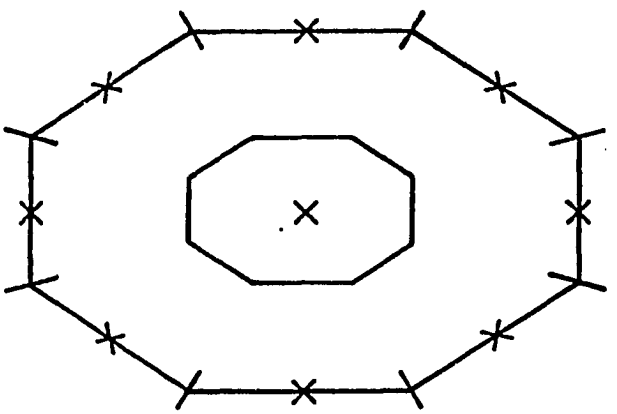

Figure A.3. Controller Power Regional Configurations for Typical Experiment.

This was verified after the experiment when the kidney was perfused with a dye. The streaming created three distinct regions of perfusion identified by the circled numbers of Figure A.2 and delineated by the alternating long and short dashed lines. Regions 1 and 3 were highly perfused relative to region 2, thus a three region one-dimensional control model was set up with model regions corresponding to perfusion regions 1,2 and 3. A new set-point temperature was calculated for each control sensor in each of the three regions. Each control sensor in a given perfusion region was assumed to be surrounded by perfusion with the same magnitude, thus each was given the set-point temperature determined for that region. Because of the lack of a communications link, perfusion was estimated using an effective perfusion model. Figure A.4 is a plot of the normalized temperature elevation, defined as $(T - T_{ART})/(T_{SET} - T_{ART})$, versus time for three temperature sensors for two tests at the same perfusion (approximately 1 kg/m^3-s average perfusion). One sensor was controlled, one was uncontrolled in a region of high perfusion and one was uncontrolled in a region of low perfusion. Figure A.4a is for a typical test utilizing the PID control scheme and Figure A.4b is for a typical test utilizing the set-point temperatures calculated by the AD1 scheme. Note that the ordinate scales are different.

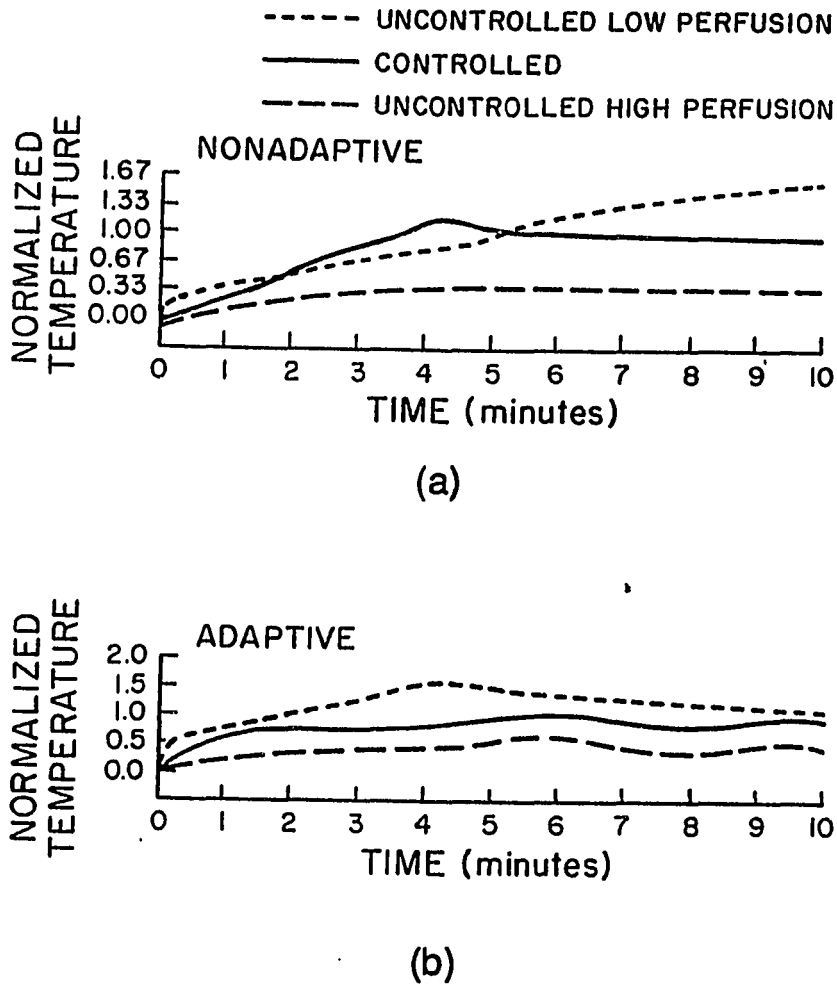

Figure A.4. Results of Typical Experiment in Kidney Model Perfused Phantom for Tests of PID and AD1 Control Schemes.

A.3 Discussion of Experimental Results

Figure A.4 compares the temperature versus time responses of different locations in the kidney model perfused phantom during a typical experiment utilizing the multi-region PID control scheme to the temperature versus time response of the same locations when the kidney model perfused phantom set-point temperatures are determined by the adaptive control scheme AD1. The uncontrolled sensor located in the low perfusion region reaches a peak normalized temperature elevation which is similar in both tests, although the final values are very different. In the PID test, the uncontrolled low-perfusion-region sensor at 10 minutes has a normalized temperature elevation, defined as $(T - T_{ART})/(T_{SET} - T_{ART})$, of approximately 1.5, whereas, the same sensor in the AD1 test has a normalized temperature elevation at 10 minutes of approximately 1.1. Similarly, the uncontrolled high-perfusion-region sensors have normalized temperature elevations of 0.3 and 0.5 respectively at 10 minutes. For these tests, a set-point temperature (T_{SET}) of three degrees above the arterial temperature (T_{ART}) was used. Thus, the temperature difference between the uncontrolled sensor in the low perfusion region and the uncontrolled sensor in the highly perfused region was approximately 3.6 °C for the PID scheme and was approximately 1.8 °C for the AD1 control scheme. Other tests showed similar improvements. Clearly, the adaptive scheme can optimize the set-point temperatures to improve the controller performance. This test also illustrates how a one-dimensional control scheme can be

applied to a two-dimensional control problem by forming regions as shown in Figure A.2 and assuming that all the sensors in a given region are surrounded by similar perfusions. The experimental results are limited in that they were obtained under very controlled conditions (the kidney model) and for very few tests. Clearly, many more experiments should be done in the kidney model, in animals and in other phantoms before these adaptive control schemes are used in hyperthermia treatments.

APPENDIX B

DIRECT MEASUREMENT OF PERFUSION -- FURTHER RESULTS

In Chapter 2, the possibility was considered of directly measuring the blood perfusion using thermal techniques. An analysis was presented for the thermal pulse-decay technique developed by Chen and Holmes (1980) and it was concluded that the technique was not applicable to the low values of perfusion that might be expected in hyperthermia treatments. In addition the claim was made that all the techniques described in Chapter 2 are ineffective at low perfusions. However, no analysis was provided to support this claim. The objective of this appendix is to present the analysis of the other thermal blood perfusion measurement techniques and to show why they are inapplicable to measuring low perfusions.

The solutions for all heated geometries for the pulse-decay technique are presented in Table B.1. With the exception of the spherical geometry, all were computed using Green's functions. For a reference on the technique of Green's functions see Haberman (1983) and Chapter 14 of Carslaw and Jaeger (1980).

Table B.1

Pulse-Decay Solutions at R=0 for Various Heated Geometries

Geometry	Initial Conditions	Solution at Center Point
Sphere	$u(R\leq 1,0) = 1$ $u(R>1,0) = 0$	$\left[\text{erf}\left(\frac{1}{2\sqrt{\tau}}\right) - \frac{1}{\sqrt{\pi\tau}}\, e^{\frac{-1}{4\tau}}\right] e^{-\gamma\tau}$
1-D Cylinder	$u(r\leq 1,0) = 1$ $u(R>1,0) = 0$	$\left[1 - e^{-1/4\tau}\right] e^{-\gamma\tau}$
2-D Cylinder	$u(R\leq 1, \lvert Z/AR\rvert \leq 1,0) = 1$ $u(R>1, \lvert Z/AR\rvert > 1,0) = 0$	$\text{erf}\left(\frac{AR}{2\sqrt{\tau}}\right)\left[1-e^{-1/4\tau}\right] e^{-\gamma\tau}$
1-D Gaussian*	$u(R,0) = e^{-R^2}$	$\left[\frac{1}{1 + 4\tau}\right] e^{-\gamma\tau}$
2-D Gaussian*	$u(R,Z,0) = e^{-R^2} e^{-(Z/AR)^2}$	$\sqrt{\frac{1}{1+4\tau(1/AR)^2}}\left(\frac{1}{1+4\tau}\right) e^{-\gamma\tau}$

* Gaussian power profiles are not only generated by ultrasonic transducer but also by lasers (See Welch, Wissler and Priebe, 1980).

The solutions for the transient temperature rise for the step-heating techniques are simply the integrals of the pulse-decay solutions given by:

$$u_{SH}(0,\tau) = \int_0^{\tau} u_{PD}(0,v)dv \ . \qquad (B.1)$$

The variables in equation (B.1) were defined in Chapter 2. The integrals are too complicated to be done analytically, therefore, a 96-point Gauss-Legendre quadrature technique given in Abramowitz and Stegun (1970) was used to numerically evaluate the solution.

For the constant temperature technique of Valvano, Allen and Bowman (1984), the solution for the power as a function of time is given by Chato (1968):

$$\frac{q}{q_{SS}} = \frac{1 + \frac{1}{\sqrt{\pi\tau}} e^{-\gamma\tau} + \sqrt{\gamma}\ \mathrm{erf}\sqrt{\gamma\tau}}{1 + \sqrt{\gamma}} \ . \qquad (B.2)$$

Again, all the variables were previously defined except q_{SS} which is the specific power at steady-state (W/m^3).

The solutions of Table B.1 can be used along with equations (B.1) and (B.2) to develop time window plots such as Figure 2.5, for all the techniques and all the heated geometries. Two examples of these results are shown in Figures B.1 and B.2. These figures illustrate clearly that the dimensionless time window sizes are not significantly different for any of the measurement techniques.

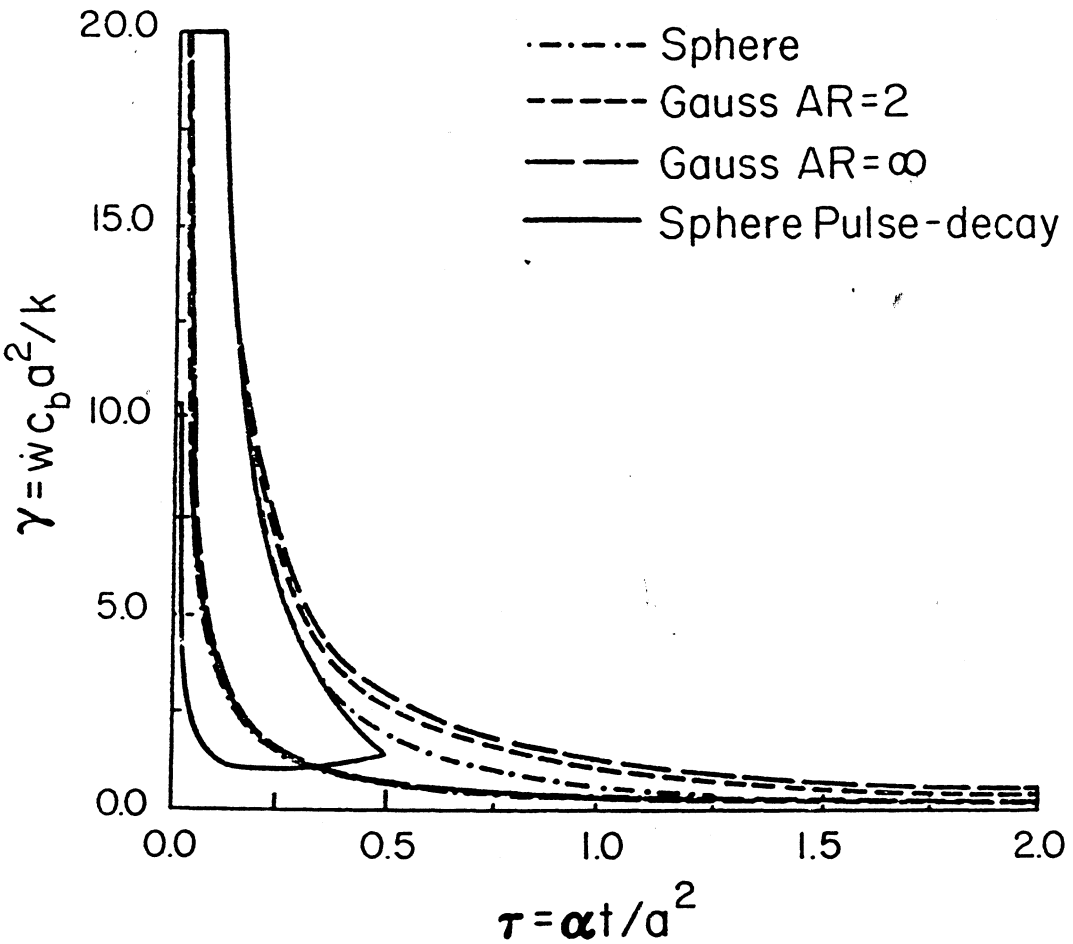

Figure B.1. Dimensionless Time Window Results for Pulse-Decay and Step-Heating Technique with Various Heated Geometries and 10% Limit Criterion

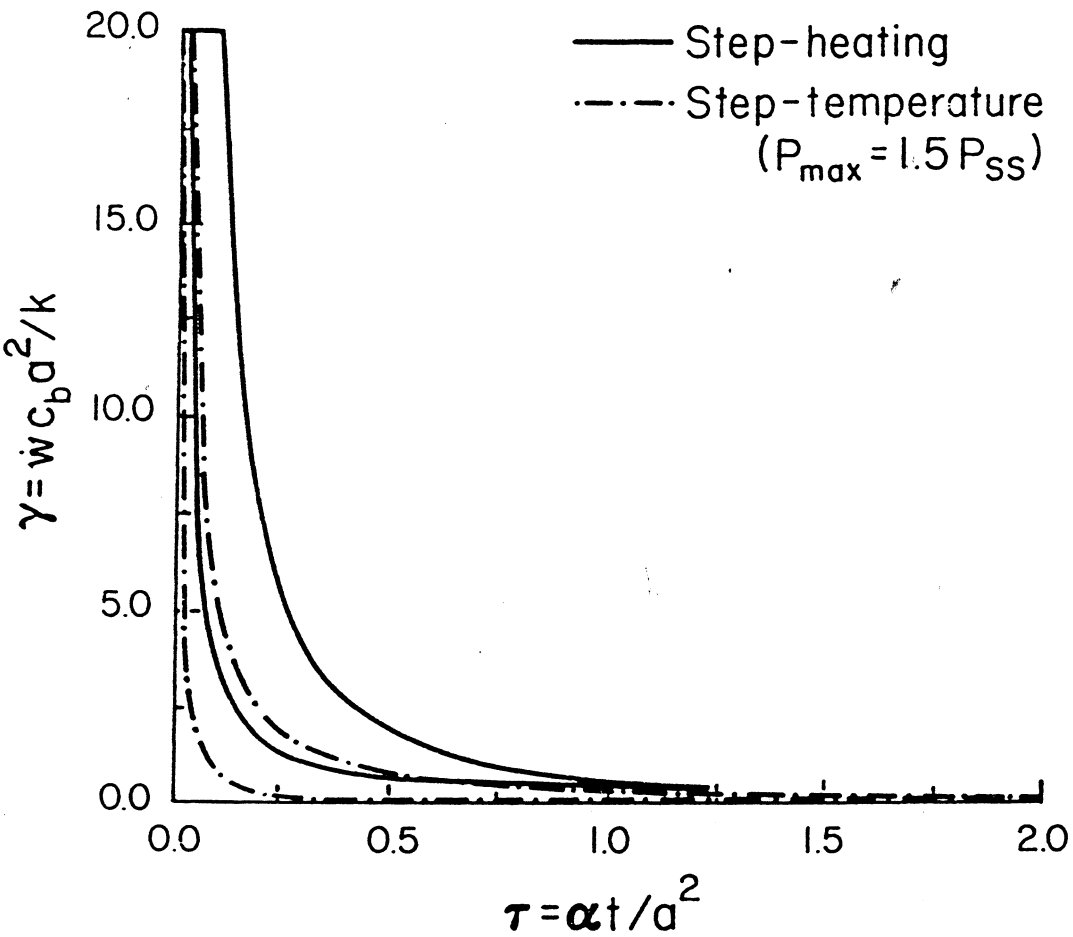

Figure B.2. Dimensionless Time Window Results for Step-Heating and Step-Temperature Techniques for Spherical Heated Geometry

Thus it may be concluded that none of the measurement techniques are applicable to measuring low values of perfusion. Further results are presented and discussed in Kress and Roemer (1987).

APPENDIX C

GAUSSIAN ESTIMATION

A Gaussian estimation technique is central to the working of the adaptive controllers designed in this dissertation. This appendix gives a short presentation of the equations used for Gaussian estimation. For a more complete treatment of the subject of parameter estimation refer to Beck and Arnold (1977).

Consider the situation where all parameters are known except the magnitudes of the perfusion vector w. The perfusion vector w is N-dimensional for an N-region model. Assume there are M temperature measurement locations. A Taylor series expansion for the predicted temperature vector $T_p \equiv [T_{p,1}, T_{p,2}, \ldots, T_{p,M}]^T$ as a function of perfusion is given by:

$$T_p(w_b,t) = T_p(w_a,t) + \nabla_w T_p(w_b - w_a) \ , \qquad (C.1)$$

where w_a and w_b are perfusion vectors a and b respectively, and $T_p(w_a,t)$ and $T_p(w_b,t)$ are the predicted temperature vectors using perfusion vectors a and b.

Assuming that one starts close to the solution, the predicted temperature vector, T_p, is approximately equal to the measured temperature vector, $T_m \equiv [T_{m,1}, T_{m,2}, \ldots, T_{m,M}]^T$. Thus equation (C.1) becomes

$$T_m \simeq T_p(w_b,t) = T_p(w_a,t) + \nabla_w T_p(w_b - w_a) \ . \qquad (C.2)$$

Defining the error vector $E = T_m - T_p$ and recognizing that $\nabla_w T_p$ is the time-dependent Jacobian (J_t) defined as:

$$J_t \equiv \begin{bmatrix} \frac{\partial T_{p,1}(t_1)}{\partial w_1} & \frac{\partial T_{p,1}(t_1)}{\partial w_2} & \cdots & \frac{\partial T_{p,1}(t_1)}{\partial w_N} \\ \frac{\partial T_{p,2}(t_1)}{\partial w_1} & \cdots\cdots & & \frac{\partial T_{p,2}(t_1)}{\partial w_N} \\ \vdots & & & \vdots \\ \frac{\partial T_{p,M}(t_1)}{\partial w_1} & \cdots\cdots & & \frac{\partial T_{p,M}(t_1)}{\partial w_N} \\ \frac{\partial T_{p,1}(t_2)}{\partial w_1} & \cdots\cdots & & \frac{\partial T_{p,1}(t_2)}{\partial w_N} \\ \vdots & & & \vdots \\ \frac{\partial T_{p,M}(t_{NT})}{\partial w_1} & \cdots\cdots & & \frac{\partial T_{p,M}(t_{NT})}{\partial w_N} \end{bmatrix} \begin{matrix} \\ \\ \\ \\ \\ \\ \\ \end{matrix} \begin{matrix} (M*NT)\ X\ N \\ \\ \\ \\ \\ \\ \\ \end{matrix} \qquad (C.3)$$

where $T_{p,i}(t_j)$ is the predicted temperature at location i at time t_j, w_i is an element (magnitude) of the perfusion vector w and NT is the number of samples of transient data. Thus, $E = J_t(w_b - w_a)$ and solving for w_b gives: $w_b = w_a + (J_t^T J_t)^{-1}(J_t^T E)$. This process is made iterative by replacing w_a with w_b, calculating a new J_t and obtaining a new w_b. The iteration can be repeated until the new perfusion vector does not change significantly from the old, that is, $||w_b - w_a||$ is less than a specified error criterion or until $||E||$ is less than a specified error criterion (generally different from the error criterion for the difference in perfusion vectors).

To actually perform an estimation, all that is required is a set of measured temperatures and a model with the geometrical

distribution of the perfusion and the measurement locations defined. Multi-dimensional estimations are no different from one-dimensional estimations as far as the Gaussian estimation routine is concerned, since its only requirement is the perfusion vector. Unknown multi-dimensional perfusion distributions can be placed in a vector form as well as one-dimensional distributions.

To estimate the specific power, the perfusion vector is replaced by a specific power vector. Also, in the transient Jacobian, derivatives are taken with respect to power magnitudes instead of perfusion magnitudes. Again a model is required except this time the geometrical distribution of the power is required. There are no measurement locations as in the perfusion estimation; instead the predicted temperatures are compared to an ideal distribution at all of the nodal locations modeled. That is, M is equal to the number of nodes in the model. Since there are always more nodes than power regions, the specific power estimation is steady-state, implying that NT equals 1.

In Chapter 3 it was stated that Tikhonov regularization of order zero was used to improve the perfusion estimation. Briefly, this technique improves the numerical properties of the (NXN) matrix $(J_t^T J_t)^{-1}$ by making it more diagonally dominant. The Tikhonov parameter is added to the diagonal elements of $(J_t^T J_t)$. Selection of the proper value for the Tikhonov parameter is complicated and is still being studied by several investigators.

APPENDIX D

PID CONTROLLER ANALYSIS

D.1 Stability of PID Controller

In order to have a very simple model, I have used the "effective perfusion" form of the bioheat transfer equation (See Roemer, Fletcher and Cetas 1985). In this formulation (which should be used with caution), the effects of conduction and perfusion are included in a single effective perfusion term. Mathematically the "effective perfusion" form is:

$$-w_e c_b T + q = \rho c \frac{dT}{dt} \tag{D.1}$$

where w_e is the effective perfusion and temperature is referenced to a constant arterial temperature. Taking the Laplace transform of equation (D.1) gives:

$$\frac{T(s)}{q(s)} = \left(\frac{1}{\rho c s + w_e c_b} \right) \tag{D.2}$$

where s is the frequency. This is the transfer function for the heating system coupled with the patient. The transfer function for a PID controller in the Laplace domain is:

$$\frac{q(s)}{e(s)} = \left(K_P + K_D s + K_I \frac{1}{s} \right) \tag{D.3}$$

where the K's are the gain constants defined earlier and e is the error signal determined as the difference between the set-point temperature and the measured (or observed) temperature. If the PID controller is arranged in series (sometimes called cascade fashion; see Kuo 1982) with the system modeled by equation (D.2) then the closed-loop transfer function, F(s), is:

$$F(s) = \frac{T(s)}{e(s)} = \frac{K_D s^2 + K_P s + K_I}{s^2(\rho c + K_D) + s(w_e c_b + K_P) + K_I} . \qquad (D.4)$$

For stability, the roots of the denominator must all lie in the left half-plane. This will always be true if the coefficients of the function in the denominator (called the characteristic function) are all of the same sign. Since the thermal properties, the effective perfusion and the controller gains are always positive the coefficients of the terms in the denominator are always positive. Consequently, the system is stable for all values of effective perfusion.

D.2 Transient Response of PID Controller

Consider the transient response to a step input of the PID controller in series with the system of equation (D.2). The transient response in the Laplace domain is:

$$F'(s) = \frac{1}{s} F(s) . \qquad (D.5)$$

Thus, the transient response in the time domain is given by:

$$\frac{T(t)}{T_{Set}} = 1. + K_1 e^{r_1 t} + K_2 e^{r_2 t} , \qquad (D.6)$$

where

$$K_l = \lim_{s \to r_l} (s - r_l) \dot{F}(s) \qquad (D.7)$$

and the r_l are the roots of the characteristic equation:

$$s^2(\rho c + K_D) + s(w_e c_b + K_P) + K_I = 0 . \qquad (D.8)$$

Thus,

$$r_{1,2} = \frac{-(w_e c_b + K_P) \pm \sqrt{(w_e c_b + K_P)^2 - 4(\rho c + K_D)K_I}}{2(\rho c + K_D)} . \qquad (D.9)$$

Values of these roots can be determined as a function of effective perfusion and controller gains. In general, higher gains (on the order of 10^5 to 10^6) give a faster transient response, however, a lower integral gain (on the order of 10^2 to 10^4) gives less oscillation. These bounds were used as guidelines in the gain studies.

APPENDIX E

THREE-DIMENSIONAL SPECTRAL EQUATIONS

This appendix summarizes the equations obtained when spectral methods are implemented in three-dimensional cartesian coordinates. The three-dimensional bioheat transfer equation, presented first as equation (2.1), is:

$$k\left[\frac{\partial^2 T}{\partial x^2} + \frac{\partial^2 T}{\partial y^2} + \frac{\partial^2 T}{\partial z^2}\right] - c_b w T + q = \rho c \frac{\partial T}{\partial t} \quad , \qquad (E.1)$$

with the additional assumptions that thermal conductivity and arterial temperature are homogeneous, metabolic power is negligible, and temperature is referenced to arterial temperature. In general, both the perfusion w and the specific power q are functions of space (x,y,z) and time (t). The solution is sought in the rectangular parallelepiped defined by: $0 \leq x \leq L_x$, $0 \leq y \leq L_y$ and $0 \leq z \leq L_z$. The boundary conditions are $T(0 \text{ or } L_x,y,z,t) = 0$, $T(x,0 \text{ or } L_y,z,t) = 0$ and $T(x,y,0 \text{ or } L_z,t) = 0$, with the initial condition $T(x,y,z,0) = f(x,y,z)$. The following spectral definitions apply; for temperature:

$$T(x,y,z,t) = \sum_{l=1}^{L} \sum_{m=1}^{M} \sum_{n=1}^{N} a_{lmn}(t) \sin\frac{l\pi x}{L_x} \sin\frac{m\pi y}{L_y} \sin\frac{n\pi z}{L_z} \quad , \qquad (E.2)$$

for perfusion:

$$wT(x,y,z,t) = \sum_{l=1}^{L} \sum_{m=1}^{M} \sum_{n=1}^{N} b_{lmn}(t) \sin\frac{l\pi x}{L_x} \sin\frac{m\pi y}{L_y} \sin\frac{n\pi z}{L_z}, \quad (E.3)$$

and for specific power:

$$q(x,y,z,t) = \sum_{l=1}^{L} \sum_{m=1}^{M} \sum_{n=1}^{N} c_{lmn}(t) \sin\frac{l\pi x}{L_x} \sin\frac{m\pi y}{L_y} \sin\frac{n\pi z}{L_z}. \quad (E.4)$$

Substitute these definitions for T, wT and q into the bioheat transfer equation and use the pseudospectral technique (cf. Figure 2.6) to determine b_{lmn} for small time steps to obtain:

$$\rho c \frac{da_{lmn}}{dt} = k\left\{-\left[\frac{l\pi}{L_x}\right]^2-\left[\frac{m\pi}{L_y}\right]^2-\left[\frac{n\pi}{L_z}\right]^2\right\}a_{lmn}- c_b b_{lmn}+ c_{lmn}. \quad (E.5)$$

Equation (E.5) can now be solved for each a_{lmn} for one small time step using any time integration technique.

Test were done using the three-dimensional adaptive control scheme. It was found that to obtain model solutions of useful accuracy, two many nodes were required, thus the CPU time expended on a VAX (8600) was too large. Despite the application of spectral methods, answers could not be obtained to sufficient accuracy in short enough time to be useful in an adaptive control scheme.

APPENDIX F

ADDITIONAL RESULTS

This appendix contains some additional results that were not included in the main text of the dissertation. The results are useful to the more interested reader.

F.1 Complete Estimation Time Results

The average CPU time required to complete the parameter estimation (in seconds on VAX 8600) were presented in Figures 3.12 and 3.17 through 3.19 for the three different adaptive control schemes for some of the tumor models. Complete results for all of the control schemes and all of the models are shown in Tables F.1 and F.2.

Table F.1

Average CPU Time to Complete Both Parameter Estimations (in seconds on VAX 8600) versus Number of Control Model Regions For Various Tumor Models using the AD1 Control Scheme Configured as in Figure 3.5

Model		LFNTPC	LFNTPFT	HFNTPC	HFNTPFT
No. of Regions	3	23	37	35	53
	4	32	43	43	65
	5	42	60	64	110
	6	49	62	68	113
	7	141	235	242	289
	8	134	227	274	320
	9	170	330	269	360
	10	234	283	271	383

Table F.2

Average CPU Time to Complete Parameter Estimations (in seconds on VAX 8600) versus Number of Control Model Regions for Various Tumor Models using the AD2 and AD3 Control Schemes Configured as in Figure 3.13

	Model		LFNTPC	LFNTPFT	HFNTPC	HFNTPFT
Number of Regions	AD2	5	23	37	35	53
		7	37	49	53	101
		9	43	52	58	97
		11	43	53	58	102
		13	38	56	50	112
	AD3	5	38	52	60	68
		7	49	63	59	116
		9	57	74	88	132
		11	65	78	91	152
		13	53	79	92	175

Note: For five temperature sensors, AD2 with five regions is equivalent to the PID and AD3 with five regions is equivalent to AD1. (No temperatures are observed.)

F.2 Temperature Dependent Perfusion

The PID and AD1 control schemes were tested using the 7 and 9 region controller configurations shown in Figure 3.5 for the LFNT simulated treatment with temperature dependent perfusion. The AD2 and AD3 control schemes were also tested with the temperature dependent perfusion model using the 7 and 9 region controller configurations shown in Figure 3.13. Perfusion was varied with respect to temperature according to equation F.1 which is for human quadriceps during hyperthermia and was taken from Lehmann (1982).

$$w(T) = \begin{cases} w_0(1.5T - 42) & (kg/m^3\text{-}s) \quad T > 42\ ^\circ C \\ w_0 & (kg/m^3\text{-}s) \quad T \leq 42\ ^\circ C \end{cases} \tag{F.1}$$

The controller performance for the temperature dependent perfusion treatments are compared to constant perfusion and time dependent perfusion simulations in Table F.3. Since the set point temperature used was 43°C, the results of the temperature dependent perfusion simulations and the constant perfusion simulations are similar.

Table F.3

Integral Square Error (°C) for Different Perfusion Variations and Various Controller Configurations for LFNT Model

		Model	PID	AD1	AD2	AD3
# of Region	7	w=Con.	1.649	1.307	1.388	1.444
		w=f(t)	1.428	1.333	1.355	1.382
		w=f(T)	1.649	1.307	1.463	1.452
	9	w=Con.	1.648	1.257	1.646	1.262
		w=f(t)	1.428	1.188	1.444	1.264
		w=f(T)	1.648	1.255	1.646	1.262

F.3 Weighted Cost Function

To emphasize low temperature errors in the tumor, a weighted cost function was implemented in the power optimization routine. The weighted cost function is given by:

$$C = \frac{1}{N}\left\{ \sum_{\substack{\text{Normal}\\\text{Nodes}}} (T-41)H(T-41) + \sum_{\substack{\text{Tumor}\\\text{Nodes}}} 10\,(42-T)H(42-T) \right\} \qquad (F.1)$$

where H(x) is the step function. Figure F.1 compares the temperature profiles for the PID control scheme at steady-state to the AD1 control scheme before and after the perfusion estimation decay to the ideal desired temperature profile for 5 region controller configuration for the LFNTPC tumor model for simulations using the weighted cost function. Comparing these results to Figure 3.6(a), it is evident that the weighted cost function did not alter the results.

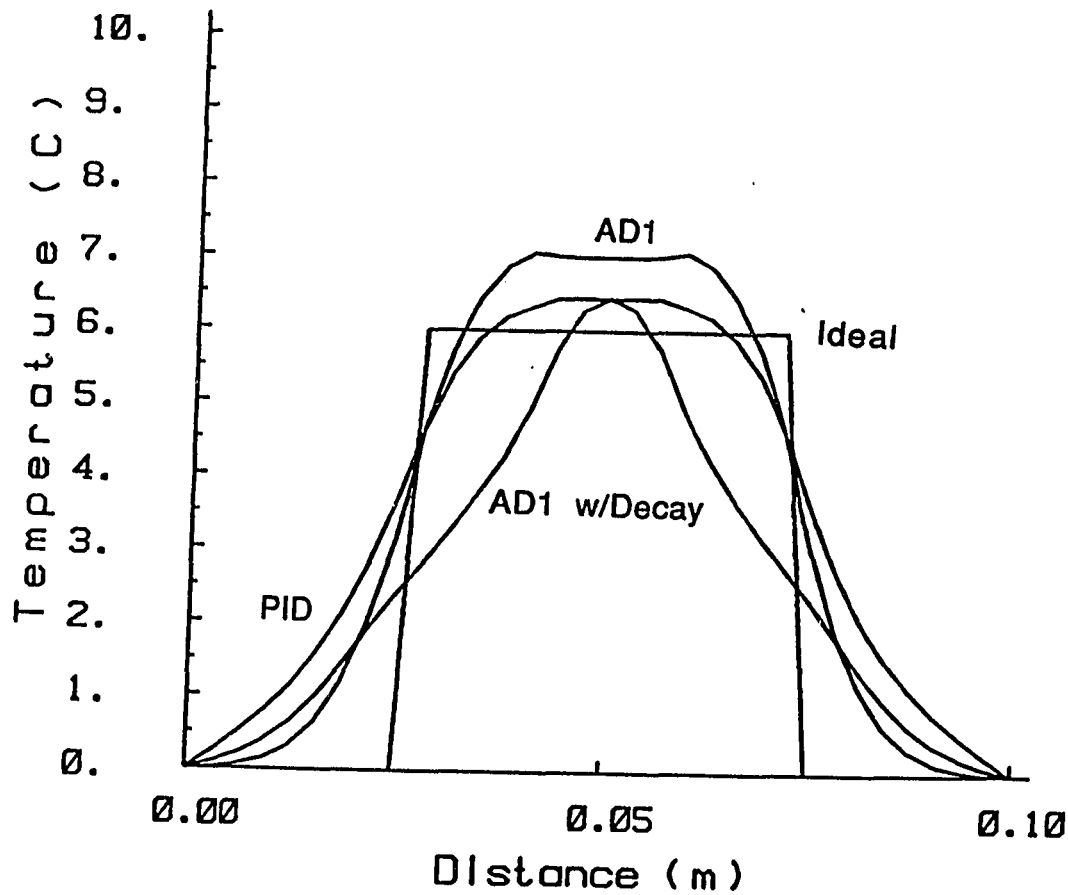

Figure F.1. Temperature Profiles for PID and AD1 (with weighted cost function) Control Schemes for LFNTPC Tumor Model.

APPENDIX G

NOMENCLATURE

Symbols

a	Characteristic heated region size: sphere or cylinder, a_r = radius; one- or two-dimensional Gaussian, a_r = 1/e relaxation length in the radial direction, a_z = 1/e relaxation length in the axial direction.
a_n	Coefficient for spectral approximation of temperature
AR	Aspect Ratio: two-dimensional cylinder, AR = $h/(2a_r)$; two-dimensional Gaussian, AR = a_z/a_r
b	Boundary operator
b_n	Coefficient for spectral approximation of product of perfusion and temperature
B	Subspace of Hilbert space **H**
c	Specific heat of tissue (J/kg-°C)
c_b	Specific heat of blood (J/kg-°C)
c_n	Coefficient for spectral approximation of internal heating term in bioheat transfer equation
e	Error signal (°C)
f	Conduction-only portion of impulse response

E	Error signal vector (°C)
F	Transfer function in Laplace space
F'	Transfer function in Laplace space for step input
h	Cylinder length (m)
H	Step function
H	Hilbert space
I_0	Modified Bessel function of zeroth order, first kind
I_1	Modified Bessel function of first order, first kind
J_t	Transient Jacobian (°C/kg/m^3-s)
k	Thermal Conductivity (W/m-°C)
K	Controller gain
K_0	Modified Bessel function of zeroth order, second kind
K_1	Modified Bessel function of first order, second kind
L_x	Length (m)
L	Linear operator
M	Matrix of coefficients for steady-state spectral methods
N	Number of modes in spectral approximation
NT	Number of time steps in decay interval
$N\tau$	Number of time steps in treatment
$p(\tau)$	Time function for dimensionless power q^*
P_N	Projection operator
q	Specific power (W/m^3)
q_n	Coefficient for spectral approximation of power
q^*	Normalized power

r	Radius (m)
R	Dimensionless radial variable (r/a_r)
R_N	Residual
$S(R,Z)$	Space function for dimensionless power q^*
t	Time (s)
T	Temperature (°C)
T_{ART}	Arterial temperature (°C)
T_I	Initial temperature after pulse (°C)
T_0	Initial temperature before perturbation (°C)
T_m	Measured temperature vector in Gaussian estimator (°C)
T_p	Predicted temperature vector in Gaussian estimator (°C)
u	Dimensionless temperature
u'	Dimensionless temperature with effect of perfusion removed
w	Blood perfusion (kg/m^3-s)
$\mathbf{w}$	Blood perfusion vector (kg/m^3-s)
$\mathbf{x}$	Position vector (m)
z	Axial variable (m)
Z	Dimensionless axial variable (z/a_z)

Greek Symbols

α	Thermal diffusivity (m^2/s)
Δt	Time step (s)
Δu	$u_k - u_{k+w}$
∇	Vector differential

∇^2	Laplace operator
γ	Dimensionless blood perfusion ($wc_b a^2/k$)
ρ	Density (kg/m^3)
σ	Power partitioning fraction
τ	Dimensionless time ($\alpha t/a_r^2$ if a_r is defined, $\alpha t/a_z^2$ if a_r is not defined)
ω	$n\pi/L_x$ in spectral approximation (1/m)
Υ	Treatment time (s)

Subscripts

ART	Arterial
b	Blood
D	Derivative
Des	Desired
e	effective
Est	Estimated
f	Final
i	Initial
I	Integral
k	Conduction only
k+w	Conduction plus perfusion
m	Measured
M	Maximum
MET	Metabolism
n	Counter

O	Observed
P	Proportional
PD	Pulse-decay
N	Operator in collocation space
r	Radial
s	Sampled
ss	Steady-state
SH	Step-heat
u	Uniform
z	Axial

LIST OF REFERENCES

Abramowitz, M. and Stegun, I., Handbook of Mathematical Functions, Dover Pub. Inc., New York, 1970.

Babbs, C.F., Vaguine, V.A.,and Jones, J.T., "A Predictive-adaptive, Multipoint Feedback Controller for Local Heat Therapy of Solid Tumors," IEEE Trans. on Microwave Theory and Tech., Vol 34, p. 604, 1986.

Baish, J.W., Foster, K.R., and Ayyaswamy, P.S., "Perfused Phantom Models of Microwave Irradiated Tissue," J. of Biomechanical Eng., Vol. 108, pp. 239-245, Aug., 1986.

Balasubramanian, T.A. and Bowman, H.F., "Temperature Field Due to a Time Dependent Heat Source of Spherical Geometry in an Infinite Medium," ASME J. of Heat Transfer, Vol. 96, No. 3, pp. 296-299, Aug., 1974.

Barlogie, B., Corry, P.M., Yip, E., Lippman, L., Johnston, D.A., Khalil, K., Tenczynski, T.F., Reilly, E., Lawson, R., Dosik, G., Rigor, B., Handerson, R., and Freireich, E.J., "Total-body Hyperthermia with and without Chemotherapy for Advanced Human Neoplasms," Cancer Research, Vol. 39, p. 1481, 1979.

Beck, J.V. and Arnold, K.J., Parameter Estimation in Engineering and Science, John Wiley, New York, 1977.

Bibbero, R.J., Microprocessors in Instruments and Control, John Wiley and Sons, New York, 1977.

Buhler, E. and Franke, D., Topics in Identification and Distributed Parameter Systems, Friedr. Vieweg and Sohn, Braunschweig, 1980.

Carslaw, H.S. and Jaeger, J.C., Conduction of Heat in Solids, Oxford University Press, 1980.

Chato, J.C., "A Method for the Measurement of the Thermal Properties of Biological Materials," Thermal Problems in Biotechnology, ASME, pp. 16-25, 1968.

Chen, M.M. and Holmes, K.R., "The Thermal Pulse-decay Method for Simultaneous Measurement of Thermal Conductivity and Local Blood Perfusion Rate of Living Tissues," J. of Biomechanical Engr., Vol. 102, p. 113, 1980.

Clegg, S.T. and Roemer, R., "A Comparative Evaluation of Unconstrained Optimization Methods Applied to the Thermal Tomography Problem," J. of Biomechanical Engineering, Vol. 107, pp. 228-233, Aug., 1985a.

Clegg, S.T. and Roemer, R.B., "A Study of the Effect of Sensor Placement and Perfusion Pattern Variations on Thermal Tomography Solutions in Hyperthermia," IEEE Trans. on Biomedical Eng., Vol. BME-32, No. 9, pp. 677-682, Sept., 1985b.

Clegg, S.T., Roemer, R.B., and Cetas, T.C., "Estimation of Complete Temperature Fields from Measured Transient Temperatures," Int. J. of Hyperthermia, Vol. 1, No. 3, pp. 265-286, 1985.

Cooley, J.W. and Tukey, J.W., "An Algorithm for the Machine Calculation of Complex Fourier Series," Mathematics of Computation, Vol. 19, pp. 297-301, 1965.

Dagan, Z., Weinbaum, S. and Jiji, L.M., "Parametric Studies on the Three-Layer Microcirculatory Model for Surface Tissue Energy Exchange," J. Biomechanical Eng., Vol. 108, pp. 89-96, 1986.

Dar, H. and Lele, P., "Design of a Power Modulator for Control of Tumor Temperature," Proceedings of the Fourth Int. Symposium on Hyperthermic Oncology, J. Overgaard editor, pp. 707-710, Taylor and Francis, London, 1984.

Dewhirst, M.W., Sim, D.A., Sapereto, S. and Conner, W.G., "Importance of Minimum Tumor Temperature in Determining Early and Long-term Responses of Spontaneous Canine and Feline Tumors to Heat and Radiation," Cancer Research, Vol. 44, pp. 43-50, 1984.

Doss, J.D., "Simulation of Automatic Temperature Control in Tissue Hyperthermia Calculations," Med. Physics, Vol. 12, pp.693-697, 1985.

Eberhart, N.C., Shitzer, A., and Hernandez, E.J., "Thermal Dilution Methods: Estimation of Tissue Blood Flow and Metabolism," Annals of the New York Academy of Science, Vol. 355, pp. 107-131, 1980.

Ferziger, J.H., Numerical Methods for Engineering Application, John Wiley and Sons, New York, 1981.

Field, S.B. and Franconi, C. editors, Physics and Technology of Hyperthermia, Martinus Nyhoff Publishers, Boston, 1987.

Gottlieb, D. and Orszag, S.A., Numerical Analysis of Spectral Methods: Theory and Applications, SIAM CBMS-NSF Regional Conference Series in Applied Mathematics Aug. 1976, No. 26, Philadelphia, Penn., 1977.

Groetsch, C.W., The Theory of Tikhonov Regularization for Fredholm Equations of the First Kind, Research Notes in Mathematics No. 105, Pitman Advanced Publishing Program, Boston, 1984.

Haberman, R., Elementary Applied Partial Differential Equations with Fourier Series and Boundary Value Problems, Prentice-Hall Inc., New Jersey,1983.

Hand, J.W., Cheetham, J.L. and Hind, A.J., "Absorbed Power Distributions from Coherent Microwave Arrays for Localized Hyperthermia," IEEE Trans. Microwave Theory and Techniques, Vol. MTT-34, pp. 484-489, 1986.

Hand, J.W. and James, J.R. eds., Physical Techniques in Clinical Hyperthermia, John Wiley, New York, 1986.

Holmes, K.R., Ryan, W., Weinstein, P., and Chen, M., "A Fixation Technique for Organs to be Used as Perfused Tissue Phantoms in Bioheat Transfer Studies," ASME WAM, 1984.

Hynynen, K., Roemer, R.B., Anhalt, D., Johnson, C., Xu, Z., Swindell, W. and Cetas, T.C., "A Scanned Focussed Multiple Transducer Ultrasonic System for Localized Hyperthermia Treatments," Int. J. of Hyperthermia, Vol. 3, p. 21, 1987.

Jiji, L.M., Weinbaum, S. and Lemons, D.E., "Theory and Experiment for the Effect of Vasculature Microstructure on Surface Tissue Heat Transfer--Part II: Model Formulation and Solution," ASME J. of Biomechanical Engineering, Vol. 106, pp. 331-341, 1984.

Johnson, C., Control System for the Application of Scanned, Focussed Ultrasound in Hyperthermia Cancer Therapy, M.S. Thesis, Electrical and Computer Engineering Department, University of Arizona, 1987.

Johnson, C., Kress, R., Roemer, R.,and Hynynen, K., "A Multipoint Feedback Control System for Scanned Focused Ultrasound Hyperthermia," Thirty-fifth Annual Meeting of the Radiation Research Society, March 1987.

Johnson, W.R., Abdelmessih, A.H., and Grayson, J., "Blood Perfusion Measurements by the Analysis of the Heated Thermocouple Probe's Temperature Transients," J. of Biomechanical Eng., Vol. 101, pp. 58-65, 1979.

Knudsen, M. and Hartmann, U., "Optimal Temperature Control with Phased Array Hyperthermia System," IEEE Trans. on Microwave Theory and Techniques, Vol. MTT-34, pp. 597-603, 1986.

Knudsen, M. and Heinzl, L., "Two-point Control of Temperature Profile in Tissue," Int. J. of Hyperthermia, Vol. 2, No. 1, pp. 21-38, 1986.

Knudsen, M. and Overgaard, J., "Identification of Thermal Model for Human Tissue," IEEE Trans. on Biomedical Eng., Vol. BME-33, No. 5, pp. 477-485, May, 1986.

Kress, R. and Roemer R.B., "A Comparative Analysis of Thermal Blood Perfusion Measurement Techniques," J. of Biomechanical Eng., Vol. 109, NO. 3, pp. 218-225, Aug., 1987.

Kuo, B.C., Automatic Control Systems, Prentice-Hall Inc., New Jersey, 1982.

Landau, Y.D., Adaptive Control, The Model Reference Approach, Control and System Theory Series, Vol. 8, Marcel Dekker Inc., New York, 1979.

Larkin, J.M., Edwards, W.S., Smith, D.E., and Clark, P.J., "Systemic Thermography: Description of a Method and Physiologic Tolerance in Clinical Subjects," Cancer, Vol. 40, pp. 3155-3159, 1977.

Lee, E.R., Samulski, T.V., Fessenden, P. and Kapp, D.S., "Controlled Scan Surface Heating," Sixth Annual NAHG Meeting, Las Vegas, Nevada, 1986.

Lehmann, J.F. ed., Therapeutic Heat and Cold, Williams and Wilkins, Baltimore, 1982.

Lele, P. and Parker, K.J., "Temperature Distributions in Tissues During Local Hyperthermia by Stationary or Steered Beams of Unfocussed or Focussed Ultrasound," Brit. J. Cancer, Vol. 45, Supplement V, pp. 108-121, 1982.

Leondes, C.T. ed., Control and Dynamic Systems Vol. 23: Decentralized/Distributed Control and Dynamic Systems, Academic Press Inc., New York, 1986.

Nikawa, Y., Watanabe, H., Kikuchi, M. and Mori,S., "A Direct-Contact Microwave Lens Applicator with a Microcomputer-Controlled Heating System for Local Hyperthermia," IEEE Trans. Microwave Theory and Techniques, Vol. MTT-34, pp. 626-630, 1986.

Ogilvie, G.K., Goss, S.A., Badger, C.W. and Burdette, E.C., "Performance of a Multisector Ultrasound Hyperthermia Applicator and Control System--Results of Animal Studies in vivo," Sixth Annual NAHG Meeting, Las Vegas, Nevada, 1986.

Oleson, J.R., Sim, D.A., and Manning, M.R., "Analysis of Prognostic Variable in Hyperthermia Treatment of 161 Patients," Int. J. of Radiation Oncology, Biology, and Physics, Vol. 10, pp. 2231-2239, 1984.

Parker, K.J., "The Generation and Analysis of Hyperthermia by Ultrasound", Ph.D. Thesis, Massachusetts Institute of Technology, Boston, MA., 1981.

Parker, K.J., "Effects of Heat Conduction and Sample Size on Ultrasonic Absorption Measurements," J. Acoust. Society of America, Vol. 77, pp. 719-725, 1985.

Patera, A.T., Mikic', B.B., and Bowman, H.F., "The Effect of Cylindrical Probe Geometry on the Accuracy of Tissue Perfusion Measurements Made with the Thermal Diffusion Probe," Bioeng. Proceedings, ASME WAM, pp. 157-159, 1978.

Pennes, H.H. "Analysis of Tissue and Arterial Blood Temperatures in the Resting Human Forearm," J. of Applied Physiology, Vol. 1, No. 2, pp. 93-122, Aug. 1948.

Pettigrew, R.T., Galt, J.M., Lugate, C.M., Horn, D.B., and Smith, A.N., "Circulatory and Biochemical Effects of Whole-body Hyperthermia," British J. of Surgery, Vol. 61, p. 727, 1974.

Ray, W.H. and Lainiotis, D.G. editors, Distributed Parameter Systems Identification, Estimation, and Control," Vol. 6 Control and Systems Theory Series, Marcel Dekker Inc., New York, 1978.

Roemer, R.B., Fletcher, A.M. and Cetas, T.C., "Obtaining Local SAR and Blood Perfusion Data from Temperature Measurements: Steady-State and Transient Techniques Compared," Int. J. Radiation Oncology Biol. Physics, Vol. 11, pp. 1539-1550, 1985.

Rude, J., Luk, K., Vova, N., Fovell, B., Findley, D. and Doggett, S., "Multipoint Feedback Control of Power: Preliminary Clinical Results," Proceedings Thirty-fifth Annual Radiation Research Society Meeting, Atlanta, Ga., p.6, 1987.

Song, W.J., Weinbaum, S. and Jiji, L.M., "A Theoretical Model for Peripheral Tissue Heat Transfer Using the Bioheat Transfer Equation of Jiji and Weinbaum," ASME J. Biomechanical Eng., Vol. 109, pp. 72-78, 1987.

Teo, K.L. and Wu, Z.S., Computational Methods for Optimizing Distributed Systems, Academic Press Inc., New York, 1984.

ter Haar, G. and Hopewell, J.W., "The Induction of Hyperthermia by Ultrasound; its Value and Associated Problems: II. Scanned-Plane Transducer," Phys. Med. Biology, Vol. 30, pp. 1327-1333, 1985.

Trembly, B.S., "The Effects of Driving Frequency and Antenna Length on Power Deposition within a Microwave-Antenna Array used for Hyperthermia," IEEE Trans. on Biomed. Eng., Vol. BME-32, pp. 152-157, Feb., 1985.

Trembly, B.S., Wilson, A.H., Sullivan, M.J., Stein, A.D., Wong, T.Z. and Strohbehn, J.W., "Control of the SAR Pattern within an Interstitial Microwave Array Through Variation of Antenna Driving Phase," IEEE Trans. on Microwave Theory and Techniques, Vol. MTT-34, pp. 568-571, No. 5, 1986.

Tzafestas, S.G. ed., Distributed Parameter Control Systems Theory and Application, Pergamon Press, New York, 1982.

Valvano, J.W., Allen, J.T., and Bowman, H.F., "The Simultaneous Measurement of Thermal Conductivity, Thermal Diffusivity, and Perfusion in Small Volumes of Tissue," J. of Biomechanical Eng., Vol. 106, pp. 192-197, 1984.

Valvano, J.W., Allen, J.T., Walsh, J.T., Hnatowich, D.J., Tomera, J.F., Brunengraber, H., Bowman, H.F., "An Isolated Rat Liver Model for the Evaluation of Thermal Techniques to Quantify Perfusion," J. of Biomechanical Eng., Vol. 106, pp. 187-191, Aug., 1984.

Van Der Zee, J., Van Putten, W.L.J., Van Den Berg, A.P., Van Rhoon, G.C., Wike Hooley, J.L., Broekmeyer-Reurink, M.P., and Reinhold, H.S., "Retrospective Analysis of the Response of Tumors in Patients Treated with a Combination of Radiotherapy and Hyperthermia," Int. J. of Hyperthermia, Vol. 2, pp. 337-350, 1986.

Voigt, R.G., Gottlieb, D. and Hussaini, Y. eds., Spectral Methods for Partial Differential Equations, SIAM, Philadelphia, 1984.

Waterman, F.M., Nerlinger, B.E., Moylan, D.J. III and Leeper, D.B., "Response of Human Tumor Blood Flow to Local Hyperthermia," Int. J. of Radiation Oncology Biol. Physics, Vol. 13, No. 1, pp. 75-82, 1987.

Weinbaum, S. and Jiji, L.M., "A New Simplified Bioheat Equation for the Effect of Blood Flow on Local Average Tissue Temperature," J. of Biomechanical Eng., Vol. 107, pp. 131-139, 1985.

Weinbaum, S., Jiji, L.M. and Lemons, D.E., "Theory and Experiment for the Effect of Vascular Microstructures on Surface Tissue Heat Transfer--Part I: Anatomical Foundation and Model Conceptualization," J. Biomechanical Eng., Vol. 106, pp. 321-330, 1984.

Welch, A.J., Wissler, E.H. and Priebe, L.A., "Significance of Blood Flow in Calculations of Temperature in Laser Irradiated Tissue," IEEE Trans. Biomedical Eng., Vol. BME-27, pp. 164-166, 1980.

Winget, J.M., Dewhirst, M.W., Engler, M.J., and Oleson, J.R., "The Use of Limited Temperature Observations to Predict Complete Temperature Fields," IEEE Eighth Annual Conference of the Engineering in Medicine and Biology Society, pp. 1507-1511, 1986.

Yakowitz, S. and Szidarovszky, F., An Introduction to Numerical Computations, Macmillan, N.Y., 1986.